BRNO UNIVERSITY OF TECHNOLOGY
VYSOKÉ UČENÍ TECHNICKÉ V BRNĚ

FACULTY OF MECHANICAL ENGINEERING
FAKULTA STROJNÍHO INŽENÝRSTVÍ

INSTITUTE OF SOLID MECHANICS, MECHATRONICS AND BIOMECHANICS
ÚSTAV MECHANIKY TĚLES, MECHATRONIKY A BIOMECHANIKY

ENERGY HARVESTING POWER SUPPLY FOR MEMS APPLICATIONS
NEZÁVISLÝ ELEKTRICKÝ ZDROJ PRO MEMS APLIKACE

DOCTORAL THESIS
DIZERTAČNÍ PRÁCE

AUTHOR — **Ing. Jan Smilek**
AUTOR PRÁCE

SUPERVISOR — **doc. Ing. Zdeněk Hadaš, Ph.D.**
ŠKOLITEL

BRNO 2018

ABSTRACT

This thesis deals with the development of an independent power source for modern low-power electronic applications. Since the traditional approach of powering small applications by means of primary or secondary batteries lowers the user comfort of using such a device due to the necessary periodical maintenance, the novel power source is using the energy harvesting approach. This approach means that the energy is scavenged from the ambience of the powered application and converted into electricity in order to satisfy the power requirements of the newest MEMS electrical devices.

The target applications for the new energy harvesting device are seen in wearable and biomedical electronic devices. That places challenging requirements on the energy harvester, as it has to harvest sufficient energy from the ambience of human body, while fulfilling practical size and weight constraints.

After the preliminary requirements setting and analyses of possible sources of energy a kinetic energy harvesting principle is selected to be employed. A series of measurements is then conducted to obtain and generalize the kinetic energy levels available in the human body during various activities. A novel design of kinetic energy harvester is then introduced and developed into the form of a functional prototype, on which the actual performance is evaluated. Aside from the actual new harvester design, the thesis introduces an original way of improving the power output of the inertial energy harvesters and provides statistical data and models for the human energy harvesting usability prediction.

KEYWORDS

Energy harvesting, human power, alternative energy source, electromechanical system, Tusi couple, principal component analysis, wearable and biomedical applications

BIBLIOGRAPHICAL REFERENCE

SMILEK, J. *Energy harvesting power supply for MEMS applications*. Brno: Brno University of Technology, Faculty of Mechanical Engineering, 2018. 156 pp. Supervisor of doctoral thesis doc. Ing. Zdeněk Hadaš, Ph.D..

ABSTRAKT

Tato práce se zabývá vývojem nezávislého elektrického zdroje pro moderní nízkopříkonové elektrické aplikace. Protože tradiční řešení napájení drobných spotřebičů s využitím baterií či akumulátorů snižuje uživatelský komfort kvůli potřebě pravidelné údržby, navrhovaný zdroj využívá principu energy harvesting. Tento princip spočívá v získávání energie přímo z okolního prostředí napájené aplikace a její přeměně na energii elektrickou, která je dále využita pro napájení moderních MEMS (mikroelektromechanických) zařízení.

Potenciální aplikací vyvíjeného zdroje je především moderní nositelná elektronika a biomedicínské senzory. Tato oblast využití ovšem klade zvýšené nároky na parametry generátoru, který musí zajistit dostatečný generovaný výkon z energie, dostupné v okolí lidského těla, a to při zachování prakticky využitelné velikosti a hmotnosti.

Po stanovení předběžných požadavků a provedení analýz vhodnosti dostupných zdrojů energie ke konverzi byla k využití vybrána kinetická energie lidských aktivit. Byla provedena série měření zrychlení na lidském těle, především v místě předpokládaného umístění generátoru, aby bylo možno analyzovat a generalizovat hodnoty energie dostupné ke konverzi v daném umístění. V návaznosti na tato měření a analýzy byl vyvinut inovativní kinetický energy harvester, který byl následně vyroben jako funkční vzorek. Tento vzorek byl pak testován v reálných podmínkách pro verifikaci simulačního modelu a vyhodnocení reálné použitelnosti takového zařízení. Kromě samotného vývoje generátoru je v práci popsán i originální způsob zvýšení generovaného výkonu pro kinetické energy harvestery a jsou prezentována statistická data a modely pro predikci využitelnosti kinetických harvesterů pro získávání energie z lidské aktivity.

KLÍČOVÁ SLOVA

Energy harvesting, lidská energie, alternativní zdroje energie, elektromechanická soustava, Tusiho mechanismus, analýza hlavních komponent, nositelné a biomedicínské aplikace

BIBLIOGRAFICKÁ CITACE

SMILEK, J. *Nezávislý elektrický zdroj pro MEMS aplikace.* Brno: Vysoké učení technické v Brně, Fakulta strojního inženýrství, 2018. 156 s. Vedoucí dizertační práce doc. Ing. Zdeněk Hadaš, Ph.D..

STATEMENT

I hereby declare that I have written this PhD thesis „Energy harvesting power supply for MEMS applications“ independently, under the supervision of doc. Ing. Zdeněk Hadaš, Ph.D. and using the listed references.

In Brno, 20.6.2018 Ing. Jan Smilek

ACKNOWLEDGEMENT

I would like to thank to my supervisor, doc. Ing. Zdeněk Hadaš, for the counselling, guidance and mentoring during my doctoral study.

Special thanks to my family and all the magnificent people, who have supported me through these last four years.

TABLE OF CONTENTS

1 INTRODUCTION

In the last twenty years there have been attempts to replace the conventional power sources for low-power and ultra-low-power electronics by alternative means. One option of achieving an independent power supply is to exploit the so called energy harvesting principle (sometimes called also power harvesting or energy scavenging). This term refers to obtaining electrical energy from energy of another type, available in the ambience of the energy harvesting unit. The other types of energy include solar energy, energy of thermal gradient, mechanical energy or electromagnetic (RF) energy. Energy harvesting is targeted at small-scale power generation in range of up to miliwatts of average power. By this definition i.e. large solar power plants cannot be considered energy harvesting sources, even though they present an alternative power source utilizing the solar energy conversion. The range of potential applications for energy harvesting devices is increasing with the dropping power consumption of modern electronic devices. Example applications, such as wireless sensors embedded in the difficult to access parts of technical systems in aerospace or civil engineering, or modern wearable and implanted health and monitoring sensors, display a growing tendency of using MEMS (microelectromechanical systems) technology, which is characterized by very low power requirements.

In relation to recent advances in the development of modern biomedical implants, namely a new generation of cochlear implants [1], the question of feasibility of using an alternative energy source for powering this implant or other wearable or biomedical MEMS application arose. Such a power source, based on the energy harvesting principle, would have to comply with challenging requirements regarding both its performance and dimensions in order not to compromise the user comfort. For this purpose it is essential to identify the feasible source of energy for conversion available from the ambient environment. The ambient power source feasibility can be evaluated by its ability to provide sufficient amount of energy for conversion. This amount is however dependent on the foreseen application to be powered up. Good requirement specification is therefore needed for the evaluation of the perspective independent power source design. It also cannot be granted in advance that the ambient energy levels will be sufficient for powering the intended application.

Equally important to the selection of ambient energy type is the conversion physical principle selection. Especially regarding the case of converting mechanical energy into electricity there are multiple conversion methods with different strengths and weaknesses. These unique points of particular transduction principles must be identified and the most advantageous principle must be selected in order to satisfy the application requirements.

This work focuses on a feasibility analysis and development of an energy harvesting-based independent power source for MEMS applications in challenging environments, where low frequency and low magnitude mechanical excitation is available, and where size and weight constraints are severely limiting the power source parameters.

2 MOTIVATION

Dropping power requirements of modern low-power and ultra-low-power electronic applications pave the way for research activities directed towards alternative power sources, which can in medium to long term horizon replace currently used conventional batteries. At the same time, the usage of biomedical sensors and the popularity of various wearable electronic gadgets shows an increasing trend. Furthermore, the concept of the internet of things, represented by a vast network of interconnected devices, is slowly making its way into the every-day life, meaning that even more small stand-alone electronic sensors and other devices will soon be used to monitor and enhance various aspects of human lives.

Multiple modern electronic MEMS applications are already in the sub-miliwatt power consumption range, as can be seen in Table 1, showing the examples of modern biomedical electronic devices with power requirements below 0.5 mW. Such power requirements can possibly be covered by theoretically inexhaustible alternative power sources, based on exploiting the unused energy in the proximity of the application.

Table 1 Examples of low power MEMS biomedical devices

Device	Reference	Reported power consumption
Pacemaker	[2]	8 μW
Neural sensor	[3]	10.5 μW
Biomonitoring system	[4]	100 μW
Cochlear implant	[1], [5]	150 μW - 211 μW
Blood Pressure Sensor	[6]	300μW
Drug pump	[7]	400 μW

The main motivation for the development of such a source is then the impracticality of maintaining a large number of independent electronic applications, including the ones used for monitoring the health of people or enhancing their life experience. While wired power supply is not feasible for the smallest devices, which are commonly wireless by design, batteries offer only a limited lifetime, often shorter than the designed lifetime of the device. Finding a feasible, maintenance-free and preferably environmentally friendly inexhaustible power source for these applications is therefore one of the major problems that need to be satisfactorily solved before the larger scale adoption of wearable and biomedical MEMS applications can happen.

3 PROBLEM DEFINITION

3.1 FEASIBLE POWER SOURCE PROBLEM

The current strategy of powering up the wearable and biomedical electronic devices by primary or secondary batteries bears the necessity of a regular maintenance. The batteries must be periodically changed or recharged, which might be an obstacle to increasing the user comfort of such electronics. In case of wearable electronics, the battery maintenance presents in most cases just a minor nuisance unless the device stops working due to lack of power in conditions, where it is being relied upon. However, for implanted electronic devices the need for maintenance due to battery change also means a need for additional surgery, putting more strain to the user of the implant.

Possible solutions can be found in the field of energy harvesting. Exploiting the otherwise unused energy in the ambience of the powered application could potentially ensure theoretically continuous and unconstrained function of the electronic devices. The challenge lies in the unpredictability and variance of the ambient energy levels in the human body and its close proximity. Harvesting power from sources that can potentially directly affect the health of the harvester user (blood pressure, heart contractions) is deemed controversial and unsafe. Solar power could theoretically be utilized, but the power output of such energy source would vary significantly depending on the time and whereabouts of the user. Moreover, exploiting this technique brings necessity to have the harvester directly exposed to the light. Some publications also analyse use of thermoelectric generators for human power harvesting, but the results are not convincing. A possibility might lie in exploiting the energy of human motion. On one hand, this approach does not endanger the user's health. On the other hand, the power output of the electromechanical energy harvester would depend on the activity levels of the user. While this might not be a problem for some wearable applications used e.g. for sport activity tracking, in biomedical sensors it could be a disadvantage, as some potential user target groups might not be very physically active. Furthermore, if the harvester is supposed to power up the electrical application 24 hours a day, 7 days a week, it needs to be able to harvest sufficient energy from the limited period of time, when its user is being physically active. In addition to that, the size and weight of the device must not be too high, in order not to affect the user comfort. For this reason it is necessary to analyse the available levels of energy for conversion, and verify, whether the energy harvesting-based power source can ensure the required performance with most of the perspective users.

3.2 THESIS GOALS

Thanks to intended placement of the independent power source –energy harvester– in the proximity of the powered application, therefore on/in the human body, there are three types of energy that are theoretically available for conversion: mechanical energy, solar energy a thermal gradient. Despite the challenges listed in the chapter above, the mechanical energy conversion still presents the least invasive technique of powering up small electrical applications. Moreover, this type of energy has high potential for every-day use, as the amounts of available mechanical energy are directly influenced by the user's behaviour, which can be adjusted to certain extent. Further work will therefore deal solely with the electromechanical energy harvesting

from human behaviour and its feasibility for powering wearable and biomedical MEMS electronic devices.

The main goals of this dissertation are twofold. Firstly, an analysis of available mechanical energy in the environment of the human body will be performed and a feasibility study of an electromechanical energy harvester placed on the human body will be conducted. The least favourable placement, represented by the human head, will be investigated as the worst-case scenario. For this, the acceleration in the area of human head will be measured on multiple testing specimen. This data will be used for statistical processing and to draw general conclusions regarding the feasibility of development of an electromechanical energy harvester for human power harvesting. In order to improve the harvester performance, a method that could potentially increase the amount of harvested power will be presented.

Based on the results of the initial analyses, a perspective electromechanical energy conversion method will be chosen and a new design of the electromechanical energy harvester for wearable and biomedical MEMS applications will be introduced. The second goal is therefore to design, optimize, manufacture and verify the prototype of electromechanical energy harvester for human power harvesting both in laboratory and in real life conditions. Even though the harvester is intended to be used for ultralow-power MEMS applications, due to expected low available energy levels the design of the harvester will have to properly utilize the advantages of selected energy conversion method and supress its weaknesses in order to comply with the expected requirements.

4 STATE-OF-THE-ART

4.1 ELECTROMECHANICAL ENERGY CONVERSION

The energy harvesting power sources utilizing mechanical energy follow the same physical principles as any other electromechanical energy transducers, be it sensors or generators. However, energy harvesting devices utilize the so-called free energy from the environment, which, if extracted without consideration, might have a negative impact on the host structure or even on the powered up application. Therefore, unlike the case of sensors, where the energy extracted to obtain the signal is negligible, or in generators, where the energy is fed with the sole intention of energy conversion, in energy harvesting devices the amount of energy extracted from the environment and the effect of the energy extraction on the host system must be considered, not to compromise the host system functional characteristics. The available methods of converting the mechanical energy into electricity are following:

4.1.1 Piezoelectric effect

The piezoelectric effect has been experimentally discovered in tourmaline and quartz crystals by Curie brothers in 1880. It was found, that certain materials exhibit an electric polarization when subjected to mechanical stress. This polarization is linearly dependent on the mechanical load. This effect and its inverse counterpart – deformation of the piezoelectric material when under the influence of electric field - is currently being exploited in sensors and actuators, but also for the purposes of energy harvesting [8].

The piezoelectric effect is rooted in the fundamental structure of a crystalline network. Certain crystalline structures have a charge balance with polarization, which must be oriented in one direction to produce piezoelectric behaviour of the material. The linear piezoelectric effect is expressed by a set of two constitutive equations [9], which can be written in the following form:

$$T_p = c_{pq}^E \cdot S_q - e_{pk} \cdot E_k \quad (1)$$

$$D_i = e_{iq} \cdot S_q + \epsilon_{ik}^S \cdot E_k \quad (2)$$

Where T_p is the stress component, c_{pq}^E is the elastic stiffness constant at the constant electric field, S_q is the mechanical strain component, e_{pk} is the piezoelectric constant, E_k is the electric field component, D_i is the electric displacement component, ϵ_{ik}^S is the permittivity component for constant strain and indices i, k, p, q refer to different directions within the material coordinate system.

The aforementioned equations can also be expressed in alternative forms, derived by equivalent modifications in order to express different variable than in the original form [8].

There are two operation modes of the piezoelectric material, exploitable for energy harvesting [10]: mode 33 and mode 31, as shown in Figure 1. In both these modes the external force is applied only in one direction, which is a common assumption in the energy harvesting devices.

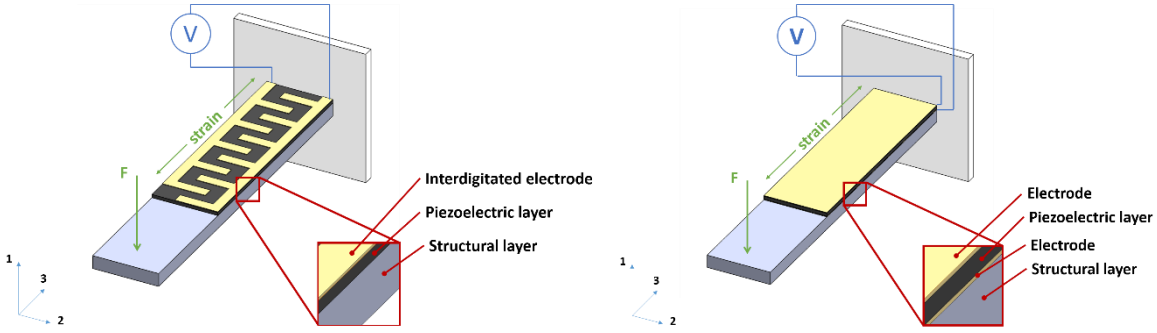

Figure 1 Piezoelectric conversion working modes: 33 (left) and 31 (right)

The electric displacement, electric field and the voltage on the electrodes are aligned along the polarization direction 3 in both modes 33 and 31. In the mode 33 (compressive mode) the vectors of mechanical stress and strain follow the same direction 3, along which the voltage is recovered. In mode 31 (transverse mode) the force is applied in direction 1, perpendicular to the direction of the recovered voltage.

Most contemporary piezoelectric energy harvester designs rely on a cantilevered beam with a proof tip mass fixed to its free end in unimorph or bimorph configuration, working in the mode 31 [11]. For maximizing the generated power, it is crucial for the piezoelectric layer working in transverse mode to be as far as possible from the neutral axis. It can be also found analytically and experimentally [12], that the piezoelectric layer should be covering only the part of the cantilever with highest deformation, namely the first 2/3 of its length, counting from the fixation line.

Other designs [13] exploit the compression mode 33 by using interdigitated electrodes on a cantilever beam or by stacking the piezoelectric layers on top of each other [14] and electrically connecting them either in series or in parallel.

Aside the mentioned basic designs, more complicated harvesters can include arrays of beams, double clamped beams or membranes for harvesting electromechanical energy in various excitation conditions.

Disadvantages of the piezoelectric materials include high frequency dependent inner impedance and rather fast degradation of the current piezoelectric materials properties [15].

4.1.2 Electromagnetic induction

The phenomenon known as electromagnetic induction was discovered in 1831 by Michael Faraday, who found that a variation of the magnetic field in time can generate an electric field. This is applicable whether the magnetic field itself changes, or the conductor is moved through it. Aside for the applications in motors and generators, the electromagnetic induction is being exploited by electrodynamic energy harvesters. These harvesters, exploiting the Faraday's law of induction for generating electromotoric force (emf) on a pickup coil placed in a time-varying magnetic field (Figure 2), are essentially miniaturized versions of rotary or linear generators with a rotor moving either in line or along a circular segment path [16], [17]. Connecting an electrical load to the coil ports then causes a current to flow, generating electrical energy. The required change of the magnetic field is usually provided by a relative movement of permanent magnet(s) with respect to the coil. Either the permanent magnet or the coil is fixed to the stationary frame of the harvester, while the other part is attached to the inertial mass. The voltage (emf) induced across the coil is calculated by the well-known formula:

$$emf = -\frac{d\psi}{dt} = -N\frac{d\Phi}{dt} \tag{3}$$

where N is the number of coil turns and Φ is total magnetic flux through the coil area. Electromagnetic generators are characterised by rather high output current level at the expenses of low voltages. Downside of this principle can be seen in using permanent magnets, leading to bulky device designs and limited scalability of such harvesters towards microstructures.

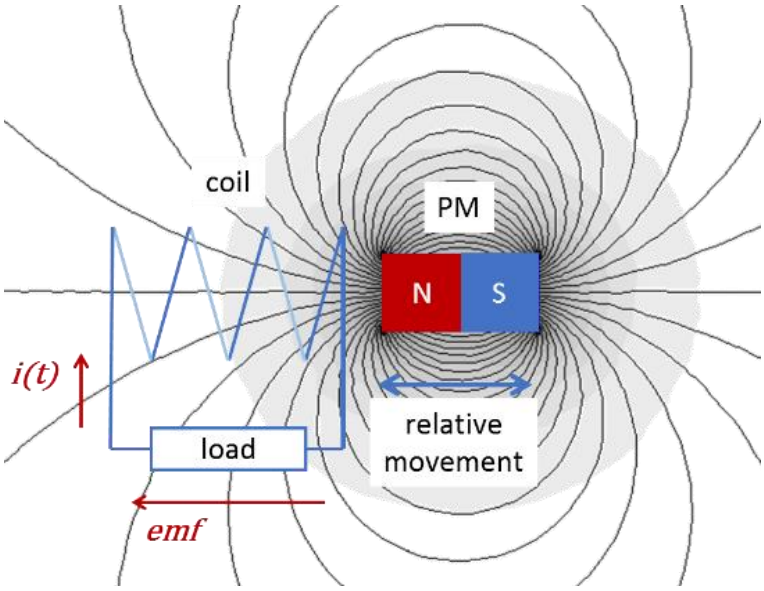

Figure 2 Electromagnetic induction principle

4.1.3 Electrostatic conversion

The principle of electrostatic energy conversion lies in exploiting a capacitor with a variable capacitance. The two electrodes of the capacitor, separated by air, vacuum or any dielectric material, move with respect to each other due to mechanical excitation. That leads to a change either in the overlapping active surface of the electrodes, or their distance from each other, causing a variation in the capacitance [18]. The electrostatic harvesters can be divided into two main groups: electret-free devices and electret-based devices. The difference between the two groups lies in the use (or lack) of the electret material between the electrodes, which eliminates the need for priming voltage to provide the initial energy for conversion.

The electret-free devices are passive structures, the function of which requires additional electrical energy to be added in order to convert mechanical energy into electricity. The most common working cycles (Figure 3) employed are the voltage-constrained cycle and the charge-constrained cycle. A correct synchronization of the energy extraction with capacitance variation is necessary in order to exploit the relative movement of the electrodes for generating electricity.

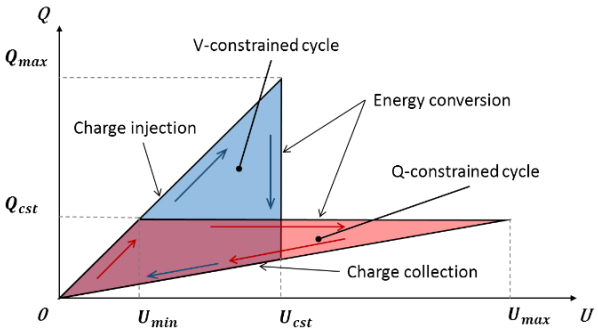

Figure 3 Electrostatic conversion working cycles

The total amount of energy converted per cycle for charge-constrained cycle is equal to:

$$E_{Q=cst} = \frac{1}{2} Q_{cst}^2 \left(\frac{1}{C_{min}} - \frac{1}{C_{max}}\right) \tag{4}$$

and for voltage constrained cycle to:

$$E_{U=cst} = \frac{1}{2} U_{cst}^2 (C_{max} - C_{min}) \tag{5}$$

The electret-based devices (Figure 4) are in principle similar to electret-free harvesters. The main difference is that a layer of electret material is added to one or both electrodes, thus polarizing it. Therefore, these devices, much like in piezoelectric materials do not rely on initial electrical energy, as the structure deformation directly induces an output voltage.

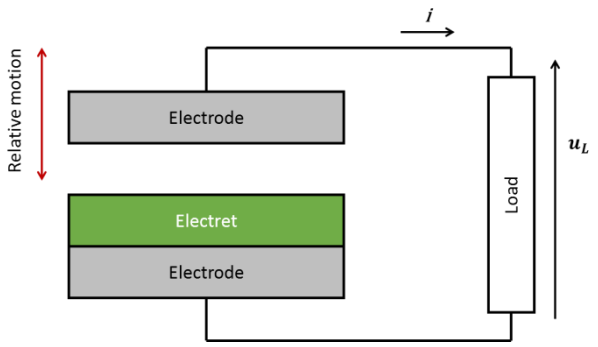

Figure 4 Electrostatic harvester using electret layer

The electrostatic conversion principle is used mainly in MEMS sensors, actuators, and energy harvesters. The common topologies of the harvesters include in-plane or out-of-plane converters with variable overlap of the electrodes or variable air gap. Commonly, interdigitated comb structures are used to maximize the electrode surface [19].

4.1.4 Magnetostriction

In magnetostrictive materials a mechanical strain will occur when they are subjected to a magnetic field in addition to strain originated from applied mechanical loading. This is known as a magnetostrictive, or Joule effect. Due to the inversion of this effect, known as magnetoelastic effect, Villari effect or just inverse magnetostrictive effect, the magnetization of these materials also changes with the variation of applied mechanical stresses in addition to the changes caused by the variance of the externally applied magnetic field.

The functional dependencies of strain and magnetic flux density can be described by mathematical functions:

$$\varepsilon = \varepsilon(\sigma, H) \quad (6)$$
$$B = B(\sigma, H) \quad (7)$$

where, ε, σ, H and B are the strain, the stress, the applied magnetic field strength, and the magnetic flux density respectively.

The most important mode of operation of magnetostrictive materials is the longitudal mode 33 [20]. Linearizing the differential response of strain and magnetization to obtain the magnetomechanical coupling for this mode leads to the following set of equations:

$$\varepsilon = S^H \sigma + d_{33} H \quad (8)$$
$$B = d_{33}^* \sigma + \mu^\sigma H \quad (9)$$

Where $S^H = \frac{\partial \varepsilon}{\partial \sigma_{|H=const}} = \frac{1}{E^H}$, E^H is the Young's modulus at constant applied magnetic field strength, $d_{33} = \frac{\partial \varepsilon}{\partial H_{|\sigma=const}}$ is the magnetostrictive strain derivative (linear coupling coefficient for mode 33), $d_{33}^* = \frac{\partial B}{\partial \sigma_{|H=const}}$ is the parameter of magnetomechanical effect for the same mode, and $\mu^\sigma = \frac{\partial B}{\partial H_{|\sigma=const}}$ is the magnetic permeability at a constant stress [20].

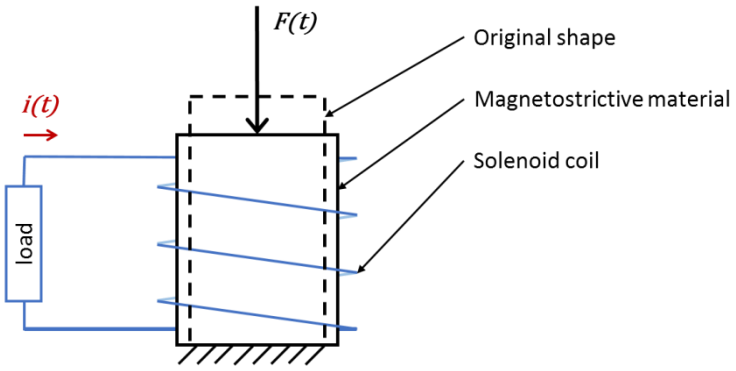

Figure 5 Principle of a Villari effect

Both magnetostrictive and magnetoelastic effects can be exploited in energy harvesting. For the direct conversion of the energy from mechanical to electrical, the magnetoelastic principle can be employed (Figure 5), utilizing a solenoid coil [21]. The change of the magnetic field caused by subjecting a magnetostrictive material to a mechanical stress induces voltage across the coil in the same manner as in electromagnetic energy harvesters [22]. The difference between the two then lies in the mechanism of magnetic field time variation.

Energy harvesting devices exploiting the direct magnetostrictive (Joule) effect consist of a sandwich of magnetostrictive and piezoelectric layers, and one or more permanent magnets. The change of external magnetic field caused by a relative movement between a permanent magnet and the magnetostrictive – piezoelectric materials sandwich causes a deformation of the magnetostrictive layer, which in turn subjects the piezoelectric layer to mechanical stress, generating voltage on electrodes through piezoelectric conversion principle.

4.1.5 Triboelectric effect

Triboelectricity has been known to humankind since antiquity, being considered mostly a negative effect that needs to be prevented. The principle of this effect lies in a contact-induced charge transfer, when one material becomes electrically charged after being contacted through friction by another material. Different materials are able to either lose or accept electrons in different amounts.

The amount of the transferred charge Δq_c is given by the product of the potential difference V_c and the capacitance between the two bodies at the critical separation distance where the charge transfer is cut off C_0:

$$\Delta q_c = C_0 V_c \tag{10}$$

The materials can be arranged by their relative polarity in an order known as triboelectric series [23]. The main obstacle for broader use of triboelectricity aside for Wimshurst machines or Van de Graaf generators was until recently seen in the limited fundamental understanding of the effect. However, recent advances in this field lead to a new type of energy transducer being used in electromechanical energy harvesting: triboelectric nanogenerator (TENG).

The theoretical and experimental analysis of this type of energy harvesters is described by many researches as can be seen from publications [24], [25], and is currently gaining increasing attention worldwide.

Triboelectric nanogenerators have demonstrated clear advantages, including high output voltages, energy-conversion efficiency, abundant choices of materials, good scalability and flexibility [26]. Following different modes of TENG (Figure 6) are currently being used: vertical contact separation mode [27], [28], lateral sliding mode [29], [30], sliding or contact freestanding triboelectric-layer modes [31], [32], and single-electrode mode [33], [34].

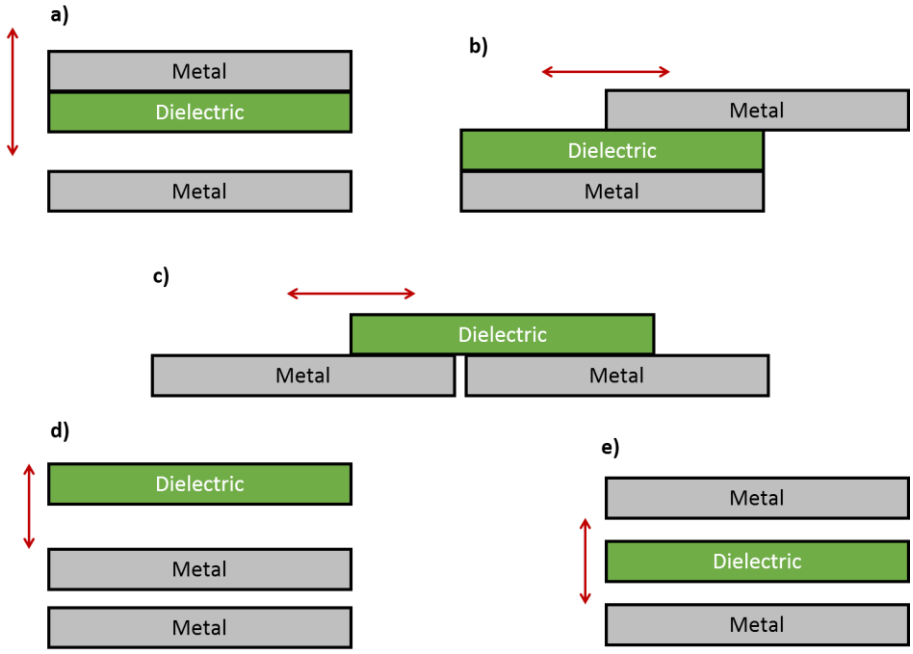

Figure 6 Different working modes of TENG: a) vertical contact separation mode, b) lateral sliding mode, c) sliding freestanding triboelectric-layer structure, d) single-electrode contact structure, e) contact freestanding triboelectric-layer structure

4.2 EXCITATION OF ELECTROMECHANICAL ENERGY HARVESTERS

Mechanical energy enters the energy conversion process in a form of excitation force or torque, acting on the harvester moving parts. This excitation can be classified according to different parameters. Knowing the excitation characteristics is a vital point for efficient design of the electromechanical energy harvester. For this reason a proper analysis of conditions in the perspective harvester placement is necessary. The classification of the mechanical excitation can be done taking into account following factors:

4.2.1 Excitation application point

4.2.1.1 Direct excitation (strain, displacement)

The excitation force is applied directly to the moving part of the harvester containing the energy transducer (Figure 7). Most energy harvesters exploiting the direct excitation use step or impulse excitation of the transducer. Typical examples include the harvester integrated into the shoe soles [35], or into the smart textiles [36], exploiting the deformation of the fabric. Furthermore, the intended implantable harvesters exploiting the deformations of the ear canal [37] or arteries [38] employ this excitation type. The dynamics of an example system with one degree of freedom, directly excited by force F is described by

$$m\ddot{q} + b\dot{q} + kq = F \tag{11}$$

where m is the mass, b is the damping, and k is the stiffness. Direct excitation of the transducer is also used in harvesters with the frequency up-conversion mechanisms [39]. Even though this type of harvesters can in principle contain the inertial proof mass, the transducer itself obtains the input mechanical energy through direct force interaction between the proof mass and the oscillator with transducer.

A specific case of the direct excitation can be seen in exploiting the turbulences in the flow of a liquid, caused by an appropriately shaped blunt body placed into the flow of a certain speed to excite e.g. piezoelectric flag-type of energy harvester [40, 41].

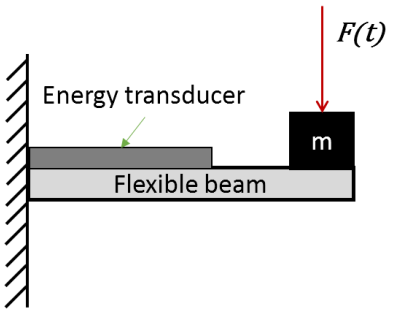

Figure 7 Directly excited system

4.2.1.2 Inertial excitation (acceleration)

Inertial energy harvesters [42] make use of an oscillating proof mass, attached to the frame of the harvester through one or more stiffness elements. The oscillation of the proof mass with the energy transducer is then excited by inertial forces caused by the movements of the harvester's frame (Figure 8). The motion of such system is described by equation

$$m\ddot{q} + b\dot{q} + kq = -\ddot{z}m \tag{12}$$

where $\ddot{z}$ denotes the acceleration of the frame. Inertial harvesters are often designed to exploit the resonance effect in order to accumulate the mechanical energy in the oscillator with the goal of increasing the power output.

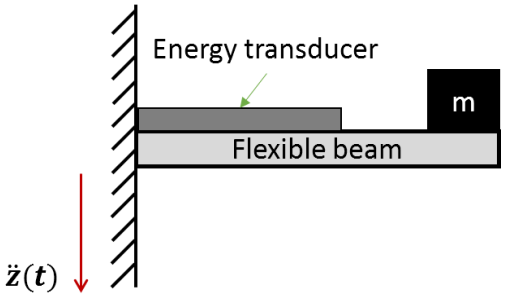

Figure 8 Inertially excited system

4.2.2 Excitation characteristic

4.2.2.1 Periodic vibration excitation

4.2.2.1.1 Harmonic excitation

The most commonly assumed excitation especially for inertial energy harvesters is the sinusoidal excitation force or acceleration with a constant frequency [43]. This ideal excitation with a single constant frequency and magnitude is however rarely present in real-world conditions.

4.2.2.1.2 Non-harmonic periodic excitation

Non-sinusoidal excitation waveforms that still comply with the requirement of periodicity are common in the energy harvesting applications. Their frequency spectra contain multiple components, which can be exploited for the energy harvester resonance tuning in case of employing the resonant mechanism [42]. In some real technical systems however, the frequencies of the excitation can be time dependent. This puts additional challenges on the harvester design, so that it can work in broader frequency band.

4.2.2.2 Random vibration excitation

Some electromechanical energy harvesters are being designed for applications, where no stable or predictable source of excitation is available [44]. If the excitation waveform cannot be predicted, it is called random excitation. An example of such excitation can be seen in earthquakes or air vibrations caused by human speech. Analysis of such an excitation requires use of statistical and probabilistic methods.

4.2.2.3 Impact excitation

A special case of energy harvester excitation are mechanical shocks or impacts [45]. An impact taking a form of a single ideal δ impulse has a flat frequency spectrum, and as such it will excite the harvester on its natural frequency no matter its tuning. Real impact impulses with finite height and non-zero width however contain discrete frequency components, the magnitudes and frequencies of which are related to the shape of the pulse. An example of impact-based harvester is the device designed for harvesting the energy of rain drops [46].

4.2.3 By excitation direction

Exploitable excitation in most technical systems is multidirectional. Electromechanical energy harvesters however are often designed as 1 degree of freedom devices, harvesting from one-dimensional motion, as these designs allow for potentially higher electromechanical coupling.

4.2.3.1 One-dimensional excitation

The vector of the excitation changes only its length with time, but remains oriented along a single line in space. This is the best case scenario for unidirectional harvesters employing a linear motion mechanism. That covers both directly excited piezoelectric stacks, and many inertial harvesters.

4.2.3.2 Two-dimensional excitation

If the excitation vector changes its direction with time, but remains within one plane, the excitation is called two-dimensional. Such excitation can be exploited by harvesters with multiple degrees of freedom. In specific cases, rotary or pendulum harvesters might also benefit from this type of excitation.

4.2.3.3 Three-dimensional excitation

Three-dimensional excitation is represented by a force or acceleration vector that changes its orientation with time in 3D space. Such excitation is common in real systems, and can even be the result of multiple sources of excitation acting on the harvester (such as multiple independent electric motors as sources of vibrations in one technical system). Ensuring sufficient electromechanical coupling in all three dimensions is challenging [47], so a proper orientation of the harvester with fewer working dimensions in these conditions is vital to maximize its power output.

4.3 ELECTROMECHANICAL ENERGY HARVESTER CLASSIFICATION

Electromechanical harvesters cover a variety of different devices, utilizing various functional principles to convert the mechanical energy into electricity. This chapter introduces some of the possible classification criteria, meant to categorise the electromechanical energy harvesters according to their similarity in some aspect. This will help with the performance comparison, where dissimilarities in the designs and functional principles can play an important role in their resulting overall performance, depending on the metric selected for comparison. The presented list of classification criteria is not exhaustive. Other aspects, such as device aspect ratio, presence of housing, total device weight, working frequency range or output voltage range might be used for classification purposes as well.

4.3.1 Energy extraction principle

Electromechanical energy harvesters employ a range of design principles in order to extract and convert the mechanical energy into electricity. Aside of the choice of the energy transduction physical principle, the design options include using a mechanical resonator, which works as a mechanical energy accumulation element and amplifies the displacement amplitude of the harvester when excited close to the resonant frequency. The electromechanical harvesters therefore can be classified by the type of resonator used, or its absence:

4.3.1.1 Non-resonant devices

Electromechanical energy harvesters that are not designed to utilize the resonance amplification effect are mostly pulse-excited or strain-based devices exploiting the direct deformation of the transducer, caused by the advantageous placement of the harvester on the host structure. The design of these devices can be fairly simple, as they completely omit the mechanical oscillator. Non-resonant harvesters [48] also do not affect the dynamic behaviour of the host structure as significantly as the resonant devices.

4.3.1.2 Direct resonators

Many harvesters employ a mechanical oscillator, connected to the frame of the harvester, and therefore also to the host structure through a stiffness element. By an appropriate tuning of the stiffness constant and the seismic mass weight the natural frequency of the oscillator can be tuned to match a frequency of an exploitable component present in the excitation spectrum [49]. This leads to the resonance amplification of the seismic mass displacement, accumulating more mechanical energy in the oscillator and increasing the power output of the harvester. The seismic mass weight of the energy must be negligible compared to the weight of the hosting structure, as its oscillation introduces a dynamic feedback into the structure. This effect is however being exploited in oscillation dampers, where the oscillations of the host structure on given frequency are supressed by the function of an accordingly tuned additional oscillator.

4.3.1.3 Parametric resonators

Parametric resonators provide another interesting option to the direct resonance mechanism commonly used in resonant-based vibration energy harvesting. A parametric resonator (Figure 9) exploits a time dependent modulation of some of the system parameters (stiffness, damping, or moment of inertia) at a frequency equal to twice the natural frequency of the system [50]. Parametric excitation of the system is usually orthogonal to the plane of the oscillator movement. Since the amplitude of oscillation of the system in parametric resonance does not saturate due to linear damping, a system driven into parametric resonance can reach over an order of magnitude higher power output than the same system working in direct resonance [51]. However, the parametric resonance requires a threshold excitation for the activation of the effect. For this reason, an auto-parametric harvesters combining the direct and parametric resonance effects were introduced [52].

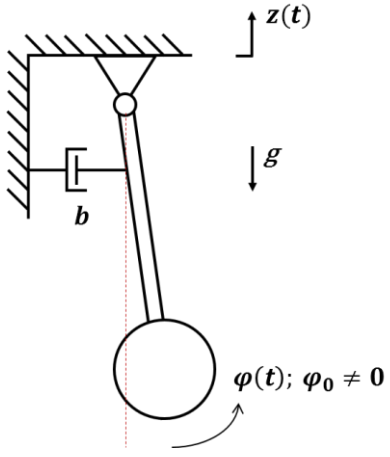

Figure 9 Parametrically excited pendulum

4.3.2 Stiffness linearity

4.3.2.1 Linear stiffness

Many inertial harvesters are designed assuming linear properties of the stiffness [53]. Even though in reality this might not be entirely true in the whole range of the possible harvester seismic mass displacements (e.g. due to displacement limiters, magnetic springs etc.), the linear approximation of the real device allows for convenient and easy modelling and analysis of the device performance, exploiting e.g. the superposition principle for output power predictions.

4.3.2.2 Nonlinear stiffness

In some applications it is desirable to exploit a nonlinearity in the stiffness in order to increase the bandwidth of resonant harvesters, making it able to cope with the variations in the excitation frequency due to skewing of the amplitude-frequency characteristics [54]. However, the non-linearity in the stiffness can trigger the system to behave chaotically under certain excitation conditions.

4.3.3 Type of movement

With respect to the motion of the internal parts of the device, the electromechanical energy harvesters can be split into three categories:

4.3.3.1 Linear trajectory

Devices with the linear motion of the internal element [55] fall within this category. Many vibration energy harvesters with linear trajectory and large displacements employ nonlinear magnetic stiffness elements [56]. Some cantilevered harvesters can be included in this category as well due to their very small displacements that can be approximated by a straight line.

4.3.3.2 Circular trajectory

Pendulum type harvesters and miniaturized conventional generators exploit oscillatory or continuous movement of the internal parts along a circular or circular segment trajectory [57]. While some devices allow for continuous rotation, others have maximum displacement limitation. Circular trajectory allows for compact devices, especially with low natural frequencies.

4.3.3.3 Other

Few electromechanical energy harvesters exploit an internal trajectory that cannot be described by the previous two types. This category includes the harvester design with free mass moving inside a spherical cavity [58] or piezoelectric cantilever harvesters with large displacements.

4.3.4 Number of DOF

Energy harvesters can be categorised into two main categories according to the number of DOF they utilise:

4.3.4.1 Single degree of freedom

Devices, which can capture and transduce vibrations or deformation into electricity in a single working direction [59]. This group contains both harvesters with linear trajectory of the proof mass and pendulum-type harvesters. The dynamics of these harvesters can be described by a single second order differential equation.

4.3.4.2 Multiple degrees of freedom

Electromechanical energy harvesters containing more than one proof mass [60], or a single proof mass that moves in multiple directions [61] fall into this category. Multiple degrees of freedom are exploited either to harvest energy from multi-directional excitation, or to extend the bandwidth of the device by using more proof masses with different natural frequency tuning (Figure 10). Arrays of cantilevered harvesters or frequency up-conversion mechanisms fall into this category.

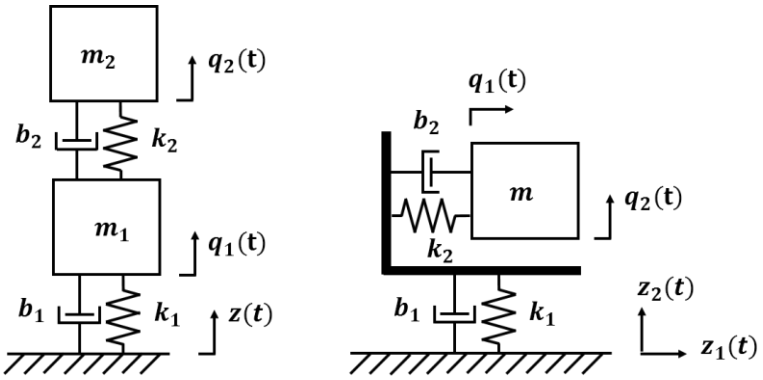

Figure 10 Different implementations of systems 2 degrees of freedom

4.4 ELECTROMECHANICAL ENERGY HARVESTERS MODELLING

There are two common approaches used for modelling and analysis of the electromechanical energy harvesting devices. Depending on the preferences, experience and compatibility with models of other interconnected systems (power management and storage, host structure) the following modelling techniques are employed:

4.4.1 Equations of motion

The electromechanical energy harvesters can generally be seen as spring–mass-damper mechanical systems with one (Figure 11) or more degrees of freedom.

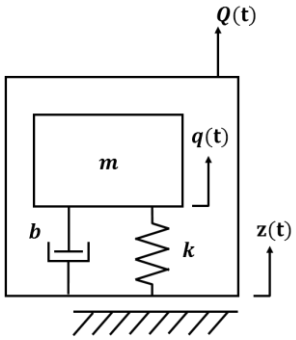

Figure 11 Spring mass damper system with one degree of freedom

The dynamics of such systems can be fully described using the energy-based approach, exploiting Lagrange equations of the second kind as shown here for an inertially excited system:

$$\frac{d}{dt}\left(\frac{dE_k}{d\dot{q}_j}\right) - \frac{dE_k}{dq_j} + \frac{dE_b}{d\dot{q}_j} + \frac{dE_p}{dq_j} = -\frac{dA}{dq_j} = -Q_j \tag{13}$$

Where $j=1 \ldots n$ in generalized coordinates q_j denotes each of n degrees of freedom of the device. E_k, E_b, and E_k denote the kinetic, dissipative and stiffness energy of the system, respectively. A is the mechanical work and Q_j stands for the generalized excitation force. Each degree of freedom then adds one differential equation of motion to the set. Depending on the design of the device, the equations might be coupled. This approach is the most commonly used method for modelling kinetic energy harvesters [62], [63].

4.4.2 Exploiting mechanical-electrical analogy

Another option is to exploit the analogy between Kirchhoff's laws and Newton's laws. Mapping the mechanical variables to electrical ones allows characterizing the whole system in the electrical domain [64]. This can be advantageous especially if the power management electronics and energy storage is being analysed together with the harvester design [65].

There are two widely used mappings (Figure 12) of mechanical variables to electrical ones: impedance analogy (force onto voltage) [66], and rotational analogy (force onto current) [67].

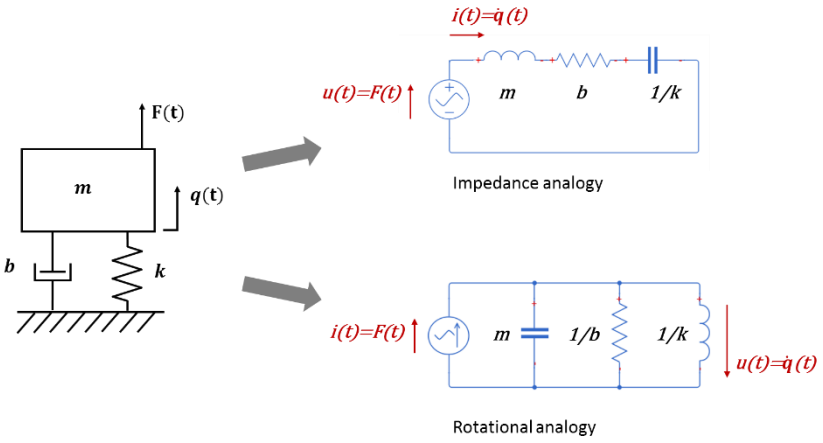

Figure 12 Two different possible mappings, exploiting mechanical-electrical analogy

The analogous differential equations for the equation of motion, impedance analogy and rotational analogy, respectively, assuming a system with one degree of freedom are:

$$m\ddot{q} + b\dot{q} + kq = F \tag{14}$$

$$L\frac{di}{dt} + Ri + \frac{1}{C}\int i\,dt = u \tag{15}$$

$$C\frac{du}{dt} + \frac{1}{R}u + \frac{1}{L}\int u\,dt = i \tag{16}$$

The analogous elements used in these equations are summarized in Table 2.

Table 2 Analogous elements for different mechanical-electrical mappings

Mechanical property		**Electrical property**			
		Impedance analogy		**Rotational analogy**	
Force	F	Voltage	u	Current	i
Velocity	$\dot{q}$	Current	i	Voltage	u
Mass	m	Inductance	L	Capacitance	C
Damping	b	Resistance	R	Conductance	$1/R$
Compliance	$1/k$	Capacitance	C	Inductance	L

4.5.1 Basic performance considerations

Teams developing inertial energy harvesters for various applications publish the parameters of their devices with very variable degree of detail, so the comparison of different designs is not straightforward.

Aside for difficulties in objectively and generally comparing designs with different working principles, there are some aspects that need to be taken into account before commencing the performance comparison. First, it should be noted that the performance of the energy harvesting device will vary significantly with the electrical load. Most of the papers publish simulation and test results with resistive load of optimal value for given conditions. Some other publications however present complex energy harvesting solutions including power management electronics consisting of combination of elements, including semiconductors, inductors and capacitors. Such electronics may further enhance (or degrade, if badly designed) the performance of the harvester and the results obtained while using it are not directly comparable to simple resistive loads. It should therefore be clear, whether the performance of the energy harvesting device only, or the performance of the whole energy harvesting solution (including power management and storage) is being evaluated.

Another point is the suitability of the harvester for given application conditions. While the performance metric can suggest that the energy harvesting device will perform sufficiently in the selected application, some practical consideration should be taken into account as well. These include predicted lifetime, possible variance in the excitation and the ability of the harvester to cope with it without user action, size of the device and the dynamic feedback it might introduce to the host system etc.

The following chapter summarizes different metrics introduced by the energy harvesting research community for possible comparison of different electromechanical devices.

4.5.2 Metrics

Multiple different metrics for the purposes of benchmarking the overall performance of energy harvesters were introduced in literature over the years [V18]:

Roundy [68] defined a metric, called the effectiveness of the harvester, taking into account the electromechanical coupling coefficient, the quality factor, the ratio of the actual harvester density to the baseline density, and the ratio of the transmission coefficient of the transduction mechanism to the maximum transduction coefficient.

A different approach taken by Beeby *et al.* [59] lies in calculating the normalized power density (NPD), where the output power of the harvester is divided by the square of acceleration magnitude and by the volume of the harvester. This approach is feasible only for devices working in resonance and does not take into account the operation frequency range of the device.

Mitcheson *et al.* [69] proposes the so called Volumetric Figure of Merit (FoM_V) derived as a ratio of useful power output to theoretical maximum power obtainable by a device with the same total volume and a gold proof mass occupying half of the total available volume. The other half is left for the proof mass displacement. This approach does not take into account the bandwidth of the harvester and devices with flatter frequency response but broader bandwidth are penalized, even though the broader operation frequency range might be advantageous in

some applications. Mitcheson therefore proposed a modification of his original volume FoM_V, multiplying the FoM_V by fractional 1dB bandwidth, in contrast with commonly used 3dB.

Another way of defining a figure of merit is presented by Sebald *et al.* [70], who proposes using the maximum obtainable power divided by the square of input acceleration magnitude and multiplied by the bandwidth. This version of FoM however does not take into consideration the size of the device, so comparing devices of different volumes is difficult.

Najafi *et al.* [71] uses a FoM defined as a modification of normalized power density, where the NPD is multiplied by the 1dB bandwidth of the harvester. That makes this metric useful for comparing harvesters operating at similar frequencies, as it does not use the fractional bandwidth.

A more recent paper, published by Ruan *et al.* [72], proposes a metric similar to the one of Najafi, utilizing the normalized power density, multiplied by the inverse of the harvester's Q factor. By definition, the Q factor corresponds to the fraction of 3dB bandwidth and resonance frequency. This makes the way Ruan's approach compensates for flatter but wider frequency responses of some harvesters similar to Mitcheson's modification of FoM, just with the 3dB instead of 1dB fractional bandwidth being considered.

An interesting metric, mainly for nonlinear harvesters, is proposed by Mallick *et al.* [73]. Instead of relying on normalized power density calculated as a function of maximum harvested power, he proposes calculating a power integral in the whole frequency range, and calculate the normalized power integral density (NPID) instead.

Different from other definitions of figure of merit, Arroyo *et al.* [74] proposes using a normalized power defined as a ratio of real output power and theoretical limit power to evaluate the harvester performance. The power normalization uses three key parameters of a generic harvester: the coupling factor, the losses coefficient and the mechanical quality factor.

Similarly, Balato *et al.* [75] presents the Harvester Ideal Utilization Factor (HIUF). This metric quantifies how close to the optimum is the harvester electrically loaded, taking into account also the diode bridge rectifiers used for power conditioning.

While other FoM definitions focus on the harvesters themselves and their comparison, the normalized power approach and the HIUF serve as tools for assessing how close to its optimal point is a particular harvester working given its parameters.

The summary of used metrics is presented in Table 3. Variables used by different authors were unified to give better possibility of direct comparison of their metrics. It should be noted that some authors take into consideration the volume of the harvester as reported, regardless of whether or not the volume reported includes necessary free space for the displacement of the proof mass. Other authors explicitly state that the volume needs to be defined as the total space occupied by the harvester during its operation. In many cases though, depending on the data published for each devices, the values reported include also the space for displacement of the proof mass.

Table 3 Metrics used for evaluating kinetic energy harvester performance

Reference	Metric	Expression	Input variables
S. Roundy [68]	Efectiveness (e)	$e = (k^2)Q^2\left(\frac{\rho}{\rho_0}\right)\left(\frac{\lambda}{\lambda_{max}}\right)$	A_0 harmonic excitation acceleration magnitude P useful power output P_f power integral over frequency P_{lim} obtainable power limit P_{max} maximum obtainable power with given excitation frequency Q quality factor V reported total volume of the harvester V_Σ volume of the harvester including the displacement Y_0 harmonic excitation displacement magnitude f_0 frequency where the maximum power is harvested $f_{1,2}$ half-power cut-off frequencies Δf bandwidth k coupling coefficient λ transmission coefficient of the transduction mechanism λ_{max} maximum transmission coefficient ρ actual density ρ_0 baseline material density ρ_{Au} density of gold ω harmonic excitation angular frequency $\delta\omega_{1dB}$ 1dB bandwidth
S. P. Beeby *et al.* [59]	Normalized Power Density (NPD)	$NPD = \frac{P}{{A_0}^2 V}$	
P. D. Mitcheson *et al.* [69]	Volumetric Figure of Merit (FoM_V)	$FoM_V = \frac{P}{\frac{1}{16}Y_0\rho_{Au}V_\Sigma^{\frac{4}{3}}\omega^3}$	
	Bandwidth Figure of Merit (FoM_{BW})	$FoM_{BW} = FoM_V \cdot \frac{\delta\omega_{1dB}}{\omega}$	
G. Sebald *et al.* [70]	Figure of Merit (FOM)	$FOM = \frac{P_{lim}}{{A_0}^2} \cdot \frac{f_2 - f_1}{f_0}$	
K. Najafi *et al.* [71]	Figure of Merit (FoM)	$FoM = \frac{P}{{A_0}^2 V} \cdot \Delta f$	
J.J. Ruan *et al.* [72]	Figure of Merit (FOM)	$FOM = \frac{P}{{A_0}^2 V_\Sigma} \cdot \frac{1}{Q}$	
D. Mallick *et al.* [73]	Normalized Power Integral Density (NPID)	$NPID = \frac{P_f}{{A_0}^2 V}$	
E. Arroyo *et al.* [74]	Normalized Power ($\underline{P}$)	$\underline{P} = \frac{P}{P_{lim}}$	
M. Balato *et al.* [75]	Harvester Ideal Utilization Factor (HIUF)	$HIUF(\omega) = \frac{P_{max}(A_0,\omega) - P(A_0,\omega)}{P_{max}(A_0,\omega)}$	

4.6 CURRENT EH DESIGNS FOR WEARABLE AND BIOMEDICAL APPLICATIONS

There are multiple electromechanical energy harvesters, designed for low frequency environments with potential use in wearable or biomedical applications. An overview of these designs is provided here. For direct performance comparison the Normalized Power Density (NPD, see 4.5.2) metric was selected, as the amount of information provided by authors of respective devices does not allow for using more complex performance metrics. The comparison (Table 4) is therefore quite rough, but it gives reader an idea of the capabilities of such devices.

Table 4 Comparison of competing kinetic energy harvesters performance

Year	Reference	Transducer	Volume [cm^3] or Dimensions [mm]	Frequency [Hz]	Acceleration [g]	Power output [μW]	NPD [$\mu W/cm^3/g^2$]
1998	[76]	electromagnetic	23.5 cm^3	2	0.3	400	189
2008	[77]	electromagnetic	ø17x55 mm	2	0.5	300	96
2009	[78]	electrostatic	20x45x? mm	2	0.4	40	?
2009	[79]	piezoelectric	25 cm^3	1	? (180° device rotation)	47	?
2010	[80]	electromagnetic	54x46x15 mm	9.25	0.5	550	59
2012	[81]	piezoelectric	125 cm^3	2	0.3	2100	187
2012	[82]	electromagnetic	34x34x18 mm	8	0.5	430	83
2013	[83]	piezoelectric	90x40x24 mm	2	? (walking, ankle placement)	51	?
2013	[84]	electromagnetic	ø 12x80 mm	6	0.5	4840	2140
2015	[85]	electromagnetic	30x10x40 mm	1.88	0.2	71	148

Some of the presented devices were tested on various placements on human subjects while walking, the published results therefore give a fair idea of expectable performance in the real-life conditions. The reported power outputs vary between 40 and 4840 μW. Confirming the intuitive expectations, the higher power outputs are reached by devices with higher working frequencies (which might however be less suitable for human power harvesting) and with larger volumes. Using the NPD to account for the size of the device and for the magnitude of the excitation, the reported devices reach values between 59 and 2140 $\mu W/cm^3/g^2$ in cases, where the data provided allows for calculation of NPD. It needs to be noted however, that NPD metrics does not take into the account the excitation frequency and thus devices with higher working frequencies might be in advantage here.

5 CHOSEN METHODOLOGY AND IMPLEMENTATION OF THE PROBLEM SOLUTION

Based on the goal definition and on the current state-of-art review, it was decided to further investigate the feasibility of an inertial electromechanical energy harvester, based on the electromagnetic energy conversion principle. This principle allows fairly straightforward implementation for low frequency devices, which will be beneficial for harvesting energy from human activities, where low excitation frequencies can be expected. Furthermore it is characterized by low inner impedance of the transducer, which can be beneficial for future power management electronics design [V10]. The downside of the selected principle lies in rather low induced voltage, making the pick-up coil design a crucial part of the development to ensure usable voltage levels.

In the first step the preliminary analysis supporting or challenging the feasibility of selected energy conversion method needs to be performed. Real-life acceleration measured on a limited number of testing human subjects is to be used as energy inputs to the simulation model. The model parameters are obtained from CAD and FEM software, with the main design parameters decided by the physical constrains placed on the harvester with respect to its maximum weight and dimensions. Furthermore, the basic application requirements are set.

Next, an algorithm exploiting a principal component analysis of the acceleration is developed to process the future measurement data. Its purpose is to find the principal direction of acceleration on selected frequency, allowing for finding the most feasible orientation of the kinetic energy harvester working axis or plane in given application. A secondary purpose of the algorithm is to correct possible misalignments of the accelerometer during measurements to mitigate a possible source of bias in the statistical analysis.

Following the results of the first analysis, a larger scale acceleration measurements are conducted to find the statistical properties of the acceleration in the human head area. The data is processed to ensure its homogeneity and employed to model the acceleration on the head of the harvester user population in order to find the theoretical power output limits of a linear kinetic energy harvester device.

Based on the results of the statistical analysis a feasibility of development of an actual kinetic energy harvester design is evaluated, and the modelling and simulation phase of the harvester development process is commenced. The design is drafted and optimized utilizing iterative simulation modelling together with CAD and FEM simulations. An optimization algorithm for the pick-up coil design is developed during this phase to maximize the electromechanical coupling. Promising results of the model allow for taking a further step, represented by an in-house manufacture of the prototype and its testing in the laboratory.

Further tests are then conducted in the real-life conditions, where the overall performance of the novel harvester design and its feasibility to power up wearable or biomedical MEMS applications is evaluated during different activities and in various placements on the human body.

Each major task in the presented problem solving methodology is covered by one or more papers published in impacted journals or international conference proceedings.

6 PRELIMINARY FEASIBILITY ANALYSIS

The feasibility analysis represents the first step in the development of the new energy harvester for powering up biomedical and wearable MEMS applications.

The example application to be powered up by the developed kinetic energy harvester is represented by a cochlear implant of new generation. Its power requirements of approximately 150 μW of average continuous power are used to define the lowest expected power output of the harvester, which would ensure function of the MEMS implant only during the harvester user activity [V15].

Acceleration during different user activities was monitored to determine the feasibility of different motions for excitation of the inertial energy harvester located in the head area, close to the cochlear implant. It was found, that most activities except for walking or jogging do not provide stable and exploitable levels of acceleration for the purposes of kinetic energy harvesting.

In order to calculate the energy necessary to supply the power to the cochlear implant for 16 hours a day, a ten months-long measurement of exploitable daily user activity was conducted. The results indicate, that average person in the productive years with semi-active life style spends only about 52 minutes a day walking, which is an activity, that can be used to harvest the energy from. The harvester would therefore have to provide 2.77 mW of average power during the assumed 52 minutes of user daily walking time, to completely satisfy the requirements of the selected application. Furthermore, this calculation does not cover the inevitable energy losses in the power management electronics and storage, which are necessary elements of the energy harvesting solution.

To get more precise results from further analyses, acceleration in the head area of five different users was measured during walking at natural and fast speeds. This data was then fed as an input to the harvester model. The multidisciplinary model [V11] was based on a virtual prototype of the harvester [V3] with one degree of freedom and nonlinear mechanical springs. The size, mass and magnetic circuit parameters of the model were obtained from FEM and CAD simulations.

A sensitivity analysis using both harmonic and real-life excitation was performed with the goal of improving the critical parameters of the model to obtain higher power output while keeping the harvester main dimensions and displacement limits. Improved model was then fed with the measured data and the harvested power on load was observed and recorded.

The results showed large variance between different users, indicating a need for larger measurement set and for determination of the user parameters, affecting the harvester power output. Final values of average harvested power on 6.6 kΩ resistive load reached between 61 μW and 238 μW during normal walking patterns, and between 100 μW and 478 μW during fast walking of the measured subjects.

The preliminary analysis was published in Microsystem Technologies journal and is included in the thesis as Annex A1.

7 SIGNAL PROCESSING ALGORITHM

During the initial measurements and analyses the question of ensuring the same orientation and alignment of the wireless accelerometer on different subjects during further planned measurements arose. Furthermore, it was found, that energy harvesting literature does not thoroughly consider the problem of the accelerometer or harvester orientation during measurements. As most of the inertial energy harvesters are devices with one degree of freedom and a single linear working axis, their correct orientation on the host system is crucial in order to maximize the power output.

An algorithm utilizing the principal component analysis of the acceleration measured in three orthogonal axes was therefore developed to solve these issues. After taking care of the uniform sampling rate of the data, the FFT is calculated. Since the measured acceleration waveforms usually contain multiple frequency components, the frequency component of interest is identified. Other frequency components are filtered out in order not to affect the further analysis.

The filtered data in time domain is then subjected to principal component analysis, which identifies the three orthogonal directions, along which the principal components of the acceleration are located (Figure 13). That means that the highest magnitude of acceleration on selected frequency of interest is located along the first principal axis, while the smallest magnitude will be found along the third axis. It needs to be noted, that different frequency components of the acceleration may also have different principal axes depending on the source of the vibrations, so the obtained principal axes might not be aligned with the principal axes of the unfiltered dataset.

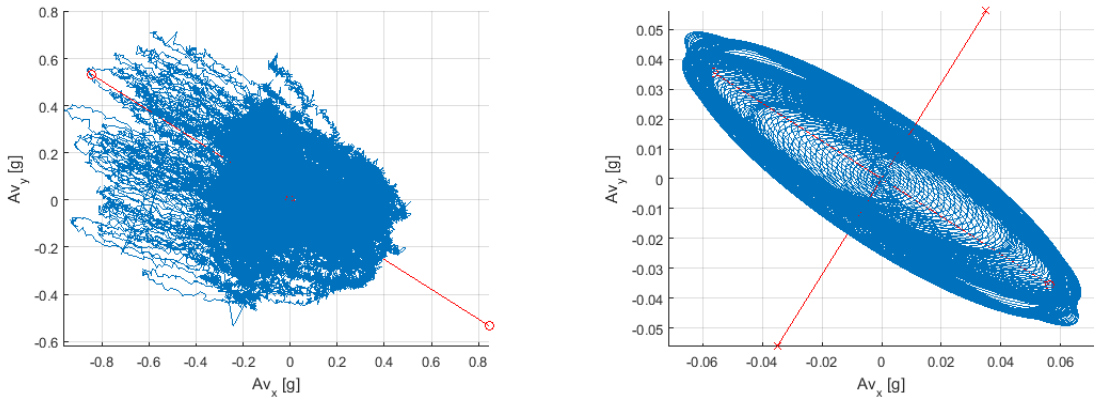

Figure 13 Original (left) and filtered (right) measured data in Cartesian space

A set of correction rotation angles denoting pitch, yaw and roll rotations necessary to align the measurement axes of the accelerometer with the found principal axes is calculated in the last step. The correction angles can then be employed to increase the power output of the kinetic energy harvester simply by rotating the working axis of the harvester with respect to originally measured directions [V4] (Figure 14).

The described method can also be used to ensure the uniform alignment of the accelerometer while measuring acceleration while walking for different people. This can be done by adopting an assumption that the principal components of the dominant acceleration peaks will be found along the same directions normal to the lateral, transversal and sagittal plane of the human body for all the people.

This correction therefore uses either static gravity acceleration or other common dominant acceleration component to rotate the data reference frame in such a way so that all processed datasets have the same orientation of the coordinate systems, regardless of the original orientation of the accelerometer during the measurements.

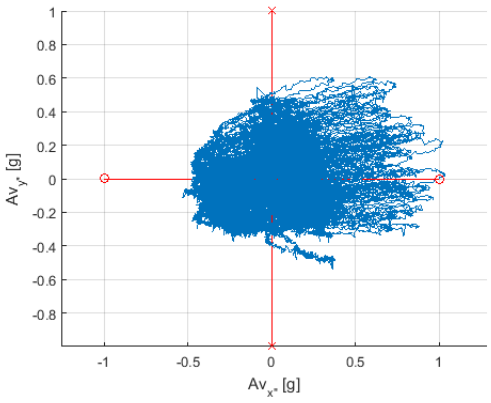

Figure 14 Acceleration data in Cartesian space after alignment of principal components with the coordinate system axes

This algorithm was published by the author of the thesis in Mechanical Systems and Signal Processing journal and is attached in the thesis as Annex A2.

8 ACCELERATION MEASUREMENTS AND ANALYSES

The acceleration measurements and processing were split into two parts. The first phase (Annex A3) served for comparison of different wireless accelerometer fixation styles and to identify the possible measurement subjects' parameters that could be affecting the measured data. 30 different testing subjects were measured while walking at natural speeds on smooth and level path. The basic parameters of the subjects, such as age, weight, height and sole thickness of shoes they were wearing during the measurements, were recorded. Measured acceleration was analysed in the frequency domain, where frequencies and magnitudes of dominant acceleration peaks in different measurement axes were compared for different sensor fixation styles and then against the recorded user parameters.

Calculating the correlation coefficients between the recorded frequencies and magnitudes of first dominant acceleration peak in the axis with highest dominant acceleration magnitude indicated, that the recorded acceleration is not linearly dependent on any of the recorded parameters with one possible exception, as correlation coefficient between magnitude of the dominant acceleration peak and the sole thickness reaches the value of 0.4.

To obtain an approximate range of theoretically harvestable power from this measured population, a simple linear model of a kinetic energy harvester was employed, assuming resonance operation, exploiting the dominant frequency with highest magnitude in each dataset.

Since the first phase of the measurements have not shown a correlation between subjects' parameters and measured frequencies and magnitudes, an alternative statistics-based approach was investigated during the second phase of signal acquisition and analysis (Annex A4). Two more sets of measurements were obtained, one of them by measuring a single testing subject multiple times, the other one measuring multiple subjects, each of them once. All the measurements were again conducted while the subjects were walking on flat level path at their respective natural speeds.

Then the data was treated using algorithm introduced in chapter 7, dynamically parsed into ten intervals in frequency domain, and finally reduced to ten frequency, magnitude and initial phase data triplets in each of the three orthogonal axes.

Before commencing the statistical analysis, the calculated rotation angles to align the coordinate system's axes with the principal axes of the dominant frequency component of the measured acceleration were observed. The distribution of the angles support the claim, that the principal axes of the acceleration during walking are parallel to the normals to the transverse, coronal and sagittal planes of the human body.

In the next step it was investigated, whether the frequency components found in the parsed frequency intervals are harmonic frequencies to the dominant frequency in each axis, and if the dominant frequencies in different axes are correlated. Both of this suggestions were supported by the calculated linear correlation coefficients, indicating a relationship both between the first dominant frequency and other frequency components in each axis, and between the dominant frequencies in different axes.

In the statistical processing part of the work, it was investigated whether the measured sample data in both datasets, each measurement reduced to ten frequency-magnitude-initial phase triplets, follow naturally assumed normal distribution. Sample mean and covariance were used to estimate the mean vector and covariance matrix of the measured data. A Kolmogorov-Smirnov

test with null hypothesis that the sample comes from the normal distribution with the estimated parameters was then used to test, whether the assumption of normal distribution of variables is valid. A two sampled K-S test was employed to check if the measured and random number simulation data come from the same distribution. This approach was then validated by repeated sub-sampling validation. The results of statistical processing revealed, that normal distributions can be assumed for all three of frequency, magnitude and initial phase parameters of each measurement. The measured dataset is therefore completely described by a normal distribution with obtained mean vector and covariance matrix. These two variables were then used to generate a statistical model of a large simulated population of walking subjects.

Developed statistical models were employed for harvested power predictions. A linear harvester model with a single degree of freedom was used for the predictions in order to exploit the superposition principle for all modelled frequency components along the working axis.

The predictions evaluate the optimal harvester parameters, namely the working frequency and quality factor combination, which will yield the highest median power output for the whole model population of 10000 samples. It was also investigated, which working axes provide sufficient levels of acceleration. It was found that while directions parallel to normals to sagittal and transverse planes contain acceleration levels suitable for generation of exploitable electrical energy, modelled acceleration frequency spectra along the normal to coronal plane offer only very low levels of harvestable energy and can therefore be neglected in further simulations. It was also found, that the normal to sagittal plane of the human body generally contains two potentially exploitable frequencies.

Complementary cumulative distribution functions were calculated for previously determined advantageous harvester natural frequency and quality factor configurations to find the lowest specific power, reachable by given percentage of the modelled user population. These simulations represent the worst-case scenario, where a linear harvester with given set of parameters would generate at least the indicated specific power per gram of its proof mass weight for given percentage of the population.

Even though the simulations clearly show the high potential of employing a low-frequency device for harvesting the human power, its actual design might suffer from technological and spatial constraints, making the actual usability of very low frequency harvester potentially limited due to e.g. large proof mass displacements, associated with low excitation frequencies.

The kinetic energy harvester for frequencies associated with human behaviour must overcome these challenges either by employing a nonlinear stiffness solution, or by a novel design, where the large displacements are not an issue [V2].

These analyses were published in Mechatronika 2016 international conference proceedings (Annex A3). The second phase analyses are submitted for publication and currently in review process in Smart Materials and Structures journal (Annex A4)

9 KINETIC ENERGY HARVESTER DESIGN, OPTIMIZATION AND FABRICATION

The previous analyses and studies indicated the feasibility of using the electromechanical energy harvesting principle for powering up MEMS electronic wearable or biomedical devices. This chapter deals with development of the kinetic energy harvester, which would be usable for harvesting human power while complying with the size and weight requirements. The target application for the harvester remains the aforementioned cochlear implant, even though the design may be universal enough to be used also for other applications with similar excitation characteristics.

The presented harvester design (Annex A5) is based on so-called Tusi couple, which is a mathematical device proposed in 13th century by a Persian mathematician Nasir al-Din al-Tusi. The basic point of the device lies in exploiting a rolling motion of a circle inside a larger circle. The points on the radius of the smaller circle generally travel along hypocycloidal paths. However, if the ratio of the circles' diameters is 2:1, as in this mechanism, the hypocycloids blend with straight lines denoting the diameter of the larger circle.

This principle is used in the novel inertial energy harvester design, as it allows for advantageous placement of the energy transducer element. Every point of the smaller circle passes through the centre of the large circle twice during one full revolution. Placing magnets along the diameter of the small circle, and a pick-up coil above the centre of the large circle would mean a possibility of a constant engagement of the coil during the small circle movement.

This configuration was exploited in the novel low frequency kinetic energy harvester design with one degree of freedom, which utilizes the unlimited displacement of the proof mass and nonlinear behaviour of the pendulum-type harvester, together with springless design and compact dimensions. Furthermore, due to the nature of the proof mass movement, this design is capable of harvesting vibrations in one working plane, as opposed to conventional designs working with a single vibrations direction. An iterative principle was employed to obtain the final variant of the device, featuring 12 permanent magnets, and two coils fixed to the lids of the harvester (Figure 15).

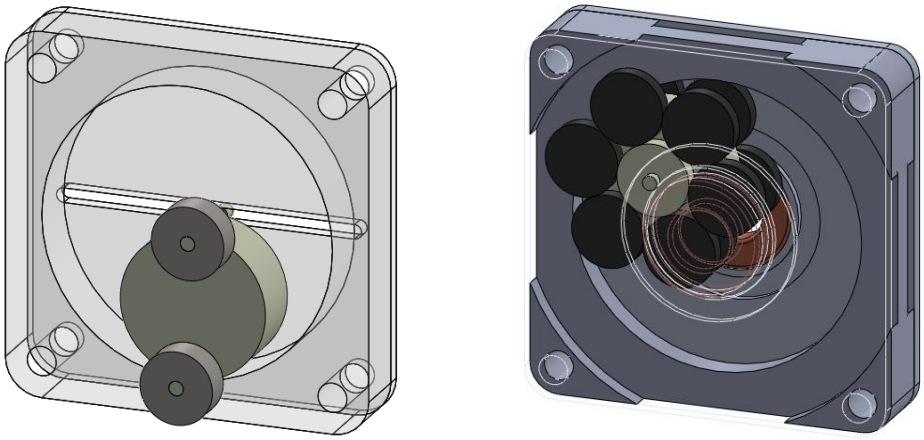

Figure 15 First (left) and final (right) version of the energy harvester design

The equation of motion governing the harvester behaviour is derived as:

$$I_{total}\ddot{q} - 0 + (b_e^* + b_m^*)\dot{q} + mgr \cdot \sin\left(\frac{r}{R-r}q\right) = -mr\left(\ddot{z}_x \cdot cos(\frac{r}{R-r}q) + \ddot{z}_y \cdot sin(\frac{r}{R-r}q)\right) \quad (17)$$

where I_{total} is the total moment of inertia with respect to the instantaneous point of contact of the rolling element and the frame, b_e^* and b_m^* are generalized electrical and mechanical damping, respectively, m is the weight of the proof mass, g is gravity acceleration constant, r and R denote radiuses of the proof mass and the frame cavity, respectively, $\ddot{z}_x$ and $\ddot{z}_y$ are frame acceleration components in the two orthogonal axes in the working plane of the harvester and q is the generalized coordinate.

The properties of the magnetic circuit have direct effect to the energy conversion effectiveness. It was therefore decided to optimize the pick-up coil dimensions of the final design in order to maximize the electromechanical coupling coefficient (Annex A6).

A greedy search algorithm was employed to expand the coil in the direction of the highest increment of magnetic flux change, one turn per iteration. The algorithm stops when the cost function, defined as power on load of a linearized model of the energy harvester, reaches its maximum. The coil configurations were tested for different load resistances to compare the differences the obtained optimal coil configurations. Dimensions (height, inner and outer diameter) of the coil were then implemented into the full simulation model of the harvester.

Simulated performance of the prototype showed promising results (Annex A5), so it was decided to manufacture and test a functional up-scaled prototype of the device. The prototype (Figure 16) was made using conventional manufacturing technology, with manually wound coreless copper coil. Testing of the prototype was performed on a linear drive, using wireless accelerometer to record the excitation waveforms.

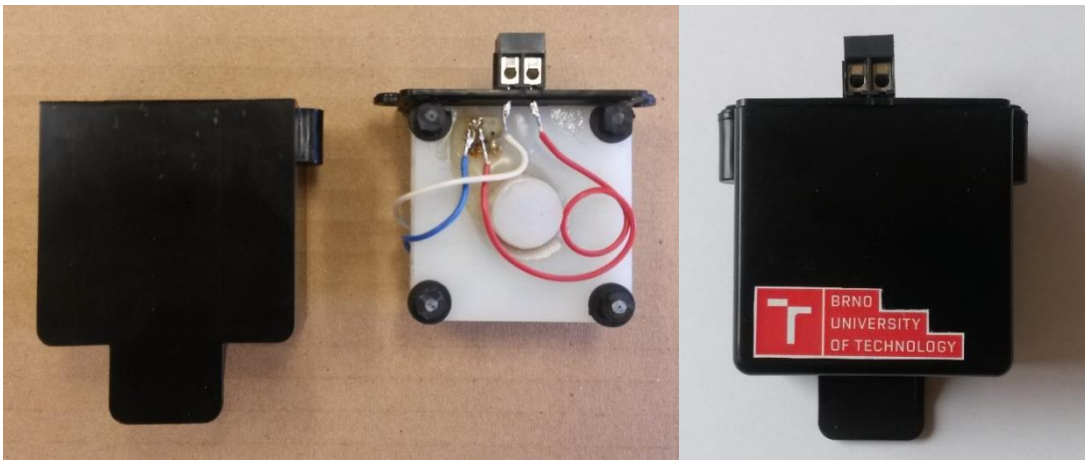

Figure 16 Packaging of the second prototype of the developed harvester

The measurements showed very good agreement with the model (Figure 17) and promising performance in context of evaluating the usability of this harvester for wearable or biomedical applications. Comparison of the performance using normalised power density metric shows, that this design is more than competitive in the field of low-frequency kinetic energy harvesters.

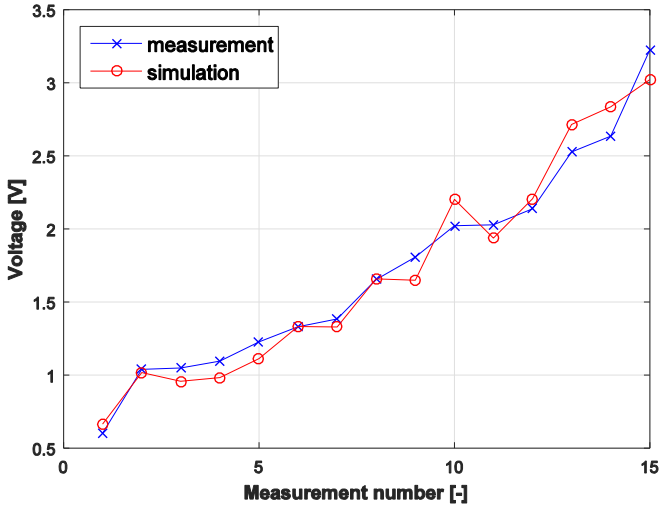

Figure 17 Fit of the simulated data with the experiment

The strengths, drawbacks and possible improvements of the design are outlined in the publication, together with introduction of the possibility of using another energy transduction principle for this design.

However, the laboratory tests are not deemed sufficient to evaluate the harvester performance in real-life conditions. For that reason it was decided to perform an additional series of measurements.

The design, modelling, optimization and testing of the harvester was published in Mechanical Systems and Signal Processing journal (Annex A5), and in Mechatronics 2017 international conference proceedings (Annex A6).

10 ENERGY HARVESTER EXPERIMENTAL EVALUATION

The additional set of measurements was obtained using a single test subject, measuring the power on load, delivered by the harvester prototype placed in one of four different locations on the human body during various defined activities. Head, belt, wrist and ankle were selected as feasible placements of the harvester for testing. Most of the works published by other researches use one or more of these particular fixation points, making this selection convenient for possible direct comparison with other designs.

The activities, recorded by NI-9234 data acquisition card and Slam Stick wireless datalogger (Figure 18), common for all harvester placements included walking at natural speed, running, climbing and descending the stairs, and jumping. Other location specific activities, chosen for high expected generated powers were also tried. These included jumping jacks, violent shaking of head or limbs or different walking patterns.

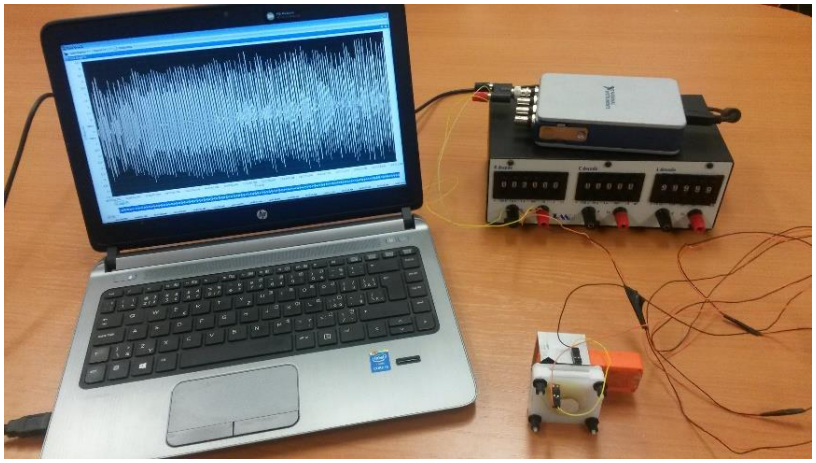

Figure 18 Measurement setup

The recorded measurements confirmed great variance in the output power depending both on the activity performed and on the placement of the harvester. The average power on load varied between 6 μW and 6.5 mW, the lower of which was harvested during nodding with the harvester fixed on the head. The higher value was recorded while the harvester was attached to the ankle of violently shaking leg.

These results indicate two main points. First, the harvester is capable of delivering sufficient power output to directly power up some of the wearable or biomedical applications. Depending on the activity level of the potential harvester user, harvester placement, and application requirements, this device might be able to cover even a daily power consumption of an electronic MEMS device by accumulating the energy harvested during the user active time. Second, the current design will mostly not be able to provide enough energy to power up the originally assumed cochlear implant. The head area of the user is the least feasible location for kinetic energy harvesting purposes, which shows also in the measurement results. However, the overall usability of the device for other wearable and biomedical MEMS applications was confirmed.

The results of these measurements are submitted to Vetomac XIV international conference, with the accepted final version of the paper being currently in press (Annex A7).

11 THESIS CONTRIBUTIONS

11.1 SCIENTIFIC CONTRIBUTION

The research works on the topic of this doctoral thesis and relevant analysis resulted in authoring and co-authoring 17 papers and one book chapter. 7 of these are directly related to the thesis, and the remaining 10 are further advancing the energy harvesting field through spin-off research, exploiting the methodology, analyses or partial results from the main research topic. Out of the 17 papers 5 are published in impacted journals, 1 is currently in the review process in an impacted journal, 10 are published in international conference proceedings and the last one is accepted for publication in proceedings of another international conference.

There are multiple important specific contributions to the field of energy harvesting from low frequency environments: first, the excitation acceleration signal processing method using principal component analysis, which can potentially bring a significant performance improvement of a kinetic energy harvester without changing its design. Second important contribution is the statistical model of acceleration in the area of a human head during walking, which can be further exploited in human power energy harvester design. Statistical approach is still rather uncommon in the energy harvesting field, and the models can provide an invaluable information for future research. Third significant contribution lies in the novel low-frequency kinetic energy harvester design. The presented design preserves some advantages of pendulum-type harvesters, such as unlimited travel path length and springless design, while allowing for more efficient placement of the energy transducer in the device, saving both space, weight and reducing the inner impedance of the harvester.

11.2 EDUCATIONAL CONTRIBUTION

The educational contribution of this doctoral thesis is supported by the two bachelor's thesis topics that were offered for elaboration. Out of the two topics, one was defended successfully in year 2016. One of the student's measurements were used as inputs for analysis found in the publication A3, resulting in the student co-authoring the conference paper. Furthermore, master's level course RAE-"Energy Harvesting" benefitted from the research activities conducted within the scope of this work. Students of this course also contributed to data gathering, used for statistical acceleration data processing in publication [V1].

11.3 ENGINEERING CONTRIBUTION

The engineering contribution of author's research activities related to the doctoral thesis is seen mainly in the valid utility model no.2017-34005 and pending national patent application for the design of the developed energy harvesting power source.

Analyses and device development related to human power harvesting were also conducted during an industrial cooperation with Huawei, where a feasibility of a piezoelectric harvester for enhancing the battery life of smart watches was investigated.

Furthermore, a UK-based firm Passive Eye, Ltd. recently expressed an interest in the device, leading to the agreement on testing the device as a possible power source for their wireless asset monitoring tags. A prototype of the energy harvester is currently undergoing testing in the UK

in the Passive Eye laboratories. The firm has also voiced their interest regarding a further co-operation with Brno University of Technology in case of satisfying harvester performance in given application.

The field relevant knowledge of energy harvesting systems development was further utilized during the work on H2020 Shift2Rail Etalon project, where the author was responsible for the completion of a deliverable focused on trackside energy harvesting systems survey and analyses.

12 CONCLUSIONS

This thesis deals with the feasibility study and the development of an energy harvesting power source for MEMS applications, with the special focus on wearable and biomedical electronic devices. After considering the available energy sources in the ambience of a human body, an electromechanical inertial energy harvester was selected as a potentially feasible solution for the defined problem situation of current unavailability of maintenance-free power source for wearable electronics.

The initial feasibility study was performed utilizing data from a ten months-long single person measurements and from five short-term measurements of different testing subjects. Promising results of the study, indicating that a useful power in the range of tens to hundreds of microwatts can be generated by a potentially implantable kinetic energy harvester model based on electromagnetic induction physical principle, showed the feasibility of the selected approach.

A signal processing method based on the principal component analysis of the excitation acceleration was then introduced. Its use lies either in improving the power output of inertial energy harvesters by alignment of their working axis with a first principal axis of the selected acceleration frequency component, or in a correction (realignment by rotation) of the measurement data to prevent measurement bias caused by misalignment of the sensor on the different measured specimen during the measurements.

Multiple sets of acceleration measurements were obtained and the data was processed to determine the properties of the acceleration obtainable from human activities, such as walking. Statistical models of acceleration in the human head area during walking were then developed in order to predict the limits of inertially excited energy harvester performance, placed in this location. It was observed that the parameters of the acceleration frequency components follow normal distributions, which can be exploited in the modelling and simulations of large harvester user populations. The simulation results further confirmed the usability of inertial energy harvester for ultra-low-power applications in the head area, so a novel concept of one degree of freedom kinetic energy harvester was introduced to exploit the observed acceleration waveforms from two orthogonal directions at the same time.

The development process was conducted with the intention of integrating the harvester as close to the powered up application as possible. Parameters and working directions of the harvester were designed utilizing the knowledge obtained from the statistical analyses and modelling. An original design of the harvester based on Tusi-couple mechanism was presented and its dynamics derived for modelling purposes. Strongly nonlinear softening characteristics of this harvester together with its unlimited circular trajectory are beneficial for applications with very low frequency of excitation acceleration and multidimensional excitation, such as human power harvesting. Comparison of the simulated results of an experimentally verified model with other low frequency harvester designs shows superiority of the novel design with respect both to the power output and to the normalized power density performance metric.

The testing of the prototype on the various locations on human body during different recorded activities showed good potential of the device for powering some of the ultra-low power sensors. The highest average power on load of 6.5 mW was recorded while the harvester was fixed on the ankle of a violently shaking leg. The average power obtained from walking by the harvester fixed on the human head, with the working plane normal to the direction of walking

reached up to 56 μW. Same activity, but harvester placement on the ankle resulted in 1.4 mW of average power on load, harvested through the duration of walking.

Aside for the focus on the human power harvesting, the harvester design attracted considerable attention within the energy harvesting industry, and over the time of writing this thesis one prototype is being evaluated by a UK-based company, which uses energy harvesting devices for powering up the wireless tags for asset monitoring.

This work presents methodology, models and physical product, which can be further developed and improved by good engineering practices. The outputs of this research are deemed to have a significant potential for larger scale utilization in the near future both in wearable and other industrial applications.

REFERENCES

[1] ŽÁK, Jaromír, Zdeněk HADAŠ, Daniel DUŠEK, Jan PEKÁREK, Vojtěch SVATOŠ, Luděk JANÁK and Jan PRÁŠEK. Model-based design of artificial zero power cochlear implant. *Mechatronics* [online]. 2015. ISSN 09574158. Available at: doi:10.1016/j.mechatronics.2015.04.018

[2] WONG, Louis S Y, Shohan HOSSAIN, Andrew TA, Jörgen EDVINSSON, Dominic H. RIVAS and Hans NÄÄS. A very low-power CMOS mixed-signal IC for implantable pacemaker applications. In: *IEEE Journal of Solid-State Circuits* [online]. 2004, p. 2446–2456. ISBN 0-7803-8267-6. Available at: doi:10.1109/JSSC.2004.837027

[3] BIEDERMAN, W., D.J. YEAGER, N. NAREVSKY, A.C. KORALEK, J.M. CARMENA, E. ALON and J.M. RABAEY. A fully-integrated, miniaturized (0.125 mm^2) 10.5 μw wireless neural sensor. *IEEE Journal of Solid-State Circuits* [online]. 2013, **48**(4), 960–970. Available at: doi:10.1109/JSSC.2013.2238994

[4] BUDINGER, Thomas F. Biomonitoring with Wireless Communications. *Annual Review of Biomedical Engineering* [online]. 2003, **5**(1), 383–412. ISSN 1523-9829. Available at: doi:10.1146/annurev.bioeng.5.040202.121653

[5] SARPESHKAR, R., C. SALTHOUSE, J.-J. SIT, M.W. BAKER, S.M. ZHAK, T.K.-T. LU, L. TURICCHIA and S. BALSTER. An ultra-low-power programmable analog bionic ear processor. *IEEE Transactions on Biomedical Engineering* [online]. 2005, **52**(4), 711–727. Available at: doi:10.1109/TBME.2005.844043

[6] M. GRAEFE, T. GOETTSCHE, P. OSYPKA K. TRIEU, H. FASSBENDER, W. MOKWA, U. URBAN, T. SCHMITZ-RODE, T. HILBEL, R. Becker. A Fully Implantable Blood Pressure Sensor for Hypertensive Patients. In: *Proceedings SENSOR 2009, Volume I* [online]. 2009, p. 145–149. Available at: doi:10.5162/sensor09/v1/b1.2

[7] SAATI, Saloomeh, Ronalee LO, Po-Ying LI, Ellis MENG, Rohit VARMA and Mark S. HUMAYUN. Mini Drug Pump for Ophthalmic Use. *Current Eye Research* [online]. 2010, **35**(3), 192–201. ISSN 0271-3683. Available at: doi:10.3109/02713680903521936

[8] BATRA, Ashok K. and Almuatasim ALOMARI. *Power Harvesting via Smart Materials* [online]. B.m.: SPIE PRESS, 2017. ISBN 9781510608498. Available at: doi:10.1117/3.2268643

[9] STANDARD, National. IEEE Standard on Piezoelectricity. *East* [online]. 1988, 74. ISSN 0885-3010. Available at: doi:10.1109/IEEESTD.1988.79638

[10] AMBROSIO, R., A. JIMENEZ, J. MIRELES, M. MORENO, K. MONFIL and H. HEREDIA. Study of Piezoelectric Energy Harvesting System Based on PZT. *Integrated Ferroelectrics* [online]. 2011, **126**(1), 77–86. ISSN 1058-4587. Available at: doi:10.1080/10584587.2011.574989

[11] SAADON, Salem and Othman SIDEK. A review of vibration-based MEMS piezoelectric energy harvesters. *Energy Conversion and Management* [online]. 2011, **52**(1), 500–504. ISSN 01968904. Available at: doi:10.1016/j.enconman.2010.07.024

[12] STEWART, Mark, Paul M. WEAVER and Markys CAIN. Charge redistribution in piezoelectric energy harvesters. *Applied Physics Letters* [online]. 2012, **100**(7), 73901. ISSN 00036951. Available at: doi:10.1063/1.3685701

[13] PARK, J. C., D. H. LEE, Jae Yeong PARK, Y. S. CHANG and Y. P. LEE. High performance piezoelectric MEMS energy harvester based on D33 mode of PZT thin film on buffer-layer with PbTiO3 inter-layer. In: *TRANSDUCERS 2009 - 15th International Conference on Solid-State Sensors, Actuators and Microsystems* [online]. 2009, p. 517–520. ISBN 9781424441938. Available at: doi:10.1109/SENSOR.2009.5285375

[14] WANG, Jianjun, Zhifei SHI, Hongjun XIANG and Gangbing SONG. Modeling on energy harvesting from a railway system using piezoelectric transducers. *Smart Materials and Structures* [online]. 2015, **24**(10), 105017. ISSN 1361665X. Available at: doi:10.1088/0964-1726/24/10/105017

[15] PILLATSCH, Pit, Eric M. YEATMAN and Andrew S. HOLMES. A piezoelectric frequency up-converting energy harvester with rotating proof mass for human body applications. *Sensors and Actuators, A: Physical* [online]. 2014. ISSN 09244247. Available at: doi:10.1016/j.sna.2013.10.003

[16] SPREEMANN, D, Y MANOLI, B FOLKMER and D MINTENBECK. Non-resonant vibration conversion. *Journal of Micromechanics and Microengineering* [online]. 2006, **16**(9), S169–S173. ISSN 0960-1317. Available at: doi:10.1088/0960-1317/16/9/S01

[17] RASOULI, Mahdi and Louis Soo Jay PHEE. Energy sources and their development for application in medical devices. *Expert review of medical devices* [online]. 2010, **7**(5), 693–709. ISSN 1745-2422. Available at: doi:10.1586/erd.10.20

[18] BOISSEAU, S, G DESPESSE and B Ahmed SEDDIK. *Small-Scale Energy Harvesting* [online]. B.m.: InTech, 2012. ISBN 978-953-51-0826-9. Available at: doi:10.5772/3078

[19] BEEBY, S P, M J TUDOR and N M WHITE. Energy harvesting vibration sources for microsystems applications. *Measurement Science and Technology* [online]. 2006, **17**(12), R175–R195. ISSN 0957-0233. Available at: doi:10.1088/0957-0233/17/12/R01

[20] BERBYUK, Viktor and Jayesh SODHANI. Towards modelling and design of magnetostrictive electric generators. *Computers & Structures* [online]. 2008, **86**(3–5), 307–313. ISSN 00457949. Available at: doi:10.1016/j.compstruc.2007.01.030

[21] FAN, Tianyu and Yoshio YAMAMOTO. Vibration-induced energy harvesting system using Terfenol-D. In: *2015 IEEE International Conference on Mechatronics and Automation (ICMA)* [online]. B.m.: IEEE, 2015, p. 2319–2324. ISBN 978-1-4799-7097-1. Available at: doi:10.1109/ICMA.2015.7237848

[22] MOHAMMADI, Saber and Aboozar ESFANDIARI. Magnetostrictive vibration energy harvesting using strain energy method. *Energy* [online]. 2015, **81**, 519–525. ISSN 03605442. Available at: doi:10.1016/j.energy.2014.12.065

[23] DIAZ, A. F. and R. M. FELIX-NAVARRO. A semi-quantitative tribo-electric series for polymeric materials: The influence of chemical structure and properties. *Journal of Electrostatics* [online]. 2004, **62**(4), 277–290. ISSN 03043886. Available at: doi:10.1016/j.elstat.2004.05.005

[24] MATSUSAKA, S., H. MARUYAMA, T. MATSUYAMA and M. GHADIRI. Triboelectric charging of powders: A review. *Chemical Engineering Science* [online]. 2010, **65**(22), 5781–5807. ISSN 00092509. Available at: doi:10.1016/j.ces.2010.07.005

[25] WANG, Zhong Lin, Long LIN, Jun CHEN, Simiao NIU and Yunlong ZI. *Triboelectric Nanogenerators* [online]. 2016. ISBN 978-3-319-40038-9. Available

at: doi:10.1007/978-3-319-40039-6

[26] ZI, Yunlong, Simiao NIU, Jie WANG, Zhen WEN, Wei TANG and Zhong Lin WANG. Standards and figure-of-merits for quantifying the performance of triboelectric nanogenerators. *Nature Communications* [online]. 2015, **6**(September), 1–8. ISSN 20411723. Available at: doi:10.1038/ncomms9376

[27] FAN, Feng-Ru, Zhong-Qun TIAN and Zhong LIN WANG. Flexible triboelectric generator. *Nano Energy* [online]. 2012, **1**(2), 328–334. ISSN 22112855. Available at: doi:10.1016/j.nanoen.2012.01.004

[28] ZHU, Guang, Caofeng PAN, Wenxi GUO, Chih Yen CHEN, Yusheng ZHOU, Ruomeng YU and Zhong Lin WANG. Triboelectric-generator-driven pulse electrodeposition for micropatterning. *Nano Letters* [online]. 2012, **12**(9), 4960–4965. ISSN 15306984. Available at: doi:10.1021/nl302560k

[29] ZHU, Guang, Jun CHEN, Ying LIU, Peng BAI, Yu Sheng ZHOU, Qingshen JING, Caofeng PAN and Zhong Lin WANG. Linear-grating triboelectric generator based on sliding electrification. *Nano Letters* [online]. 2013, **13**(5), 2282–2289. ISSN 15306984. Available at: doi:10.1021/nl4008985

[30] WANG, Sihong, Long LIN, Yannan XIE, Qingshen JING, Simiao NIU and Zhong Lin WANG. Sliding-triboelectric nanogenerators based on in-plane charge-separation mechanism. *Nano Letters* [online]. 2013, **13**(5), 2226–2233. ISSN 15306984. Available at: doi:10.1021/nl400738p

[31] WANG, Sihong, Yannan XIE, Simiao NIU, Long LIN and Zhong Lin WANG. Freestanding triboelectric-layer-based nanogenerators for harvesting energy from a moving object or human motion in contact and non-contact modes. *Advanced Materials* [online]. 2014, **26**(18), 2818–2824. ISSN 15214095. Available at: doi:10.1002/adma.201305303

[32] WANG, Sihong, Simiao NIU, Jin YANG, Long LIN and Zhong Lin WANG. Quantitative measurements of vibration amplitude using a contact-mode freestanding triboelectric nanogenerator. *ACS Nano* [online]. 2014, **8**(12), 12004–12013. ISSN 1936086X. Available at: doi:10.1021/nn5054365

[33] YANG, Ya, Hulin ZHANG, Jun CHEN, Qingshen JING, Yu Sheng ZHOU, Xiaonan WEN and Zhong Lin WANG. Single-electrode-based sliding triboelectric nanogenerator for self-powered displacement vector sensor system. *ACS Nano* [online]. 2013, **7**(8), 7342–7351. ISSN 19360851. Available at: doi:10.1021/nn403021m

[34] NIU, Simiao, Ying LIU, Sihong WANG, Long LIN, Yu Sheng ZHOU, Youfan HU and Zhong Lin WANG. Theoretical investigation and structural optimization of single-electrode triboelectric nanogenerators. *Advanced Functional Materials* [online]. 2014, **24**(22), 3332–3340. ISSN 16163028. Available at: doi:10.1002/adfm.201303799

[35] XIE, Longhan and Mingjing CAI. Increased piezoelectric energy harvesting from human footstep motion by using an amplification mechanism. *Applied Physics Letters* [online]. 2014, **105**(14), 143901. ISSN 0003-6951. Available at: doi:10.1063/1.4897624

[36] EDMISON, J., M. JONES, Z. NAKAD and T. MARTIN. Using piezoelectric materials for wearable electronic textiles. In: *Proceedings - International Symposium on Wearable Computers, ISWC* [online]. 2002, p. 41–48. ISBN 0769518168. Available at: doi:10.1109/ISWC.2002.1167217

[37] DELNAVAZ, Aidin and Jeremie VOIX. Energy Harvesting for In-Ear Devices Using Ear Canal Dynamic Motion. *IEEE Transactions on Industrial Electronics* [online]. 2014, **61**(1), 583–590. ISSN 0278-0046. Available at: doi:10.1109/TIE.2013.2242656

[38] PFENNIGER, Alois, Lalith N WICKRAMARATHNA, Rolf VOGEL and Volker M KOCH. Design and realization of an energy harvester using pulsating arterial pressure. *Medical engineering & physics* [online]. 2013, **35**(9), 1256–65. ISSN 1873-4030. Available at: doi:10.1016/j.medengphy.2013.01.001

[39] FAN, Kangqi, Jianwei CHANG, Fengbo CHAO and Witold PEDRYCZ. Design and development of a multipurpose piezoelectric energy harvester. *Energy Conversion and Management* [online]. 2015, **96**, 430–439. ISSN 01968904. Available at: doi:10.1016/j.enconman.2015.03.014

[40] ABDELKEFI, A, A H NAYFEH and M R HAJJ. Enhancement of power harvesting from piezoaeroelastic systems. *Nonlinear Dynamics* [online]. 2012, **68**(4), 531–541. ISSN 0924-090X. Available at: doi:10.1007/s11071-011-0234-9

[41] MICHELIN, Sébastien and Olivier DOARÉ. Energy harvesting efficiency of piezoelectric flags in axial flows. *Journal of Fluid Mechanics* [online]. 2013, **714**, 489–504. ISSN 00221120. Available at: doi:http://dx.doi.org/10.1017/jfm.2012.494

[42] YUN, Jaeseok, Shwetak N. PATEL, Matthew S. REYNOLDS and Gregory D. ABOWD. Design and Performance of an Optimal Inertial Power Harvester for Human-Powered Devices. *IEEE Transactions on Mobile Computing* [online]. 2011, **10**(5), 669–683. ISSN 1536-1233. Available at: doi:10.1109/TMC.2010.202

[43] TANG, Xiudong and Lei ZUO. Enhanced vibration energy harvesting using dual-mass systems. *Journal of Sound and Vibration* [online]. 2011, **330**(21), 5199–5209. ISSN 0022460X. Available at: doi:10.1016/j.jsv.2011.05.019

[44] KHAN, Farid, Farrokh SASSANI and Boris STOEBER. Nonlinear behaviour of membrane type electromagnetic energy harvester under harmonic and random vibrations. *Microsystem Technologies* [online]. 2014, **20**(7), 1323–1335. ISSN 0946-7076. Available at: doi:10.1007/s00542-013-1938-1

[45] CARMAN, S Moss and A Barry and I Powlesland and S Galea and G P. A broadband vibro-impacting power harvester with symmetrical piezoelectric bimorph-stops. *Smart Materials and Structures*. 2011, **20**(4), 45013. ISSN 0964-1726.

[46] ONG, Z.-Z., V.-K. WONG and J.-H. HO. Performance enhancement of a piezoelectric rain energy harvester. *Sensors and Actuators, A: Physical* [online]. 2016, **252**, 154–164. Available at: doi:10.1016/j.sna.2016.10.035

[47] CEPNIK, Clemens, Roland LAUSECKER and Ulrike WALLRABE. Review on Electrodynamic Energy Harvesters—A Classification Approach. *Micromachines* [online]. 2013, **4**(2), 168–196. ISSN 2072-666X. Available at: doi:10.3390/mi4020168

[48] HEIDRICH, Nicola, Fabian KNÖBBER, Vladimir POLYAKOV, Volker CIMALLA, Wilfried PLETSCHEN, Ram Ekwal SAH, Lutz KIRSTE, Steffen LEOPOLD, Stefan HAMPL, Oliver AMBACHER and Vadim LEBEDEV. Corrugated piezoelectric membranes for energy harvesting from aperiodic vibrations. *Sensors and Actuators A: Physical* [online]. 2013, **195**, 32–37. ISSN 09244247. Available at: doi:10.1016/j.sna.2013.02.001

[49] NGUYEN, Son D. and Einar HALVORSEN. Nonlinear Springs for Bandwidth-Tolerant Vibration Energy Harvesting. *Journal of Microelectromechanical Systems* [online]. 2011, **20**(6), 1225–1227. ISSN 1057-7157. Available at: doi:10.1109/JMEMS.2011.2170824

[50] SCAPOLAN, Matteo, Maryam Ghandchi TEHRANI and Elvio BONISOLI. Energy harvesting using parametric resonant system due to time-varying damping. *Mechanical Systems and Signal Processing* [online]. 2016. ISSN 10961216. Available at: doi:10.1016/j.ymssp.2016.02.037

[51] SESHIA, Yu Jia and Jize Yan and Kenichi Soga and Ashwin A. Parametric resonance for vibration energy harvesting with design techniques to passively reduce the initiation threshold amplitude. *Smart Materials and Structures*. 2014, **23**(6), 65011. ISSN 0964-1726.

[52] JIA, Yu and Ashwin A. SESHIA. An auto-parametrically excited vibration energy harvester. *Sensors and Actuators A: Physical* [online]. 2014, **220**, 69–75. ISSN 09244247. Available at: doi:10.1016/j.sna.2014.09.012

[53] GATTI, G., M. J. BRENNAN, M. G. TEHRANI and D. J. THOMPSON. Harvesting energy from the vibration of a passing train using a single-degree-of-freedom oscillator. *Mechanical Systems and Signal Processing* [online]. 2016, **66**–**67**, 785–792. ISSN 10961216. Available at: doi:10.1016/j.ymssp.2015.06.026

[54] STANTON, Samuel C., Clark C. MCGEHEE and Brian P. MANN. Nonlinear dynamics for broadband energy harvesting: Investigation of a bistable piezoelectric inertial generator. *Physica D: Nonlinear Phenomena* [online]. 2010, **239**(10), 640–653. ISSN 01672789. Available at: doi:10.1016/j.physd.2010.01.019

[55] YUEN, Steve C L, Johnny M H LEE, Wen J. LI and Philip H W LEONG. An AA-sized vibration-based microgenerator for wireless sensors. *IEEE Pervasive Computing* [online]. 2007, **6**(1), 64–72. ISSN 15361268. Available at: doi:10.1109/MPRV.2007.4

[56] MANN, B. P. and B. A. OWENS. Investigations of a nonlinear energy harvester with a bistable potential well. *Journal of Sound and Vibration* [online]. 2010, **329**(9), 1215–1226. ISSN 0022460X. Available at: doi:10.1016/j.jsv.2009.11.034

[57] SASAKI, Ken, Yuji OSAKI, Jun OKAZAKI, Hiroshi HOSAKA and Kiyoshi ITAO. Vibration-based automatic power-generation system. *Microsystem Technologies* [online]. 2005, **11**(8), 965–969. ISSN 1432-1858. Available at: doi:10.1007/s00542-005-0506-8

[58] BOWERS, Benjamin J and David P ARNOLD. Spherical, rolling magnet generators for passive energy harvesting from human motion. *Journal of Micromechanics and Microengineering* [online]. 2009, **19**(9), 94008. ISSN 0960-1317. Available at: doi:10.1088/0960-1317/19/9/094008

[59] BEEBY, S.P., R.N. TORAH, M.J. TUDOR, P. GLYNNE-JONES, T. O'DONNELL, C.R. SAHA and S. ROY. A micro electromagnetic generator for vibration energy harvesting. *Journal of Micromechanics and Microengineering* [online]. 2007, **17**(7). Available at: doi:10.1088/0960-1317/17/7/007

[60] WANG, Wei, Rong Jin HUANG, Chuan Jun HUANG and Lai Feng LI. Energy harvester array using piezoelectric circular diaphragm for rail vibration. *Acta Mechanica Sinica/Lixue Xuebao* [online]. 2014, **30**(6), 884–888. ISSN 05677718. Available

at: doi:10.1007/s10409-014-0115-9

[61] CHING, N.N.H., H.Y. WONG, W.J. LI, P.H.W. LEONG and Z. WEN. A laser-micromachined multi-modal resonating power transducer for wireless sensing systems. *Sensors and Actuators, A: Physical* [online]. 2002, **97**–**98**, 685–690. Available at: doi:10.1016/S0924-4247(02)00033-X

[62] GUAN, Mingjie and Wei-Hsin LIAO. Design and analysis of a piezoelectric energy harvester for rotational motion system. *Energy Conversion and Management* [online]. 2016, **111**, 239–244. ISSN 01968904. Available at: doi:10.1016/j.enconman.2015.12.061

[63] COTTONE, F, L GAMMAITONI, H VOCCA, M FERRARI and V FERRARI. Piezoelectric buckled beams for random vibration energy harvesting. *Smart Materials and Structures* [online]. 2012, **21**(3), 35021. ISSN 0964-1726. Available at: doi:10.1088/0964-1726/21/3/035021

[64] AHMAD, Mahmoud Al, Amro M ELSHURAFA, Khaled N SALAMA and H N ALSHAREEF. Modeling of MEMS piezoelectric energy harvesters using electromagnetic and power system theories. *Smart Materials and Structures* [online]. 2011, **20**(8), 85001. ISSN 0964-1726. Available at: doi:10.1088/0964-1726/20/8/085001

[65] HADAS, Zdenek, Vojtech VETISKA, Jan VETISKA and Jiri KREJSA. Analysis and efficiency measurement of electromagnetic vibration energy harvesting system. *Microsystem Technologies* [online]. 2016, **22**(7), 1767–1779. ISSN 0946-7076. Available at: doi:10.1007/s00542-016-2832-4

[66] LIANG, Junrui and Wei-Hsin LIAO. Impedance Modeling and Analysis for Piezoelectric Energy Harvesting Systems. *IEEE/ASME Transactions on Mechatronics* [online]. 2012, **17**(6), 1145–1157. ISSN 1083-4435. Available at: doi:10.1109/TMECH.2011.2160275

[67] CAMMARANO, A, S A NEILD, S G BURROW, D J WAGG and D J INMAN. Optimum resistive loads for vibration-based electromagnetic energy harvesters with a stiffening nonlinearity. *Journal of Intelligent Material Systems and Structures* [online]. 2014. ISSN 1045-389X. Available at: doi:10.1177/1045389X14523854

[68] ROUNDY, S. On the Effectiveness of Vibration-based Energy Harvesting. *Journal of Intelligent Material Systems and Structures* [online]. 2005, **16**(10), 809–823. ISSN 1045-389X. Available at: doi:10.1177/1045389X05054042

[69] MITCHESON, P.D., E.M. YEATMAN, G.K. RAO, A.S. HOLMES and T.C. GREEN. Energy Harvesting From Human and Machine Motion for Wireless Electronic Devices. *Proceedings of the IEEE* [online]. 2008, **96**(9), 1457–1486. ISSN 0018-9219. Available at: doi:10.1109/JPROC.2008.927494

[70] SEBALD, Gael, Hiroki KUWANO, Daniel GUYOMAR and Benjamin DUCHARNE. Experimental Duffing oscillator for broadband piezoelectric energy harvesting. *Smart Materials and Structures* [online]. 2011, **20**(10), 102001. ISSN 0964-1726. Available at: doi:10.1088/0964-1726/20/10/102001

[71] NAJAFI, K., T. GALCHEV, E. E. AKTAKKA, R. L. PETERSON and J. MCCULLAGH. Microsystems for energy harvesting. In: *2011 16th International Solid-State Sensors, Actuators and Microsystems Conference, TRANSDUCERS'11* [online]. 2011, p. 1845–1850. ISBN 9781457701573. Available

at: doi:10.1109/TRANSDUCERS.2011.5969888

[72] RUAN, J.J., R.A. LOCKHART, P. JANPHUANG, A.V. QUINTERO, D. BRIAND and N. DE ROOIJ. An automatic test bench for complete characterization of vibration-energy harvesters. *IEEE Transactions on Instrumentation and Measurement* [online]. 2013, **62**(11). Available at: doi:10.1109/TIM.2013.2265452

[73] MALLICK, Dhiman, Andreas AMANN and Saibal ROY. Interplay between electrical and mechanical domains in a high performance nonlinear energy harvester. *Smart Materials and Structures*. 2015, **24**(12), 122001.

[74] ARROYO, E., A. BADEL, F. FORMOSA, Y. WU and J. QIU. Comparison of electromagnetic and piezoelectric vibration energy harvesters: Model and experiments. *Sensors and Actuators A: Physical* [online]. 2012, **183**, 148–156. ISSN 09244247. Available at: doi:10.1016/j.sna.2012.04.033

[75] BALATO, M., L. COSTANZO and M. VITELLI. Resonant electromagnetic vibration energy harvesters: The harvester ideal utilization factor. In: *Proceedings - 2016 IEEE International Power Electronics and Motion Control Conference, PEMC 2016* [online]. 2016. ISBN 9781509017980. Available at: doi:10.1109/EPEPEMC.2016.7752090

[76] AMIRTHARAJAH, R. and A.P. CHANDRAKASAN. Self-powered signal processing using vibration-based power generation. *IEEE Journal of Solid-State Circuits* [online]. 1998, **33**(5). Available at: doi:10.1109/4.668982

[77] SAHA, C. R., T. O&APOS;DONNELL, N. WANG and P. MCCLOSKEY. Electromagnetic generator for harvesting energy from human motion. *Sensors and Actuators, A: Physical* [online]. 2008, **147**(1), 248–253. ISSN 09244247. Available at: doi:10.1016/j.sna.2008.03.008

[78] NARUSE, Y, N MATSUBARA, K MABUCHI, M IZUMI and S SUZUKI. Electrostatic micro power generation from low-frequency vibration such as human motion. *Journal of Micromechanics and Microengineering* [online]. 2009, **19**(9), 94002. ISSN 0960-1317. Available at: doi:10.1088/0960-1317/19/9/094002

[79] RENAUD, Michael, Paolo FIORINI, Rob VAN SCHAIJK and Chris VAN HOOF. Harvesting energy from the motion of human limbs: the design and analysis of an impact-based piezoelectric generator. *Smart Materials and Structures* [online]. 2009, **18**(3), 35001. ISSN 0964-1726. Available at: doi:10.1088/0964-1726/18/3/035001

[80] ARNOLD, Shuo Cheng and David P. A study of a multi-pole magnetic generator for low-frequency vibrational energy harvesting. *Journal of Micromechanics and Microengineering*. 2010, **20**(2), 25015. ISSN 0960-1317.

[81] PILLATSCH, P, E M YEATMAN and A S HOLMES. A scalable piezoelectric impulse-excited energy harvester for human body excitation. *Smart Materials and Structures* [online]. 2012, **21**(11), 115018. ISSN 0964-1726. Available at: doi:10.1088/0964-1726/21/11/115018

[82] JO, S.E., M.S. KIM and Y.J. KIM. Electromagnetic human vibration energy harvester comprising planar coils. *Electronics Letters* [online]. 2012, **48**(14), 874. ISSN 00135194. Available at: doi:10.1049/el.2012.0969

[83] WEI, Sheng, Hong HU and Siyuan HE. Modeling and experimental investigation of an impact-driven piezoelectric energy harvester from human motion. *Smart Materials and*

Structures [online]. 2013, **22**(10), 105020. ISSN 0964-1726. Available at: doi:10.1088/0964-1726/22/10/105020

[84] MUNAZ, Ahmed, Byung-Chul LEE and Gwiy-Sang CHUNG. A study of an electromagnetic energy harvester using multi-pole magnet. *Sensors and Actuators A: Physical* [online]. 2013, **201**, 134–140. ISSN 09244247. Available at: doi:10.1016/j.sna.2013.07.003

[85] BERDY, D.F., D.J. VALENTINO and D. PEROULIS. Kinetic energy harvesting from human walking and running using a magnetic levitation energy harvester. *Sensors and Actuators A: Physical* [online]. 2015, **222**, 262–271. ISSN 09244247. Available at: doi:10.1016/j.sna.2014.12.006

LIST OF AUTHORED PUBLICATIONS

IMPACTED JOURNALS

[V1] **SMILEK, Jan**, Tomas GRISA and Zdenek HADAS. Statistical modelling of acceleration in the human head area for energy harvester performance prediction. *Smart Materials and Structures* [in review]

[V2] **SMILEK, Jan**, Zdenek HADAS, Jan VETISKA and Steve BEEBY. Rolling mass energy harvester for very low frequency of input vibrations. *Mechanical Systems and Signal Processing* [online]. 2018. ISSN 08883270. Available at: doi:10.1016/j.ymssp.2018.05.062

[V3] HADAS, Zdenek, Ludek JANAK and **Jan SMILEK**. Virtual prototypes of energy harvesting systems for industrial applications. *Mechanical Systems and Signal Processing* [online]. 2018, **110**, 152–164. ISSN 08883270. Available at: doi:10.1016/j.ymssp.2018.03.036

[V4] BAI, Yang, Pavel TOFEL, Zdenek HADAS, **Jan SMILEK**, Petr LOSAK, Pavel SKARVADA and Robert MACKU. Investigation of a cantilever structured piezoelectric energy harvester used for wearable devices with random vibration input. *Mechanical Systems and Signal Processing* [online]. 2018, **106**, 303–318. ISSN 08883270. Available at: doi:10.1016/j.ymssp.2018.01.006

[V5] **SMILEK, Jan** and Zdenek HADAS. Improving power output of inertial energy harvesters by employing principal component analysis of input acceleration. *Mechanical Systems and Signal Processing* [online]. 2017, **85**, 801–808. ISSN 08883270. Available at: doi:10.1016/j.ymssp.2016.09.020

[V6] **SMILEK, Jan** and Zdenek HADAS. A study of kinetic energy harvesting for biomedical application in the head area. *Microsystem Technologies* [online]. 2016, **22**(7), 1535–1547. ISSN 0946-7076. Available at: doi:10.1007/s00542-015-2766-2

PROCEEDINGS OF INTERNATIONAL CONFERENCES

[V7] **SMILEK, Jan** and Zdenek HADAS. Experimental evaluation of Tusi couple based energy harvester for scavenging power from human motion. In*: Proceedings of VETOMAC 14th international conference on vibration Engineering and Technology of Machinery*. [in press]

[V8] **SMILEK, Jan** and Zdenek HADAS. Coil Optimization for Linear Electromagnetic Energy Harvesters with Non-uniform Magnetic Field. In: Tomáš BŘEZINA a Ryszard JABŁOŃSKI, ed. *Mechatronics 2017. Advances in Intelligent Systems and Computing* [online]. Cham: Springer International Publishing, 2018, s. 735–742. ISBN 978-3-319-65960-2. Available at: doi:10.1007/978-3-319-65960-2_90

[V9] **SMILEK, Jan**, JANAK Luděk, RUBES, Ondřej, HADAS, Zdenek. Smart Skins for Structural Health Monitoring in Aerospace Applications. In *Proceedings of the EASN*

Association Conference - 7th EASN International Conference. 7th EASN International Conference Proceedings. European Aeronautics Science Network, 2017. s. 59-65. ISSN: 2523-5052.

[V10] HADAS, Zdenek, **Jan SMILEK** and Ondrej RUBES. Analyses of electromagnetic and piezoelectric systems for efficient vibration energy harvesting. In: Luis FONSECA, Mika PRUNNILA a Erwin PEINER, ed. *Proceedings of SPIE - The International Society for Optical Engineering* [online]. 2017, s. 1024619. ISBN 9781510609938. Available at: doi:10.1117/12.2265206

[V11] **SMILEK, Jan**, Ludek JANAK and Zdenek HADAS. Modular Multidisciplinary Models for Prototyping Energy Harvesting Products. In: *15th International Conference on Global Research and Education, INTER-ACADEMIA 2016* [online]. 2017, s. 395–401. ISBN 9783319464893. Available at: doi:10.1007/978-3-319-46490-9_53

[V12] **SMILEK, Jan**, Filip CIESLAR and Zdenek HADAS. Measuring acceleration in the area of human head for energy harvesting purposes. In: *Proceedings of the 2016 17th International Conference on Mechatronics - Mechatronika, ME 2016*. 2017. ISBN 9788001058831.

[V13] JANAK, Ludek, Zdenek HADAS and **Jan SMILEK**. Reliability assessment of electromechanical energy harvesting systems establishment of devices' key characteristics for application in safety-critical systems. In: *Proceedings of the 2016 17th International Conference on Mechatronics - Mechatronika, ME 2016*. 2017. ISBN 9788001058831.

[V14] RUBES, Ondrej, **Jan SMILEK**, Martin BRABLC and Zdenek HADAS. Nonlinear redesign of vibration energy harvester: Linear operation test and nonlinear simulation of extended bandwidth. In: *2016 IEEE International Power Electronics and Motion Control Conference (PEMC)* [online]. B.m.: IEEE, 2016, s. 737–742. ISBN 978-1-5090-1798-0. Available at: doi:10.1109/EPEPEMC.2016.7752086

[V15] **SMILEK, Jan** and Zdenek HADAS. Assessment of MEMS energy harvester for medical applications. In: José Luis SÁNCHEZ-ROJAS a Riccardo BRAMA, ed. *Proceedings of SPIE - The International Society for Optical Engineering* [online]. 2015, s. 95170N. Available at: doi:10.1117/12.2178473

[V16] HADAS, Zdenek, Vojtech VETISKA, **Jan SMILEK**, Ondrej ANDRS and Vladislav SINGULE. Efficiency of electromagnetic vibration energy harvesting system. In: José Luis SÁNCHEZ-ROJAS a Riccardo BRAMA, ed. *Proceedings of SPIE - The International Society for Optical Engineering* [online]. 2015, s. 95171H. ISBN 9781628416398. Available at: doi:10.1117/12.2178448

[V17] RUBES, Ondrej, **Jan SMILEK** and Zdenek HADAS. Development of vibration energy harvester fabricated by rapid prototyping technology. In: *Proceedings of the 16th International Conference on Mechatronics - Mechatronika 2014* [online]. B.m.: IEEE, 2014, s. 178–182. ISBN 978-80-214-4816-2. Available at: doi:10.1109/MECHATRONIKA.2014.7018255

[V18] HADAS, Zdenek and **Jan SMILEK**. Efficiency of vibration energy harvesting systems. In: KANOUN, Olga, ed. *Energy Harvesting for Wireless Sensor Networks, Technology, Components and System Design* [in press]. Berlin, Boston: De Gruyter Oldenbourg, 2019. ISBN 978-3-11-044368-4. Available at: https://www.degruyter.com/view/product/462297

LIST OF ABBREVIATIONS

DOF	Degrees of freedom
EH	Energy harvester
FOM	Figure of merit
FoM_{BW}	Bandwidth figure of merit
FoM_{V}	Volumetric figure of merit
HIUF	Harvester ideal utilization factor
MEMS	Microelectromechanical system
NPD	Normalized power density
NPID	Normalized power integral density
TENG	Triboelectric nanogenerator

LIST OF FIGURES

LIST OF TABLES

LIST OF ANNEXES

ANNEX A1

SMILEK, Jan and Zdenek HADAS.

A study of kinetic energy harvesting for biomedical application in the head area.

Microsystem Technologies [online]. 2016, **22**(7), 1535–1547. ISSN 0946-7076. Available at: doi:10.1007/s00542-015-2766-2

Impact factor: 1.195

Microsyst Technol (2016) 22:1535–1547
DOI 10.1007/s00542-015-2766-2

TECHNICAL PAPER

A study of kinetic energy harvesting for biomedical application in the head area

Jan Smilek[1] · **Zdenek Hadas**[1]

Received: 5 August 2015 / Accepted: 10 December 2015 / Published online: 30 December 2015

Abstract This paper is focused on determining a suitability of using a kinetic energy harvester placed in the area of the human head for supplying power to a new generation of cochlear implants. Placement-dependant volumetric and mass constraints of the harvester are discussed, and the requirements for its power output are set based on the power demands on the state-of-the-art cochlear implants. Measured acceleration data for different activities are presented together with a statistics of a random user behaviour during the course of 10 months. Nonlinear simulation model based on CAD geometry and FEM analyses is developed and its parameters are optimized using the sensitivity analysis in order to generate the maximum power. Real life acceleration data are then employed to feed the input of the simulation model of energy harvester to predict the obtainable power output. The feasibility of employing the energy harvesting to power the selected biomedical application is discussed based on simulation results.

1 Introduction

The basic idea of energy harvesting is based on converting some type of available energy from the ambience of the harvester into usable electric energy. For at least 20 years energy harvesting has been investigated as a possible source of power for wireless applications (Starner 1996), that would be for one reason or another difficult to connect to the power grid. These include wireless sensor nodes in industrial structural or health monitoring systems (Aktakka and Najafi 2014), aerospace (Hadas et al. 2014) or transportation (Yoon et al. 2013). Other applications include wearable electronics and gadgets (Dai and Liu 2012) and also biomedical sensors and actuators (Chen et al. 2010). Available power is a crucial limiting factor for independent devices, and most of the mentioned applications rely on the battery as a primary source of power. Energy harvesting, if implemented, serves as a secondary power source meant to extend the service life until the next battery replacement or recharge. With the ongoing miniaturization of the electronic devices, their increasing power efficiency and decreasing power consumption however, the energy harvesters could serve as the primary power source for some ultra-low power applications.

The progress of electronic devices miniaturization has also allowed a significant increase in the utilization of advanced electronic medical devices for monitoring and assisting in treatment of various physiological conditions. These devices, be it pacemakers, drug pumps, cochlear implants, or other sensors, are currently limited by the unavailability of an independent and battery-less power source, that would ensure their reliable function. The issue of satisfying the power demands of biomedical applications by energy harvesting from human body was addressed in multiple papers over time, e.g. (Romero et al. 2010; Rasouli and Phee 2010; Sudano et al. 2011; Yun et al. 2011; Cadei et al. 2014), providing an observable trend of decreasing power demands of the new devices (Table 1).

Energy harvesting represents a promising opportunity for a development of an autonomous power source to supply the new generation of low-power biomedical devices. Human body stores vast amounts of energy, needed for its function. For more than a decade there have been reported

✉ Jan Smilek
smilek@fme.vutbr.cz

[1] Faculty of Mechanical Engineering, Brno University of Technology, Technicka 2896/2, 616 69 Brno, Czech Republic

Table 1 Evolution of the biomedical applications power consumption (Rasouli and Phee 2010; Cadei et al. 2014)

Device	Power consumption (2010)	Power consumption (2014) (μW)
Cochlear implant	200 μW	145
Neurostimulator	1–100 mW	50
Pacemaker	<100 μW	8

attempts to scavenge and exploit human power in order to power up various applications.

Aside for energy harvesters utilizing a thermal gradient between human body and ambient environment (Lay-Ekuakille et al. 2009; Leonov et al. 2011; Kim et al. 2014), most of the reported devices exploit mechanical energy. Mechanical energy can be scavenged either directly from the movements of the heart, lungs and diaphragm (Dagdeviren et al. 2014), from the deformation of the arteries (Pfenniger et al. 2013), from the impacts during walking (Wei et al. 2013), or indirectly with the use of an inertial proof mass (Chapman et al. 2008). The energy harvesters exploiting human power are being developed for various intended placement locations, depending on their application. Harvester size thus range from large scale devices, such as knee braces (Li et al. 2009) or knee (Almouahed et al. 2011) and hip (Morais et al. 2011) prostheses, backpacks (Granstrom et al. 2007) and shoe inserts (Zhu et al. 2013), to miniature MEMS harvesters, designed to power up implanted biomedical sensors (Beker et al. 2013).

Possible ways of converting mechanical energy to electricity include electromagnetic induction, piezoelectric effect, electrostatic conversion and triboelectric effect.

Exploiting the piezoelectric effect is common for small scale harvesters, as it allows for easy integration with MEMS technologies. When subjected to mechanical strain, materials with piezoelectric property exhibit polarization. That can be utilized to collect energy from human movement. The published designs range from optimized single linear (Benasciutti et al. 2009) or non-linear (Wickenheiser 2011) oscillating cantilevers to MEMS devices relying on direct deformation (Delnavaz and Voix 2014). Impact based devices generating electric energy from random mechanical shocks have also been investigated (Renaud et al. 2009; Pillatsch et al. 2012).

Electromagnetic energy harvesters, based on Faraday's law of electromagnetic induction, are employed mainly in larger-scale applications, as the necessity to use permanent magnets and coils with sufficient number of turns result in bulky configuration. Electromagnetic energy harvesters are usually designed to work in a narrow bandwidth around resonant frequency, but in order to increase the exploitable excitation frequency range the nonlinear (Khan et al. 2014a), wideband (Patel and Khamesee 2013), or parametric frequency-increased (Galchev et al. 2011) harvesters were also designed. Some designs also employ a hybrid energy conversion approach, utilizing both piezoelectric and electromagnetic conversion (Li et al. 2013).

Electrostatic energy harvesters utilize a variable distance or overlap of the electrodes, caused by the mechanical excitation. As this principle does not require use of any smart materials, it is widely used for MEMS energy harvesters with potential use for harvesting power from human movement (Naruse et al. 2009). A major downside of exploiting this energy conversion principle is the need for a priming voltage source to provide the initial potential difference between the electrodes. Most of the designs also require a mechanical stops to limit the movement of the proof mass. Aside of resonance-based harvester, a self-synchronous non-resonant electrostatic MEMS energy harvester was introduced (Miao et al. 2006).

Recently published progress in characterization of the well-known triboelectric effect has led to a rapid development of triboelectric nanogenerators. Possible applications for this new type of energy harvesters lies also in sensing or harvesting the energy from the human body motion (Wang 2013).

This paper focuses on assessing a kinetic energy harvester placed in the head area of the user. For this reason, a different behavioural patterns of perspective users have to be taken into account. A paper by (Goll et al. 2011), dealing with the levels of harvestable energy in the human head area during different activities concludes, that up to 7 mW of power could be harvested in the most optimistic scenario. However, as stated, this result is highly dependent on the size of the harvester, and also on the user behaviour.

2 Measurements

The acceleration available in the area of human head during different activities was measured in order to obtain real-life excitation waveforms for the intended kinetic energy harvester.

Initial measurements for determining the range of recorded actions and obtaining preliminary results were conducted utilizing a three-axis accelerometer with a data acquisition card and SignalExpress software from NI to capture the data. Due to the inconvenience of using a wired measurement setup, further measurements were done using three-axis MIDE Slam Stick vibration data logger with the set sampling rate of 3200 Hz. The acceleration limits of all three axes measurements are ±15 g. The data logger was fixed to the head of test subjects with a tight rubber band in such a way, that the measurement axes corresponded with fore-aft, lateral and vertical axis of the human skull

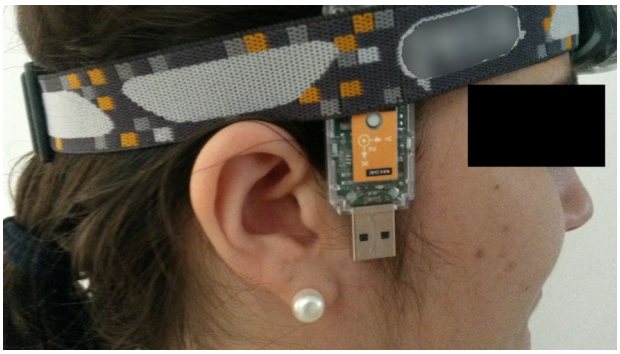

Fig. 1 Vibration measurement setup

(Fig. 1). Acceleration readings were recorded for 100 s during each measurement.

In order to cover a broader range of possible excitation patterns, the original plan covered following actions to be measured on test users: fast walk; walk at natural pace; working by the desk while being seated; and random movements during chatting while standing. However, the initial measurements revealed that while walking at arbitrary speed provides a periodic excitation with exploitable magnitudes and dominant frequencies, working by the desk and random movements provide random vibrations with very low magnitudes and flat frequency spectra (Fig. 2). For further measurements therefore only the walking patterns were recorded, as it is expected to provide significantly better excitation for the harvester.

Data from five healthy subjects, four males and one female, aged between 21 and 35 years, were measured while walking on different speeds. In the first measurement the subjects were instructed to walk on a level ground with their natural pace, during the second measurement they were walking at increased speed equal to their fast pace. Measurements were done in a real-life environment without the use of treadmills, therefore the natural walking pace of the subjects was not artificially influenced by the speed settings. The Frequency spectra of the measured datasets indicate, that the highest magnitudes of acceleration can be observed along the vertical axis of the human head (Fig. 3), the displacement axis of the investigated harvester was therefore aligned with the vertical axis of the skull.

Evaluation of the measurement results reveals that the spectra contain also higher frequencies between 2 and 30 Hz superimposed on the dominant sinusoid. These higher frequency peaks differ considerably in their magnitudes depending on the individual walking styles (Figs. 3, 4) and must be considered in the simulations as they will influence the simulated power output, as seen in chapter 6.

It is also notable, that even though the dominant frequencies and vibration magnitudes naturally differ for different measured subjects (Table 2), they are well in accordance

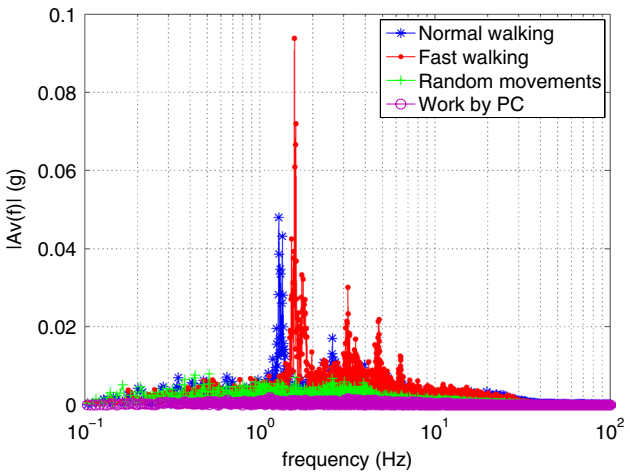

Fig. 2 Comparison of frequency spectra during different activities

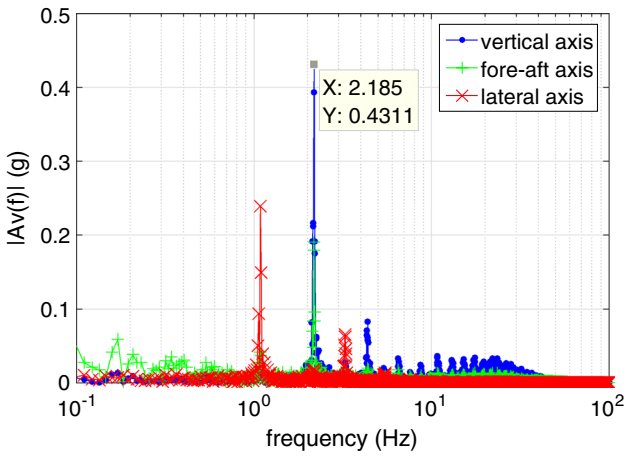

Fig. 3 Comparisons of vibration frequencies and magnitudes in different axes during fast walk: subject 3

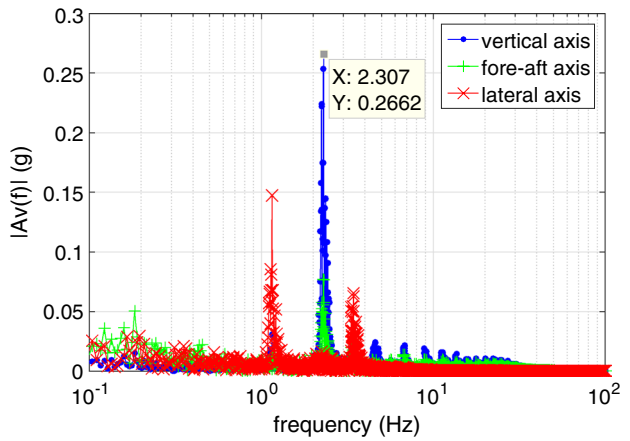

Fig. 4 Comparisons of vibration frequencies and magnitudes in different axes during fast walk: subject 4

Table 2 Measurement subjects data

Subject data					Normal walk		Fast walk	
No.	Sex	Age	Height (cm)	Weight (kg)	1st Dominant frequency (Hz)	Magnitude (g)	1st Dominant frequency (Hz)	Magnitude (g)
1	m	26	183	75	1.69	0.26	1.86	0.41
2	m	35	180	98	1.79	0.30	2.05	0.20
3	m	26	191	69	1.94	0.32	2.19	0.43
4	m	25	177	77	1.95	0.26	2.31	0.27
5	f	21	159	57	2.05	0.33	2.44	0.45

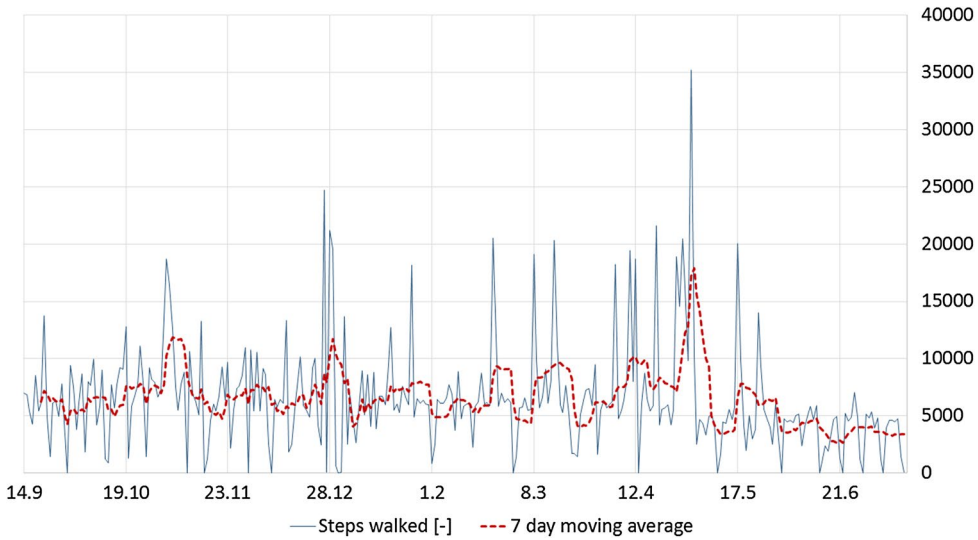

Fig. 5 Measured daily numbers of steps during 10 months

with the measurements done by other research groups (Accoto et al. 2009).

The second part of the measurements utilizes a set of data, acquired between September 2013 and July 2014 from the pedometer application in a mobile phone, which was carried by its user virtually all the time. The data (Fig. 5) therefore show the walking habits of an average company employee, commuting to work during the work days and occasionally going for trips during weekends.

Statistical processing of this data revealed, that the average number of steps per day reached 6559 steps. Due to a small number of outstanding data points the median of the dataset is considerably lower—only 5877 steps per day. Mode of the dataset, 5868 steps, represents the middle point of the most numerous class between 3912 and 7824 steps (Fig. 6), and is used in further energy balance calculations.

3 Preliminary requirements and design

The basic constraints set on the investigated harvester are set due to its application and placement. Since it is intended to serve as a main power source for a new type of cochlear implant based on the bank of piezoresistive mechanical filters (Žák et al. 2015), the power output requirement is set to 150 μW of power during the function of the implant. The dimension limits are set based on the size of usable space in the human skull (Fig. 7), which is about 20 × 20 × 5 mm. That equals to a volume of 2 cm^3 available for the harvester. Taking into account the demanded power output, the harvester will need to achieve a power density of at least 75 $\mu W/cm^3$ with the kinetic energy levels available from the human movements.

Adopting the premise that an average potential user of the cochlear implant with the kinetic energy harvester as a power source will sleep 8 h a day, the longest time period when the implant can be required to work during the day is 16 h. That, using the equation for energy W being equal to time integral of power $p(t)$:

$$W = \int p(t)dt, \tag{1}$$

and assuming the estimated implant power demand of 150 μW, results in at most 8.64 J of energy necessary every day to ensure the proper function of the cochlear implant. Taking into account the measurement results, it is possible to assume that most of this energy will have to be harvested from walking, due to low vibration magnitudes of

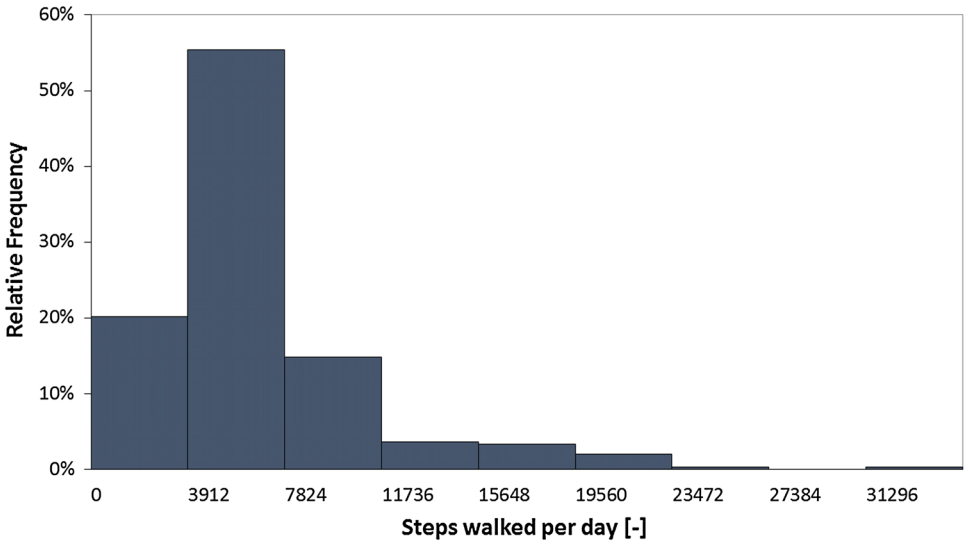

Fig. 6 Relative frequency distribution of 10 months measurement

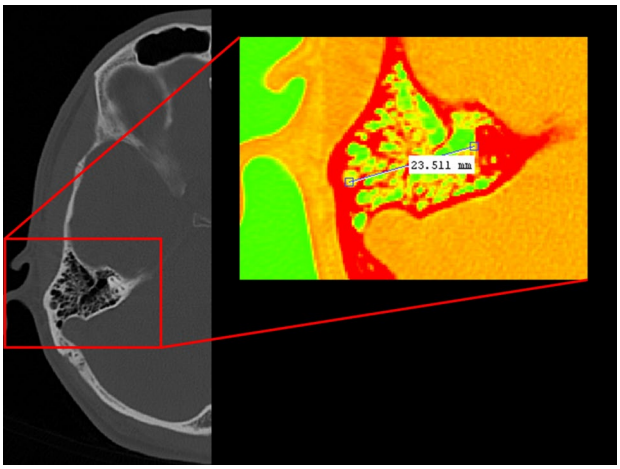

Fig. 7 Intended placement of the investigated harvester inside the human skull cavity

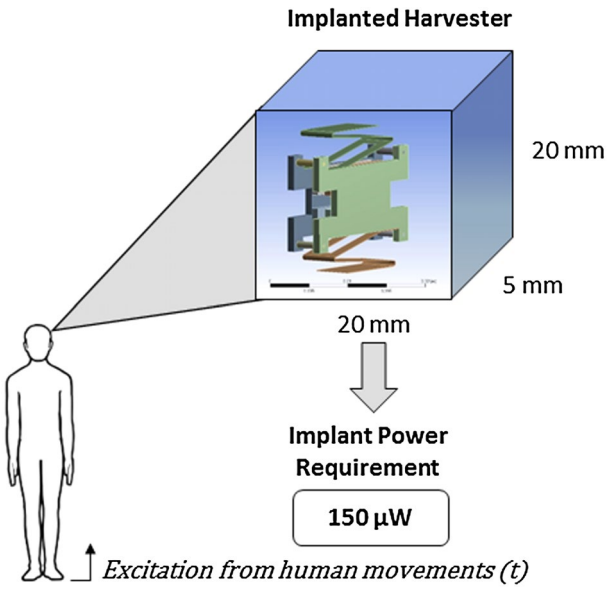

Fig. 8 Schematic drawing of the harvester with basic power and dimension constraints

the other activities. Considering the calculated mode of 5868 steps per day to be the most common step count, it can be concluded that on average it is necessary to harvest 1.47 mJ of energy with every step. Assuming that most of the time people walk at their natural pace and taking into consideration the average normal speed step frequency of 1.88 Hz calculated from Table 2, an estimation of an average 0.87 walking hours is made. Combining this information together with the necessary energy for the function of the implant yields the worst-case requirement of almost 2.77 mW of power being harvested during walking to ensure the function of the cochlear implant for 16 h. However, since the electronics of the implant require power input only when the implant is activated, the real amount of energy necessary should be significantly lower, as it is not likely that the user will be talked to straight 16 h a day.

Based on the previous experience and simple modelling, the electromagnetic induction conversion principle was chosen for preliminary design. The design employs a stationary multilayer printed coil and a mechanical oscillator with permanent magnets (Fig. 8). The natural frequency of the oscillator is tuned by adjusting the parameters of the mechanical springs.

4 Modelling

The modelling phase of the study combined CAD and FEM modelling approaches with the simulation modelling

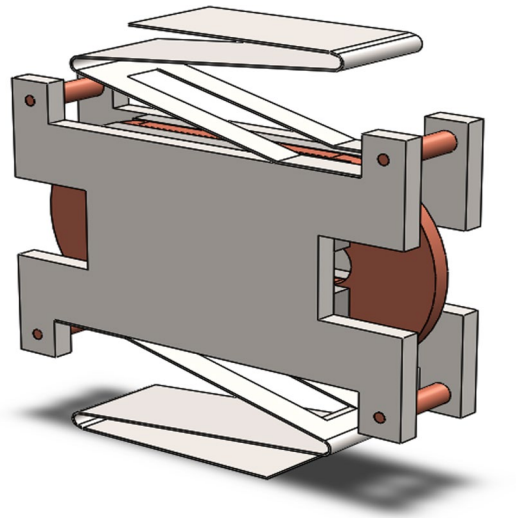

Fig. 9 Initial harvester design

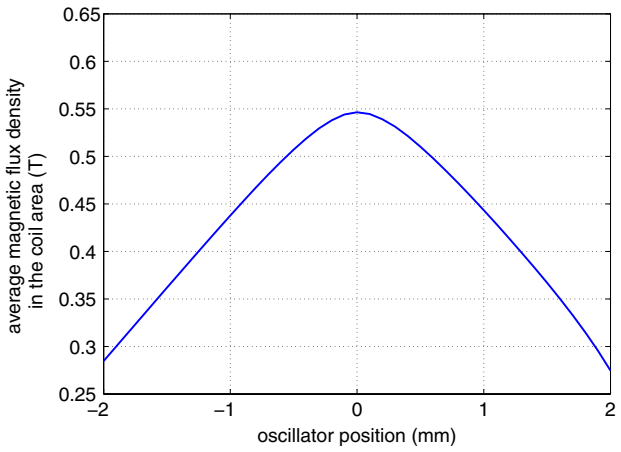

Fig. 10 Dependance of the average magnetic flux density in the coil area on the oscillator position

of the harvester dynamics. First, the design concept of the harvester was created in CAD software (Fig. 9) in order to obtain the inertial properties of the harvester oscillator. Due to the requirements of the oscillator magnetic circuit, the material of the proof mass was selected to be a ferromagnetic steel. NdFeB and permanents magnets were chosen to achieve a high average magnetic flux density in the air gap. The maximum displacement of the oscillator is set to 2 mm, secured by the mechanical limits of the springs.

Due to the design of the harvester, the average magnetic flux density through the coil is varying during the movement of the oscillator. The issue of modelling the non-uniform magnetic field was addressed by (Khan et al. 2014b). In this paper it was decided to use the FEM software to calculate the average magnetic flux density through the coil

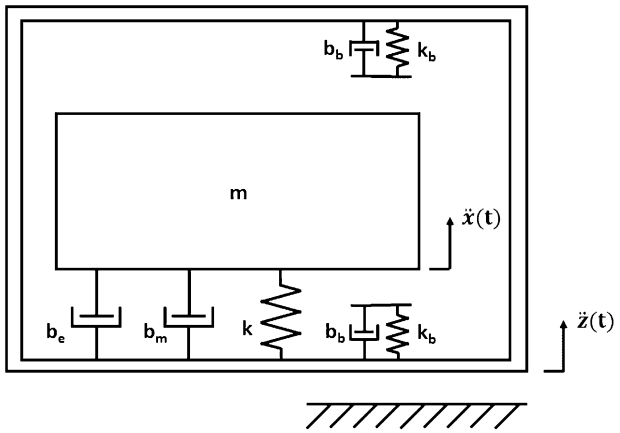

Fig. 11 1DOF model of nonlinear energy harvester

in the whole range of relative positions of the coil and the oscillator (Fig. 10). The result of the FEM analysis was then used in the simulation model in the form of a look-up table.

The simulation model is built in Matlab/Simulink with the use of well-known motion equation of the mass-spring-damper system with one degree of freedom (Fig. 11):

$$\ddot{x} + \frac{[b_e(x) + b_m(x)]}{m}\dot{x} + \frac{k(x)}{m}x = -\ddot{z}, \tag{2}$$

Where x denotes the relative displacement of the proof mass m. The harvester is excited by the vibrations of the frame $\ddot{z}$.

Spring stiffness k and mechanical damping b_m are nonlinear due to the implementation of mechanical limits/bumpers, where a part of the kinetic energy is being dissipated when the oscillating mass comes into the contact with them:

$$k(x) = \begin{cases} k + k_b & x > x_{max} \\ k & x_{min} < x < x_{max} \\ k + k_b & x < x_{min} \end{cases} \tag{3}$$

$$b_m(x) = \begin{cases} b + b_b & x > x_{max} \\ b & x_{min} < x < x_{max} \\ b + b_b & x < x_{min} \end{cases} \tag{4}$$

Electrical damping b_e is also nonlinear due to the distribution of magnetic flux density B. For the proposed design, where the magnetic flux density is perpendicular to the movement of the oscillator, the electromotive force can be calculated according to Faraday's law as:

$$emf = -N\frac{d\Phi}{dt} = -NlB(x)\dot{x}, \tag{5}$$

where l denotes the effective length of the coil, and N is the number of coil turns. If there is an electrical load connected

to the ports of the harvester, the velocity-dependant damping force

$$F_e = b_e \dot{x}. \tag{6}$$

extracts the kinetic energy from a system in the form of electricity. Calculating the power extracted by the damping force

$$p(t) = F_e \dot{x} = b_e \dot{x}^2, \tag{7}$$

and setting it equal to the obtained electrical power, calculated as squared *emf* divided by sum of load and coil resistance R_L and R_C, respectively:

$$p(t) = \frac{emf^2}{(R_L + R_C)}, \tag{8}$$

yields the position dependent electrical damping b_e:

$$b_e(x) = \frac{emf^2}{(R_L + R_C)\dot{x}^2} = \frac{(NlB(x))^2}{R_L + R_C}. \tag{9}$$

In the proposed design, the electrical damping is also nonlinear due to the non-uniform distribution of the magnetic flux density B in the air gap. For the purpose of setting the initial load resistance, the analytic calculation of harvested power on the output was derived by solving a linearized version of (2) combined with (7):

$$P_{loadlinear} = b_e \cdot \frac{\left(A_v \frac{\omega}{\Omega^2}\right)^2}{\left[\frac{\omega(b_e+b_m)}{m\Omega^2}\right]^2 + \left[1 - \left(\frac{\omega}{\Omega}\right)^2\right]^2} \cdot \left(\frac{R_L}{R_L + R_C}\right) \tag{10}$$

where A_v denotes the amplitude of excitation vibrations, ω stands for excitation frequency and $\Omega = \sqrt{\frac{k}{m}}$ is the natural frequency of the harvester. The load resistance in Eq. (10) can be formulated as a function of electrical damping using (9) in order to find the extreme value of electrical power on the load depending on the electrical damping b_e:

$$\frac{dP_{loadlinear}}{db_e} = 0 \tag{11}$$

The value of electrical damping obtained from (11) provides an initial parameter, adjustable either by modifying the magnetic circuit, or by changing the load resistance to better utilize the real-life excitation waveforms.

5 Sensitivity study and model modifications

Feeding the above described modification of the original model (Smilek and Hadas 2015) with the measured acceleration data did not result in expected power output, which was ranging between 24 μW, harvested from normal walk of subject 4; and 176 μW, obtained from fast walk of subject 5.

It was thus decided to rework and improve the design. Due to the nonlinearity of the model, multiple case studies were performed to find the optimum values of tuneable parameters.

First the impact of changing the ratio of magnet and steel pole shoes thickness on the magnetic flux density in the air gap was analysed. The outer dimensions of the harvester and the width of the air gap were set as constants. Two designs, variant 1 with two pairs of permanent magnets and variant 2 with one pair, (Fig. 12) were investigated.

By performing a chain of consecutive FEM analyses for different ratios of magnet thickness to total wall thickness, it was found that the ratio of 0.4 results in the strongest magnetic field in the air gap. It is also apparent from the results (Fig. 13) that using two pairs of permanent magnets with the air gap between each pair is more efficient than using a single pair of magnets with doubled thickness.

In the following step, a sensitivity analysis for the mass of the oscillator, mechanical and electrical damping was conducted using harmonic excitation with 0.3 g magnitude and frequency of 1.8 Hz to imitate the first dominant frequency and magnitude of the vibrations acquired from the measurements. Design variables for the analysis were selected based on the easiness of their adjustability.

The natural frequency of the harvester was tuned up to 11.5 Hz. If a linear harvester model was used, it would be possible to further lower the natural frequency of the harvester by changing the spring design and/or the mass properties in order to better match the dominant frequency of the excitation vibrations. That would in return lead to increased harvested power.

In the studied case however, due to the implementation of displacement limiters and influence of the static gravity acceleration, there are two issues preventing us from taking this path. The first one lies in unacceptably high displacements of the mechanical oscillator working near resonance on a frequency around 2 Hz. This would require either expanding the dimensions envelope to accommodate larger space for oscillator movement or, since the envelope expansion is not a feasible option, it would cause the oscillator to hit the bumpers periodically and lose kinetic energy during the impacts. The other challenge is caused by the fact that due to the pre-straining of the low-stiffness spring by the force caused by static gravity acceleration the oscillator would be resting on the lower limiter and the harvested power would drop.

It could be an option to exploit vibrations from different direction to avoid the spring pre-straining. That would, however, worsen the overall performance due to the lower magnitude of input vibrations. For these reasons the design was kept as described and subjected to the sensitivity study.

Results of this analysis show that the performance of the harvester can be only negligibly improved by adding

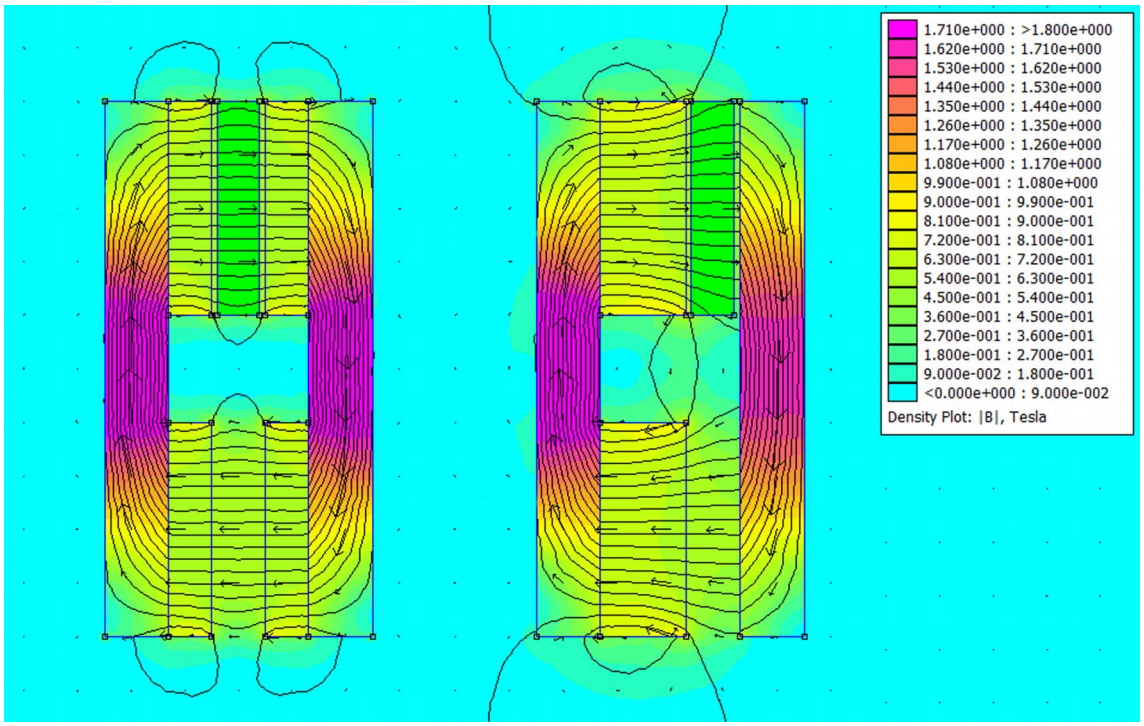

Fig. 12 FEM analyses of two designs of the magnetic circuit. Coil area highlighted in *green* (color figure online)

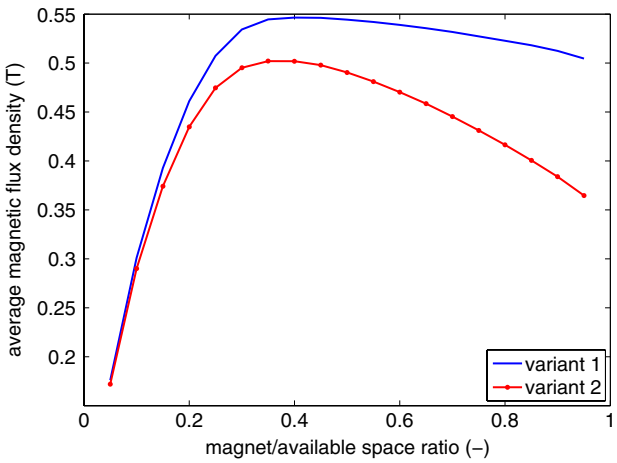

Fig. 13 Results of optimal magnets thickness analyses for two pairs of magnets (variant 1) and one pair of magnets (variant 2)

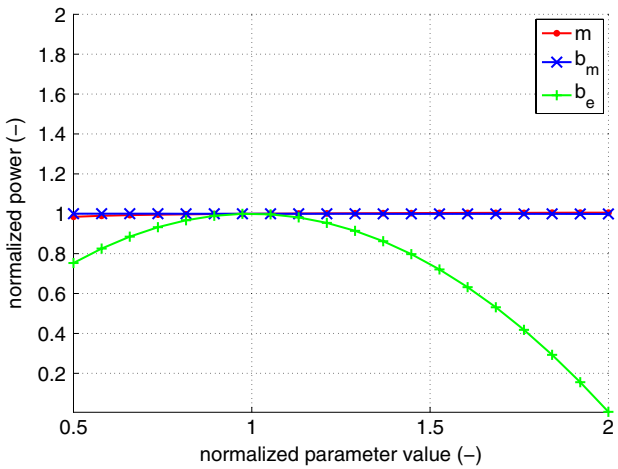

Fig. 14 Results of sensitivity analysis with harmonic excitation

more weight to the oscillator or by lowering the mechanical damping coefficient (Fig. 14). Since the harvester in this analysis works with a small displacement without hitting the limiters and the nonlinearity in the electrical damping is not significant enough, the electrical damping, even though calculated by (11) for a linear harvester with the same excitation and natural frequencies as used in the analysis, is apparently close to the optimum and its change would not yield any improvement of the performance.

However, running another sensitivity study, this time with the real acceleration data as the input, revealed that adding the weight actually does have much larger effect to the performance than originally anticipated, as the real data contain also frequencies closer to the resonant frequency of the harvester. For the same reason also the load value, provided by the load matching Eq. (11) and verified by previous analysis as the optimal for harmonic excitation does not provide the best performance with the real data, and

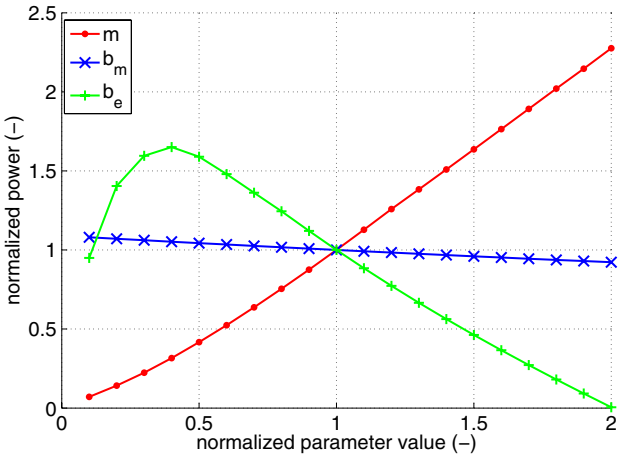

Fig. 15 Results of sensitivity analysis with real-life excitation

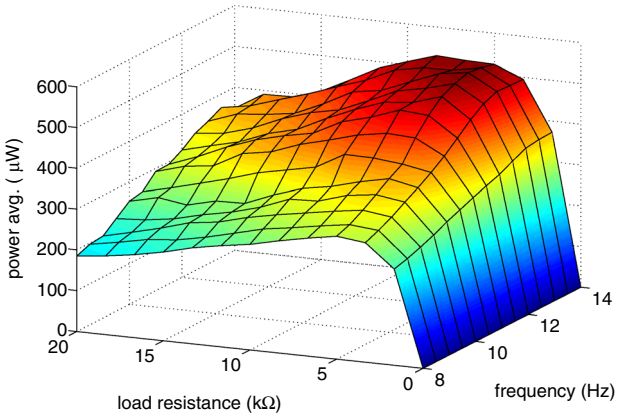

Fig. 17 Dependance of harvested power on natural frequency of the harvester and load resistance for subject no. 5 during fast walk

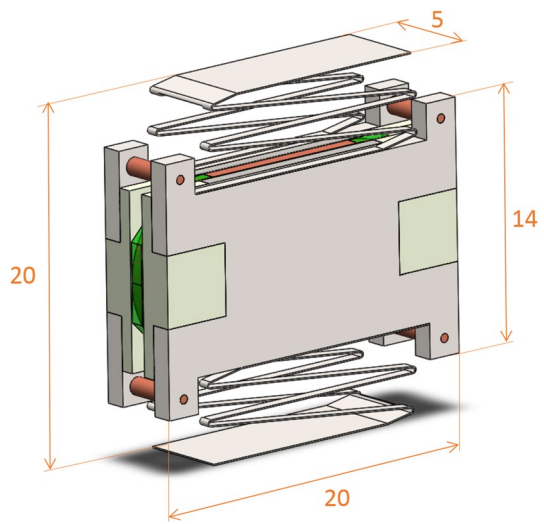

Fig. 16 Modified CAD model of the harvester with added balast and optimized wall *thickness*

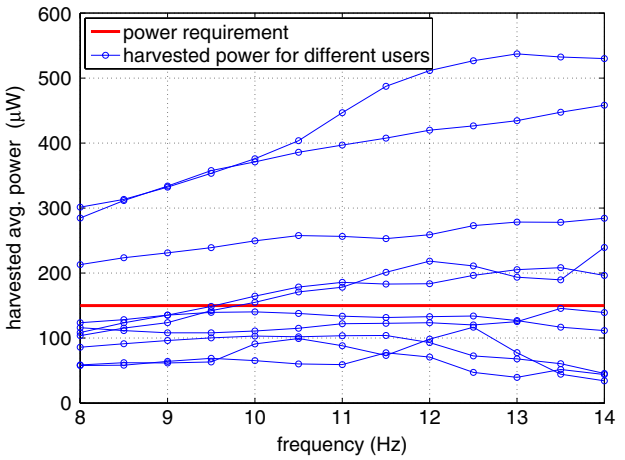

Fig. 18 Highest simulated power output dependances on natural frequency for all measurements

the electrical load needs to be adjusted in order to lower to value of electrical damping (Fig. 15).

Based on results of these studies, the CAD model of the harvester was modified to accommodate the suggested change in mass. Adding a shaped wolfram weights increased the total weight of the harvester to 9.5 g, instead of the original of 5 g. All the additional mass is placed within previously empty volume of space, therefore the outer dimensions of the harvester remain unchanged (Fig. 16).

The last step of modifications comprised of series of simulations in order to determine the most suitable natural frequency of the harvester, adjustable by changing the spring stiffness. For every resonant frequency tried, it was necessary to run a sweep with different electrical loads (Fig. 17), since the calculated load was proved to be overdamping the system in case of broader excitation frequency range.

The natural frequency and electrical load sweeps with different datasets showed, that the harvester generally provides the most power when the oscillator moves throughout the whole available displacement range without hitting the bumpers. This also means, that for every user the optimal spring stiffness and thus the natural frequency is slightly different, depending on their walking style and speed.

The highest reached power at every frequency within investigated range between 8 and 14 Hz was saved for all the users and both walking patterns and compared against the minimum harvested power requirement (Fig. 18). Results show, that the natural frequency of the harvester between 11.5 and 12 Hz yields highest minimum power harvested from all the walking patterns recorded. Frequency 12 Hz was therefore selected as the natural

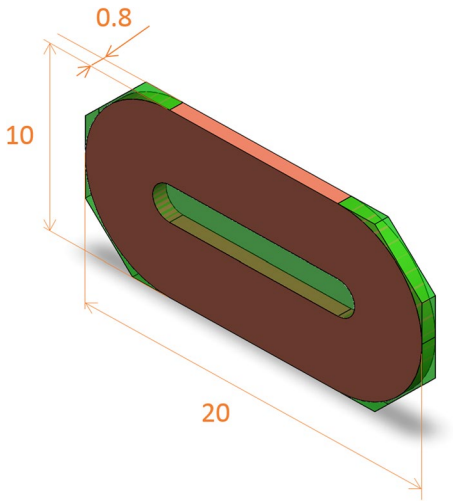

Fig. 19 CAD model of the coil with dimensions

Table 3 Final parameters of the modelled harvester

Oscillator parameters	
Outer dimensions	20 × 20 × 5 mm
Total weight	m = 9.5 g
Mechanical damping	$b_m = 0.01$ Ns/m
Average magnetic flux in the air gap	B = 0.27–0.55 T (see Fig. 9)
Natural frequency	Ω = 12 Hz
Coil parameters	
Coil dimensions	20 × 10 × 0.8 mm
Conductive path cross-section dimensions	4 × 0.8 mm
Conductor diameter	d = 25 µm
Number of turns	N = 2000
Effective length of one turn	l = 12 mm
Resistance	$R_C = 2.4$ kΩ
Load	
Resistance	$R_L = 6.6$ kΩ

frequency of the harvester, as it provides more than sufficient power levels for users with more dynamic style of walking, while harvesting maximum obtainable power from users with softer walking style. Due to the redesign of the springs to adjust the natural frequency of the harvester the stiffness in directions perpendicular to the direction of oscillator movement dropped. A mechanical guidance for the oscillator will therefore be necessary and needs to be taken into consideration in the estimation of the total mechanical damping.

The electrical load resistance 6.6 kΩ was selected as optimal for the harvester with 2 mm maximum displacement and the multilayer printed coil with 2.4 kΩ resistance (Fig. 19). Intended conductor thickness is 25 µm and

Table 4 Harvested amounts of power from different subjects and activities

Subject No.	Harvested average power (µW)	
	Normal walk	Fast walk
1	81	100
2	84	170
3	238	377
4	61	110
5	228	478

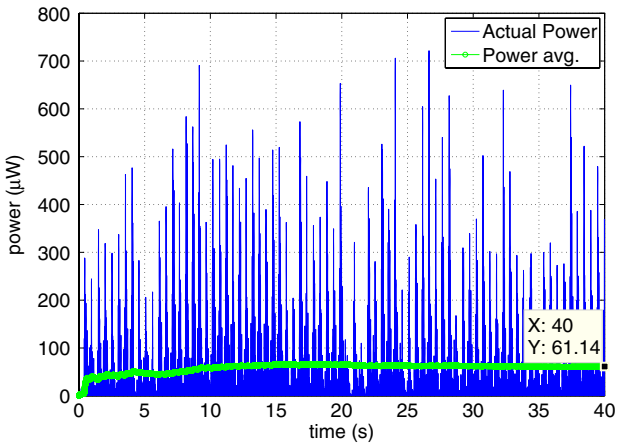

Fig. 20 Simulation results with the lowest amount of harvested power (subject 4, normal walk)

the coil cross-section dimensions are 4 × 0.8 mm, which leads to the estimation of 16 layers necessary to reach the designed number of 2000 turns. The coil is intended to be manufactured by stacking thin printed circuit boards with inductors printed on them (Olivo et al. 2013). The Final parameters of the harvester used for power output simulations are summarized in Table 3.

6 Simulation results

In order to verify the feasibility of the selected natural frequency and load value of the harvester, numerous simulations were run with the finalized version of the model for all the measured excitation waveforms. The length of each simulation was set to 40 s in order to ensure better reliability of the result than shorter times, used in previous analyses. Simulated power on the load resistor for each user can be observed from Table 4.

Results show, that even though satisfying the requirements for powering the cochlear implant for full 16 h a day might still be challenging, ensuring momentary function of the implant by harvesting the energy from the harvester

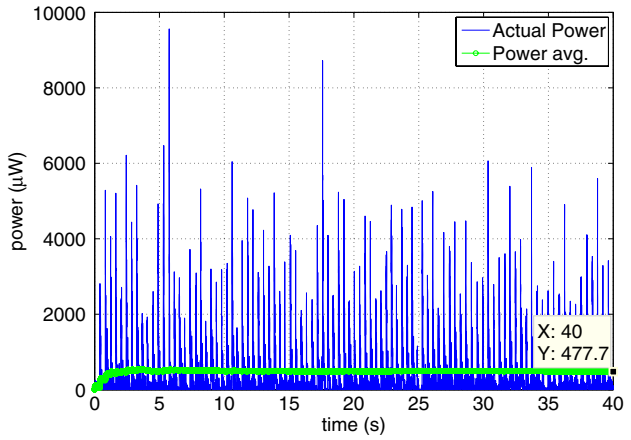

Fig. 21 Simulation results with the highest amount of harvested power (subject 5, fast walk)

placed in the human head during walking could present a feasible approach for the future biomedical applications.

Obtained simulation results display an order of magnitude difference between lowest and highest reached average power (Figs. 20, 21). The results also indicate, that the walking style of different users has a considerable impact on the harvested power. Even though the dominant frequencies and magnitudes of vibrations during walking are similar for all the tested subjects, the individual walking style contributes with higher frequencies close to the natural frequency of the harvester as was discussed in chapter 2. Even though the magnitudes of these higher frequency vibrations are much lower than the magnitude of vibrations on dominant frequencies, they account for a significant differences between the results.

7 Conclusions

The study of the kinetic energy harvester based on the electromagnetic conversion principle was done to investigate the feasibility of implanting such a harvester into the human head to power up a selected biomedical application. The basic harvester design comprises of an oscillator with a proof mass, consisting of a magnetic circuit and an additional ballast, a stationary multilayer printed coil and mechanical springs. The maximum displacement of the oscillator was set to 2 mm. Tuning the harvester to work in resonance was not feasible due to the low excitation frequencies, low spring stiffness and large displacements connected with it. Instead, the harvester was tuned in such a way, that the excitation frequencies are lower than the natural frequency, but the natural frequency is still low enough for the harvester to be able to extract sufficient amount of power from the available excitation. The initial harvester design was modified for higher power output based on the results of the sensitivity study for three different design variables—mass of the oscillator, mechanical and electrical damping. Further design optimization is intended to be conducted using the methods of artificial intelligence (Hadas et al. 2012).

To better understand the real-life excitation patterns, the acceleration in the area of human head was measured during different walking speeds on five different subjects. The measurement of daily step count was also conducted in order to analyse, how much time does an average user daily spend by walking, and how much energy is needed to be harvested during this period to ensure the function of the powered implant for the time its user might be needing it during the day.

Results of the simulations indicate, that the implanted harvester could be able to cope with the momentary power demands of the cochlear implants, but with the investigated design it will most likely not provide the calculated highest necessary energy of 8.64 J per day, which equals to 2.77 mW of average power generated during the walking time, to keep the implant operating even when its user is not walking. Moreover, the power output of the harvester is highly dependent on walking style, and possibly also on the footgear used and the walking surface, therefore proper tuning of the harvester for a whole range of users and their walking styles might be challenging. The simulated power outputs differ by almost an order of magnitude, between 61 and 478 μW. It remains to be a question of feasibility to adjust the harvester for every specific user to provide an optimal power output. The simulations also do not take into account further losses caused by the power management electronics, the efficiency of which usually ranges between 60 and 90 %.

At the moment, even though the proposed energy harvester could not entirely satisfy the requirements for powering up the cochlear implant, it would still improve the usage comfort for a user of such a device, as the battery replacement or recharging interval would be extended. With future technology advances and further optimization of the new cochlear implants however, we believe that it will become possible to eliminate the need for the battery recharging from other sources entirely. Possible focus points to improve the performance of the miniature energy harvesters for biomedical applications could include for example optimizing the rotary inertial energy harvesters (Jang et al. 2011) to better utilize the small available volume of space or employing hybrid harvesters to take advantage of multiple kinetic energy transducers. Another option could lie in changing the strategy and exploiting directly the deformation of the ear canal during movements of the jaw.

Acknowledgments This work is an output of research and scientific activities of NETME Centre, supported through project NETME

CENTRE PLUS (LO1202) by financial means from the Ministry of Education, Youth and Sports in Czech Republic under the "National Sustainability Programme I".

References

Accoto D, Calvano M, Campolo D et al (2009) Energetic analysis for self-powered cochlear implants. In: Conference proceedings: annual international conference of the IEEE engineering in medicine and biology society. Annual Conference 2009. IEEE Engineering in Medicine and Biology Society, pp 4860–4863. doi:10.1109/IEMBS.2009.5332449

Aktakka EE, Najafi K (2014) A micro inertial energy harvesting platform with self-supplied power management circuit for autonomous wireless sensor nodes. IEEE J Solid-State Circuits 49:2017–2029. doi:10.1109/JSSC.2014.2331953

Almouahed S, Gouriou M, Hamitouche C et al (2011) The use of piezoceramics as electrical energy harvesters within instrumented knee implant during walking. IEEE/ASME Trans Mechatron 16:799–807. doi:10.1109/TMECH.2011.2159512

Beker L, Zorlu O, Goksu N, Kulah H (2013) Stimulating auditory nerve with MEMS harvesters for fully implantable and self-powered cochlear implants. In: 2013 Transducers and eurosensors XXVII: the 17th international conference on solid-state sensors, actuators and microsystems (Transducers and eurosensors XXVII). IEEE, pp 1663–1666

Benasciutti D, Moro L, Zelenika S, Brusa E (2009) Vibration energy scavenging via piezoelectric bimorphs of optimized shapes. Microsyst Technol 16:657–668. doi:10.1007/s00542-009-1000-5

Cadei A, Dionisi A, Sardini E, Serpelloni M (2014) Kinetic and thermal energy harvesters for implantable medical devices and biomedical autonomous sensors. Meas Sci Technol 25:012003. doi:10.1088/0957-0233/25/1/012003

Chapman P, DiBerardino L, Hsiao-Wecksler E (2008) Design and optimization of a biomechanical energy harvesting device. In: 2008 IEEE power electronics specialists conference. IEEE, pp 4062–4069

Chen I-M, Phee SJ, Luo Z, Lim CK (2010) Personalized biomedical devices and systems for healthcare applications. Front Mech Eng China 6:3–12. doi:10.1007/s11465-011-0209-z

Dagdeviren C, Yang BD, Su Y et al (2014) Conformal piezoelectric energy harvesting and storage from motions of the heart, lung, and diaphragm. Proc Natl Acad Sci USA 111:1927–1932. doi:10.1073/pnas.1317233111

Dai D, Liu J (2012) Human powered wireless charger for low-power mobile electronic devices. IEEE Trans Consum Electron 58:767–774. doi:10.1109/TCE.2012.6311316

Delnavaz A, Voix J (2014) Energy harvesting for in-ear devices using ear canal dynamic motion. IEEE Trans Ind Electron 61:583–590. doi:10.1109/TIE.2013.2242656

Galchev T, Kim H, Najafi K (2011) Micro power generator for harvesting low-frequency and nonperiodic vibrations. J Microelectromechanical Syst 20:852–866. doi:10.1109/JMEMS.2011.2160045

Goll E, Zenner H-P, Dalhoff E (2011) Upper bounds for energy harvesting in the region of the human head. IEEE Trans Biomed Eng 58:3097–3103. doi:10.1109/TBME.2011.2163407

Granstrom J, Feenstra J, Sodano HA, Farinholt K (2007) Energy harvesting from a backpack instrumented with piezoelectric shoulder straps. Smart Mater Struct 16:1810–1820. doi:10.1088/0964-1726/16/5/036

Hadas Z, Kurfurst J, Ondrusek C, Singule V (2012) Artificial intelligence based optimization for vibration energy harvesting applications. Microsyst Technol 18:1003–1014. doi:10.1007/s00542-012-1432-1

Hadas Z, Vetiska V, Huzlik R, Singule V (2014) Model-based design and test of vibration energy harvester for aircraft application. Microsyst Technol 20:831–843. doi:10.1007/s00542-013-2062-y

Jang S-J, Kim I-H, Jung H-J, Lee Y-P (2011) A tunable rotational energy harvester for low frequency vibration. Appl Phys Lett 99:134102. doi:10.1063/1.3644130

Khan F, Stoeber B, Sassani F (2014a) Modeling and simulation of linear and nonlinear MEMS scale electromagnetic energy harvesters for random vibration environments. Sci World J. doi:10.1155/2014/742580

Khan F, Stoeber B, Sassani F (2014b) Modeling of linear micro electromagnetic energy harvesters with nonuniform magnetic field for sinusoidal vibrations. Microsyst Technol 21:683–692. doi:10.1007/s00542-014-2359-5

Kim M-K, Kim M-S, Lee S et al (2014) Wearable thermoelectric generator for harvesting human body heat energy. Smart Mater Struct 23:105002. doi:10.1088/0964-1726/23/10/105002

Lay-Ekuakille A, Vendramin G, Trotta A, Mazzotta G (2009) Thermoelectric generator design based on power from body heat for biomedical autonomous devices. In: 2009 IEEE international workshop on medical measurements and applications. IEEE, pp 1–4

Leonov V, Fiorini P, Vullers RJM (2011) Theory and simulation of a thermally matched micromachined thermopile in a wearable energy harvester. Microelectron J 42:579–584. doi:10.1016/j.mejo.2010.08.002

Li Q, Naing V, Donelan JM (2009) Development of a biomechanical energy harvester. J Neuroeng Rehabil 6:22. doi:10.1186/1743-0003-6-22

Li P, Gao S, Cai H (2013) Modeling and analysis of hybrid piezoelectric and electromagnetic energy harvesting from random vibrations. Microsyst Technol 21:401–414. doi:10.1007/s00542-013-2030-6

Miao P, Mitcheson PD, Holmes AS et al (2006) Mems inertial power generators for biomedical applications. Microsyst Technol 12:1079–1083. doi:10.1007/s00542-006-0152-9

Morais R, Silva NM, Santos PM et al (2011) Double permanent magnet vibration power generator for smart hip prosthesis. Sensors Actuators A Phys 172:259–268. doi:10.1016/j.sna.2011.04.001

Naruse Y, Matsubara N, Mabuchi K et al (2009) Electrostatic micro power generation from low-frequency vibration such as human motion. J Micromech Microeng 19:094002. doi:10.1088/0960-1317/19/9/094002

Olivo J, Carrara S, De Micheli G (2013) A study of multi-layer spiral inductors for remote powering of implantable sensors. IEEE Trans Biomed Circuits Syst 7:536–547. doi:10.1109/TBCAS.2012.2225620

Patel P, Khamesee MB (2013) Electromagnetic micro energy harvester for human locomotion. Microsyst Technol 19:1357–1363. doi:10.1007/s00542-013-1820-1

Pfenniger A, Wickramarathna LN, Vogel R, Koch VM (2013) Design and realization of an energy harvester using pulsating arterial pressure. Med Eng Phys 35:1256–1265. doi:10.1016/j.medengphy.2013.01.001

Pillatsch P, Yeatman EM, Holmes AS (2012) A scalable piezoelectric impulse-excited energy harvester for human body excitation. Smart Mater Struct 21:115018. doi:10.1088/0964-1726/21/11/115018

Rasouli M, Phee LSJ (2010) Energy sources and their development for application in medical devices. Expert Rev Med Devices 7:693–709. doi:10.1586/erd.10.20

Renaud M, Fiorini P, van Schaijk R, van Hoof C (2009) Harvesting energy from the motion of human limbs: the design and analysis of an impact-based piezoelectric generator. Smart Mater Struct 18:035001. doi:10.1088/0964-1726/18/3/035001

Romero E, Warrington RO, Neuman MR (2010) Powering biomedical devices with body motion. In: Conference proceedings

annual international conference on IEEE Engineering in Medicine and Biology Society IEEE Engineering Medicine and Biology Society annual conference 2010:3747–3750. doi:10.1109/IEMBS.2010.5627542

Smilek J, Hadas Z (2015) Assessment of MEMS energy harvester for medical applications. In: Proceedings of SPIE 9517:95170 N–95170 N–8

Starner T (1996) Human-powered wearable computing. IBM Syst. J. 35:618–629

Sudano A, Accoto D, Francomano MT et al (2011) Optimization of kinetic energy harvesters design for fully implantable cochlear implants. In: Conference proceedings of annual international conference IEEE Engineering Medicine and Biology Society IEEE Engineering Medicine and Biology Society annual conference 2011:7678–7681. doi:10.1109/IEMBS.2011.6091892

Wang ZL (2013) Triboelectric nanogenerators as new energy technology for self-powered systems and as active mechanical and chemical sensors. ACS Nano 7:9533–9557. doi:10.1021/nn404614z

Wei S, Hu H, He S (2013) Modeling and experimental investigation of an impact-driven piezoelectric energy harvester from human motion. Smart Mater Struct 22:105020. doi:10.1088/0964-1726/22/10/105020

Wickenheiser AM (2011) Design optimization of linear and nonlinear cantilevered energy harvesters for broadband vibrations. J Intell Mater Syst Struct 22:1213–1225. doi:10.1177/1045389X11418859

Yoon Y-J, Park W-T, Li KHH et al (2013) A study of piezoelectric harvesters for low-level vibrations in wireless sensor networks. Int J Precis Eng Manuf 14:1257–1262. doi:10.1007/s12541-013-0171-2

Yun J, Patel SN, Reynolds MS, Abowd GD (2011) Design and performance of an optimal inertial power harvester for human-powered devices. IEEE Trans Mob Comput 10:669–683. doi:10.1109/TMC.2010.202

Žák J, Hadaš Z, Dušek D et al (2015) Model-based design of artificial zero power cochlear implant. Mechatronics. doi:10.1016/j.mechatronics.2015.04.018

Zhu G, Bai P, Chen J, Lin Wang Z (2013) Power-generating shoe insole based on triboelectric nanogenerators for self-powered consumer electronics. Nano Energy 2:688–692. doi:10.1016/j.nanoen.2013.08.002

ANNEX A2

SMILEK, Jan and Zdenek HADAS

Improving power output of inertial energy harvesters by employing principal component analysis of input acceleration

Mechanical Systems and Signal Processing [online]. 2017, **85**, 801–808. ISSN 08883270. Available at: doi:10.1016/j.ymssp.2016.09.020

Impact factor: 4.116

Mechanical Systems and Signal Processing 85 (2017) 801–808

Contents lists available at ScienceDirect

Mechanical Systems and Signal Processing

journal homepage: www.elsevier.com/locate/ymssp

Improving power output of inertial energy harvesters by employing principal component analysis of input acceleration

Jan Smilek*, Zdenek Hadas

Faculty of Mechanical Engineering, Brno university of Technology, Technicka 2896/2, 616 69 Brno, Czech Republic

ARTICLE INFO

Keywords:
Energy harvesting
Principal component analysis
Signal processing
Excitation acceleration

ABSTRACT

In this paper we propose the use of principal component analysis to process the measured acceleration data in order to determine the direction of acceleration with the highest variance on given frequency of interest. This method can be used for improving the power generated by inertial energy harvesters. Their power output is highly dependent on the excitation acceleration magnitude and frequency, but the axes of acceleration measurements might not always be perfectly aligned with the directions of movement, and therefore the generated power output might be severely underestimated in simulations, possibly leading to false conclusions about the feasibility of using the inertial energy harvester for the examined application.

1. Introduction

Energy harvesting as a mean of obtaining useful electrical energy from ambient energy of surrounding environment has become a mature research field with well characterized principles. Sources of harvestable energy and devices for its conversion to electric energy vary depending on the application. Possible options might include one or more of following sources and transduction methods [1]: solar energy, transduced through photovoltaic cells; thermal gradient, convertible utilizing TEG generators; RF electromagnetic waves, exploitable using antennas, or kinetic energy, which can be converted with electromechanical energy harvesters.

Basic classification of electromechanical energy harvesters can be done by assigning them into two groups according to the operation principle: direct force harvesters and inertial harvesters [2]. While direct force devices exploit the direct application of the loading force to the transducer and the dynamics of such a system is mostly dominated by the loading force, inertial harvesters utilize the kinematic excitation of the frame to achieve a relative oscillatory movement between the proof mass and the frame of the harvester.

Another way of classification is based on the transduction physical principle. Commonly employed conversion methods include Faraday's induction law [3–5], piezoelectric effect [6–10], electrostatic effect [11,12], magnetostriction [13,14], and newly also triboelectric effect [15,16].

This paper is focused on a method for potential improvement of the power output of inertial energy harvesters by locating and exploiting principal directions of acceleration with given frequency in a measured dataset.

2. Inertial energy harvesters

Inertial harvesters can be understood as accumulators of mechanical energy, which is being stored in the system in as kinetic

* Corresponding author.
E-mail address: smilek@fme.vutbr.cz (J. Smilek).

http://dx.doi.org/10.1016/j.ymssp.2016.09.020
Received 18 May 2016; Received in revised form 18 August 2016; Accepted 10 September 2016

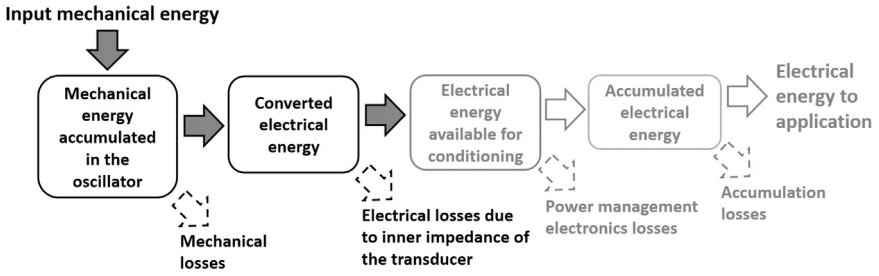

Fig. 1. Energy flow in the energy harvesting system.

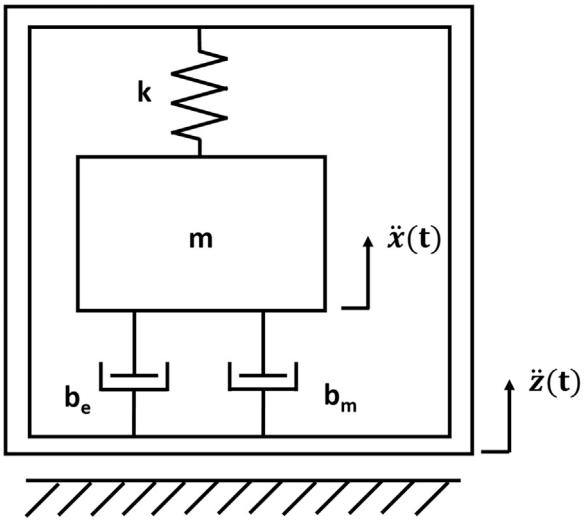

Fig. 2. Model of 1dof inertial energy harvester.

energy of the proof mass and potential energy in the spring element. During the operation a part of the accumulated mechanical energy is being extracted and converted into electrical energy by one of the transducing principles, using either electrodynamic or electrostatic damping force. Some part of the energy is inevitably lost due to the mechanical losses (Fig. 1).

Let us assume that given 1 degree of freedom (dof) inertial harvester consisting of proof mass m with electrodynamic damping characteristics given by combination of mechanical and electrical damping b_m and b_e, respectively, contains linear stiffness k and is excited by vibrations of the frame $\ddot{z}$ (Fig. 2).

Its dynamics is described by the well-known motion equation

$$\ddot{x}+\frac{[b_e + b_m]}{m}\dot{x}+\frac{k}{m}x=-\ddot{z} \tag{1}$$

where x represents the displacement of the proof mass. Natural frequency of such a system is found as $\Omega=\sqrt{\frac{k}{m}}$ and its damping ratio as

$$b_p=\frac{b_e + b_m}{2m\Omega} \tag{2}$$

The quality factor of the harvester is given by

$$Q=\frac{1}{2b_p}=\frac{m\Omega}{b_e + b_m} \tag{3}$$

Motion Eq. (1) can then be rewritten as

$$\ddot{x}+\frac{\Omega}{Q}\dot{x}+\Omega^2 x=-\ddot{z} \tag{4}$$

In case of harmonic excitation $\ddot{z}=Av\cos(\omega t)$ the power output of the linear energy harvester is proportionally dependent on the

square of the input acceleration magnitude Av of given frequency ω:

$$P_{el}=b_e\bullet\frac{\left(Av\frac{\omega}{\Omega^2}\right)^2}{\left[\frac{\omega\left(b_e+b_m\right)}{m\Omega^2}\right]^2+\left[1-\left(\frac{\omega}{\Omega}\right)^2\right]^2} \tag{5}$$

Formula (5) can be used to calculate the frequency dependency of the power output of the system. By exploiting the superposition property of linear systems it is possible to calculate an estimate of a steady-state power output with arbitrary periodic input acceleration waveform by decomposing the input acceleration into harmonic components. It is obvious, that increasing the magnitude of input vibrations component with frequency equal to natural frequency of the harvester will lead to significant power generation improvement. Raising the magnitude of input vibrations is usually not feasible in real-life applications. However, the same effect can be achieved by proper orientation of the harvester. Given that the excitation acceleration is measured with 3-axis accelerometer with orthogonal axes of measurement, it is likely that the measurement axes were not aligned with the principal axes of the acceleration and thus only orthogonal projections of the actual acceleration vector are apparent in the measured data and used for harvester excitation.

3. Pre-processing of the measured acceleration data

Measuring the acceleration with a 3-axis accelerometer allows for displaying the time change of the acceleration vector in the 3 dimensional Cartesian space. The measured instantaneous excitation acceleration $\ddot{z}$ can then be found in the vector form $\ddot{z}=(\ddot{z}_x, \ddot{z}_y, \ddot{z}_z)$, where the vector components correspond with the measured data from three orthogonal directions. If the measurement is done with constant sampling rate, the time distance of each pair of neighboring measured values remains constant. Total least squares approach thus can be used to find the direction which contains highest variance of the acceleration magnitude – the first principal direction.

In the general case the measured data containing a single frequency will form an ellipsoid, as the accelerations in principal directions along the axes of the ellipsoid might not be in phase with each other (Fig. 3). In case of all three phases being the same, the ellipsoid will degenerate into a line in space, which would be the best case scenario for the purposes of exciting the energy harvester with 1 dof. Finding the principal direction of acceleration with the highest variance in time, and identifying the rotation angles to transform the original coordinate system linked with the measurement device/energy harvester to align it with this principal direction will ensure, that highest magnitude of acceleration will be used for excitation of the energy harvester. This way, the highest power output for given application and transducer will be achieved.

Real measured data contain noise and possibly wider spectrum of frequencies (Figs. 4 and 5). As the principal directions of different frequency components are not necessarily the same, it is essential to filter out frequencies other than the frequency of interest from the vibration spectrum. We filtered the measured data in time domain (Fig. 6) using inverse notch filter, implemented as narrow band pass 2nd order Butterworth filter with cut-off frequencies ± 0.05 Hz around the desired isolation frequency.

4. Locating the principal acceleration direction

Filtered data containing only the frequency of interest can be subjected to principal component analysis (pca) in order to obtain the principal axes of vibration. The pca routine fits the m-dimensional data points with a set of m orthogonal lines, equations of which are obtained by solving the total least squares optimization problem. The sum of squared orthogonal distances of the data points from the sought lines is thus minimized.

One possible approach to this lies in performing singular value decomposition (svd) of a measured dataset. If the mean-centered measured data is stored in a form of 3×n matrix $\boldsymbol{D}$, columns of which contain the Cartesian coordinates of the acceleration vector end point measured in n time instants, the $\boldsymbol{D}$ can be decomposed into

$$\boldsymbol{D}=\boldsymbol{U}\boldsymbol{\Sigma}\boldsymbol{V}^T \tag{6}$$

where $\boldsymbol{U}$ is a matrix of left eigenvectors, describing the components rotations, $\boldsymbol{\Sigma}$ is a diagonal matrix of singular values sorted in a descending order along the diagonal, and $\boldsymbol{V}$ is a 3×3 matrix of right eigenvectors, containing orthonormal vectors associated with the singular values. The vector associated with the highest singular value is the principal component of the data, and is located in the first column of $\boldsymbol{V}$. Matrix $\boldsymbol{V}$ can be also understood as a rotation matrix, describing the transformation of the original coordinate system linked with the measurement axes to the new coordinate system, associated with the principal directions of data.

Another option is working with a covariance matrix $\boldsymbol{C}$

$$\boldsymbol{C}=\frac{1}{n}\boldsymbol{D}^T\boldsymbol{D} \tag{7}$$

The 3×3 sized covariance matrix $\boldsymbol{C}$ is symmetric and positive definite and its singular value decomposition therefore yields the same result as its eigenvalue decomposition:

$$\boldsymbol{C}=\boldsymbol{V}\boldsymbol{\Lambda}\boldsymbol{V}^T=\boldsymbol{V}\frac{\boldsymbol{\Sigma}^2}{n}\boldsymbol{V}^T \tag{8}$$

Where $\boldsymbol{\Lambda}$ is the diagonal matrix of eigenvalues sorted in decreasing order. The sought base vectors are stored again in the columns of

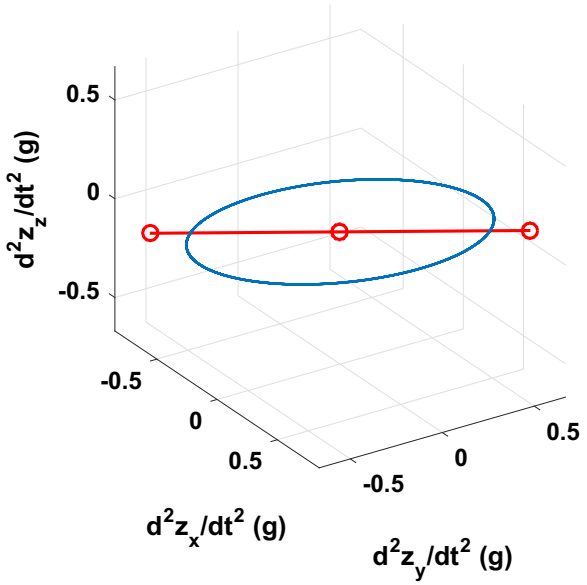

Fig. 3. Representation of the noiseless acceleration vector end point in 3D Cartesian space. Red circle in the center represents the mean value of the data. (For interpretation of the references to color in this figure legend, the reader is referred to the web version of this article)

the rotation matrix $\boldsymbol{V}$.

5. Identification of the rotation angles

Once the desired new orientation of the coordinate system linked with the harvester is known, the succession of rotational angles must be found. It is known, that an arbitrary orientation of the coordinate system in space can be achieved by a sequence of three rotations around different axes. In this paper we find the succession of angles for extrinsic rotations (rotations around fixed coordinate system) around axes z-y-x, known also as yaw-pitch-roll rotations. This succession can be reversed to obtain the same final orientation with intrinsic rotation axes x-y'-z", which might be easier to implement on the real system.

It needs to be checked whether the final rotation matrix obtained from pca follows the convention of right-handed coordinate system. When necessary, one of the columns of **V** can be multiplied by −1 to achieve the desired right-handed orientation.

Assuming that the coordinates of the points in Cartesian system are stored in row vectors, the post-multiplication of the vectors with the rotation matrix can be used for transformation. In that case the final transformation matrix $\boldsymbol{V}$ can be written as

$$\boldsymbol{V}=\left[x''^{T}\quad y'^{T}\quad z'^{T}\right]=\boldsymbol{R}_z\boldsymbol{R}_y\boldsymbol{R}_x \tag{9}$$

where $\boldsymbol{R}_z$, $\boldsymbol{R}_y$ and $\boldsymbol{R}_x$ are transformation matrices, each of which rotates the coordinate system around the given axis:

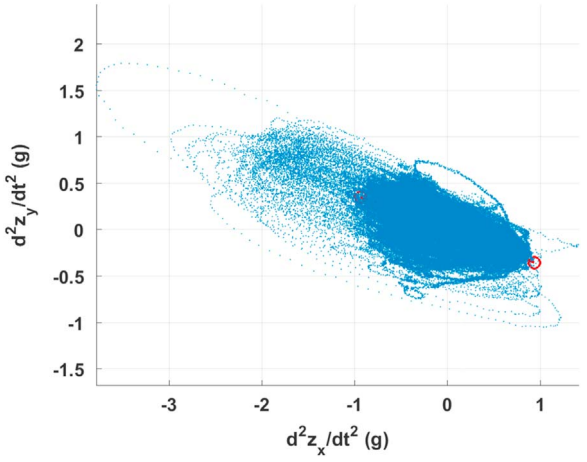

Fig. 4. Projection of the measured data with multiple frequencies into XY plane.

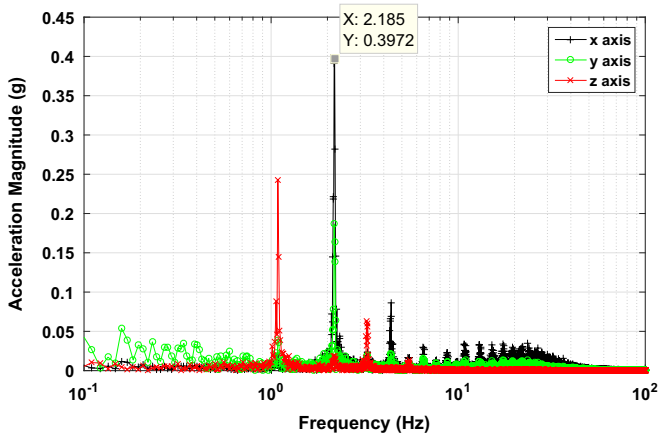

Fig. 5. FFT of the measured acceleration data with noticeable multiple peaks on different frequencies and in different measurement directions.

$$\boldsymbol{R}_z=\begin{bmatrix}\cos\psi & -\sin\psi & 0\\ \sin\psi & \cos\psi & 0\\ 0 & 0 & 1\end{bmatrix}, \tag{10}$$

$$\boldsymbol{R}_y=\begin{bmatrix}\cos\theta & 0 & \sin\theta\\ 0 & 1 & 0\\ -\sin\theta & 0 & \cos\theta\end{bmatrix}, \tag{11}$$

$$\boldsymbol{R}_x=\begin{bmatrix}1 & 0 & 0\\ 0 & \cos\phi & -\sin\phi\\ 0 & \sin\phi & \cos\phi\end{bmatrix}, \tag{12}$$

The rotation angles ϕ, θ, ψ are found by using goniometric functions, exploiting the knowledge of original coordinates of coordinate system axes and their desired new positions.

$$\psi=atan2\left(\frac{x''_2}{x''_1}\right) \tag{13}$$

$$\theta=-asin(x'_3) \tag{14}$$

$$\phi=atan2\left(\frac{y'_3}{y'_2}\right) \tag{15}$$

where x''_n is the n-th coordinate of the x axis after first two rotations around z and y. y'_n is the n-th coordinate of the y axis after the first rotation around x. This can be found also as a sequence of backward rotations of the known y'' axis vector:

$$y'=y\boldsymbol{R}_x{}^T=y''\boldsymbol{R}_z\boldsymbol{R}_y \tag{16}$$

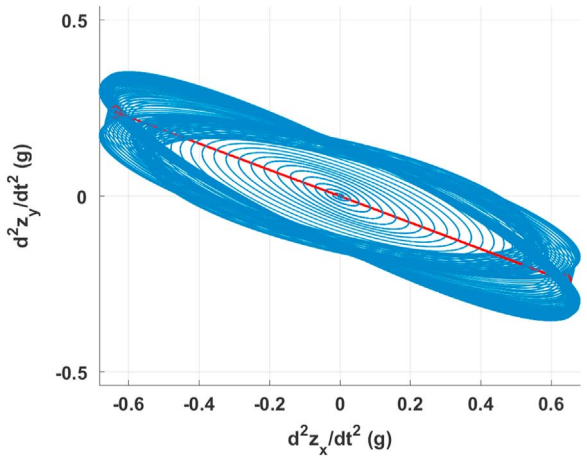

Fig. 6. Filtered frequency of interest from the measured data. Red line indicates the first principal direction of the filtered acceleration data.

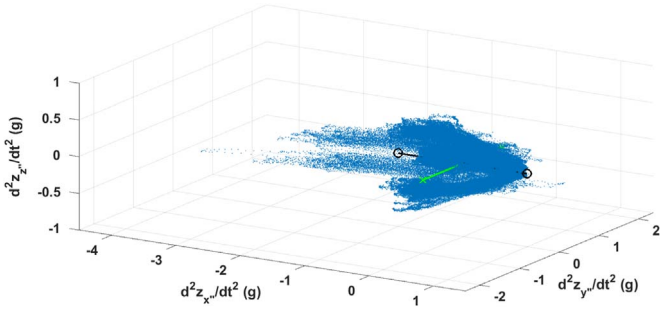

Fig. 7. Rotated measurement data with first two principal components of the frequency of interest indicated as black and green lines, respectively.

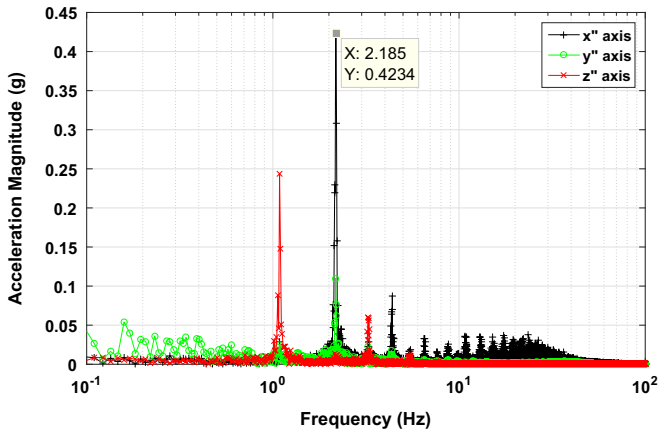

Fig. 8. FFT of the rotated measurement data. The magnitude of the acceleration with desired frequency of interest is maximized along the new x axis.

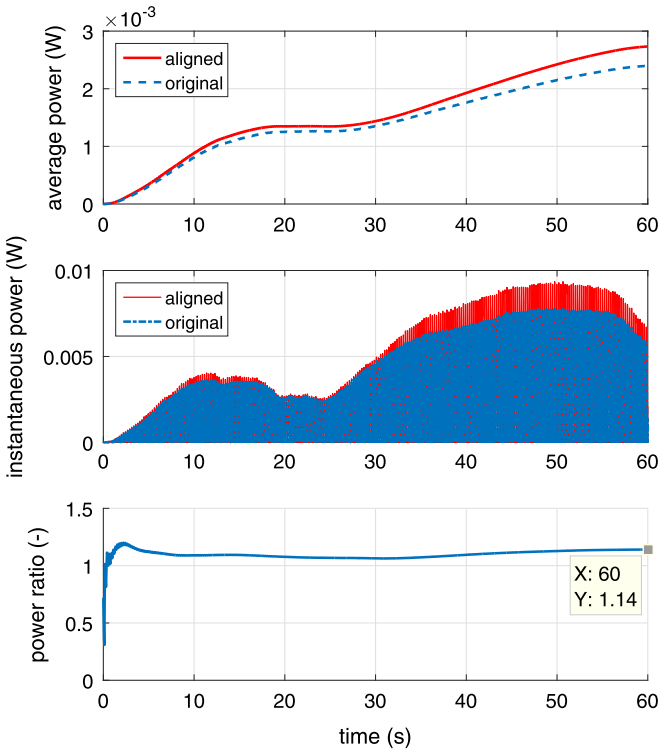

Fig. 9. Comparison of the harvester performance before and after the alignment with the principal axis of acceleration.

Table 1
Simulated improvements in the power output after aligning the harvester working axis with the principal component of the excitation acceleration.

Measured system	Frequency of interest (Hz)	Highest measured acceleration component (g)	First principal component of acceleration (g)	Rotation Angles ϕ, θ, ψ (rad)	Harvester power output ratio (dimensionless)
Human walking - wrist	1.12	0.269	0.427	0.7237–0.6568–2.2941	2.72
Human walking – head	2.19	0.397	0.423	0.17540.0052–0.3604	1.14
Helicopter TGB [17]	17.07	0.792	0.980	2.42150.36852.1387	1.50
Helicopter RAGB [17]	34.15	0.723	0.742	−0.27390.24350.0692	1.07
Helicopter APU [17]	34.15	0.810	0.906	−0.0914–0.46030.0425	1.25
Unspecified technical system I	58.23	0.723	0.723	000	1.00
Unspecified technical system II	62.47	0.188	0.237	00–0.7371	1.40
CNC machine I	66.7	0.083	0.099	00–0.6148	1.41
CNC machine II	200	0.033	0.034	00–0.3164	1.09

Applying the rotation succession on the measured data represents changing the orientation of the harvester and leads to aligning the principal components of the acceleration with the new axes of the coordinate system (Figs. 7 and 8).

6. Simulations

The presented method was used to process measured data from several different applications. The power output comparison was then simulated, using a generic spring-mass-damper model of a linear kinetic energy harvester with a single degree of freedom. The model was built according to (4) with Q factor 50 and viscous damping force evenly distributed between the mechanical and electrical damping. The weight of the simulated proof mass was 10 g and the harvester was tuned to the frequency of interest of each application.

For exciting the harvester model with the measured data the axis with the highest magnitude of the acceleration component at the frequency of interest was used. That ensures obtaining the maximum power output with the harvester aligned with the measurement axes of the accelerometer. Then the transformed data was used for excitation, simulating aligning the working axis of the harvester with the calculated principal axis of acceleration.

Comparison of the average power, instantaneous power and ratio of average generated power for new and original orientation of the harvester placed on human head is visible on Fig. 9.

Data from 9 measurements on 7 different systems with application potential for energy harvesting were used to evaluate possible gains of the proposed method for improving the power output of energy harvesters.

Results (Table 1) indicate, that in 8 out of 9 cases the measured axes of acceleration were not perfectly aligned with the principal axes of the acceleration. Therefore a simple rotation of the harvester without changing any other parameters could significantly improve the generated power output. Acceleration measurements in last four rows in Table 1 were done using two-axis accelerometer, and thus a single rotation is sufficient to achieve the optimum position of the harvester with respect to the measured data.

7. Conclusions

This paper presents a way of processing the acceleration data in order to better estimate the power output capabilities of kinetic energy harvesters. The presented method relies on finding the principal components of the acceleration with a selected frequency and on aligning the working axis of the harvester along the largest principal component direction. In most cases this method provides an easy to implement way of improving the performance of 1 dof kinetic energy harvester. Additionally, in case of using multiple dof harvester with perpendicular working axes, the method reveals also the second-best working direction with the same frequency. Furthermore, by exploiting an iterative approach it is possible to find the principal acceleration directions of multiple frequencies for wideband multiple dof harvester. Knowledge of the real data characteristics obtained by this method can thus provide a valuable information for the feasibility study and design optimization phase of the perspective inertial energy harvesters.

Acknowledgments

This work is an output of research and scientific activities of NETME Centre, supported through project NETME CENTRE PLUS (LO1202) by financial means from the Ministry of Education, Youth and Sports in Czech Republic under the “National Sustainability Programme I”.

References

[1] A. Harb, Energy harvesting: state-of-the-art, Renew. Energy 36 (2011) 2641–2654. http://dx.doi.org/10.1016/j.renene.2010.06.014.
[2] P.D. Mitcheson, Energy harvesting for human wearable and implantable bio-sensors, in: Conf. Proc. IEEE ENG. MEd. Biol. Soc., 2010, pp. 3432–3436. ⟨http://www.scopus.com/inward/record.url?eid=2-s2.0-84903867307&partnerID=tZOtx3y1⟩.
[3] T. Galchev, H. Kim, K. Najafi, Micro power generator for harvesting Low-frequency and nonperiodic vibrations, J. Microelectromech. Syst. 20 (2011) 852–866. http://dx.doi.org/10.1109/JMEMS.2011.216l0045.
[4] H. Liu, Y. Qian, C. Lee, A multi-frequency vibration-based MEMS electromagnetic energy harvesting device, Sens. Actuators A Phys. 204 (2013) 37–43. http://dx.doi.org/10.1016/j.sna.2013.09.015.
[5] T.-W. Ma, H. Zhang, N.-S. Xu, A novel parametrically excited non-linear energy harvester, Mech. Syst. Signal Process. 28 (2012) 323–332. http://dx.doi.org/10.1016/j.ymssp.2012.01.017.
[6] K. Fan, J. Chang, F. Chao, W. Pedrycz, Design and development of a multipurpose piezoelectric energy harvester, Energy Convers. Manag 96 (2015) 430–439. http://dx.doi.org/10.1016/j.enconman.2015.03.014.
[7] A.G.A. Muthalif, N.H.D. Nordin, Optimal piezoelectric beam shape for single and broadband vibration energy harvesting: modeling, simulation and experimental results, Mech. Syst. Signal Process. 54- 55 (2015) 417–426. http://dx.doi.org/10.1016/j.ymssp.2014.07.014.
[8] A. Syta, C.R. Bowen, H.A. Kim, A. Rysak, G. Litak, Responses of bistable piezoelectric-composite energy harvester by means of recurrences, Mech. Syst. Signal Process. 76–77 (2016) 823–832. http://dx.doi.org/10.1016/j.ymssp.2016.01.021.
[9] P. Pillatsch, E.M. Yeatman, A.S. Holmes, Magnetic plucking of piezoelectric beams for frequency up-converting energy harvesters, Smart Mater. Struct. 23 (2014) 25009 ⟨http://stacks.iop.org/0964-1726/23/i=2/a=025009⟩.
[10] M. Guan, W.-H. Liao, Design and analysis of a piezoelectric energy harvester for rotational motion system, Energy Convers. Manag 111 (2016) 239–244. http://dx.doi.org/10.1016/j.enconman.2015.12.061.
[11] C.P. Le, E. Halvorsen, E.M. Yeatman, O. Sorasen, Microscale electrostatic energy harvester using internal impacts, J. Intell. Mater. Syst. Struct. 23 (2012) 1409–1421. http://dx.doi.org/10.1177/1045389×12436739.
[12] S.D. Nguyen, E. Halvorsen, Nonlinear springs for bandwidth-tolerant vibration energy harvesting, J. Micro. Syst. 20 (2011) 1225–1227. http://dx.doi.org/10.1109/JMEMS.2011.2170824.
[13] S. Mohammadi, A. Esfandiari, Magnetostrictive vibration energy harvesting using strain energy method, Energy 81 (2015) 519–525. http://dx.doi.org/10.1016/j.energy.2014.12.065.
[14] M. Li, Y. Wen, P. Li, J. Yang, X. Dai, A rotation energy harvester employing cantilever beam and magnetostrictive/piezoelectric laminate transducer, Sens. Actuators A Phys. 166 (2011) 102–110. http://dx.doi.org/10.1016/j.sna.2010.12.026.
[15] G. Zhu, P. Bai, J. Chen, Z. Lin Wang, Power-generating shoe insole based on triboelectric nanogenerators for self-powered consumer electronics, Nano Energy 2 (2013) 688–692. http://dx.doi.org/10.1016/j.nanoen.2013.08.002.
[16] F.-R. Fan, Z.-Q. Tian, Z. Lin Wang, Flexible triboelectric generator, Nano Energy 1 (2012) 328–334. http://dx.doi.org/10.1016/j.nanoen.2012.01.004.
[17] Z. Hadas, C. Ondrusek, V. Singule, M. Kluge, Vibration power generator for aeronautics applications, in: Proc. 10th Anniv. Int. Conf. Eur. Soc. Precis. Eng. Nanotechnology, EUSPEN 2008, euspen, 2008, pp. 46–50. ⟨http://www.scopus.com/inward/record.url?eid=2-s2.0-84908312361&partnerID=tZOtx3y1⟩.

ANNEX A3

SMILEK, Jan, Filip CIESLAR and Zdenek HADAS

Measuring acceleration in the area of human head for energy harvesting purposes

In: *Proceedings of the 2016 17th International Conference on Mechatronics - Mechatronika, ME 2016*. 2017. ISBN 9788001058831.

Measuring Acceleration in the Area of Human Head for Energy Harvesting Purposes

Jan Smilek*, Filip Cieslar* and Zdenek Hadas*
* Faculty of Mechanical Engineering, Brno University of Technology, Technicka 2896/2, 616 69 Brno, Czech Republic
e-mail: *smilek@fme.vutbr.cz, 162529@vutbr.cz, hadas@fme.vutbr.cz*

***Abstract*—This paper deals with measurements and statistical processing of the acceleration data measured in the area of the human head. Kinetic energy harvesters require such levels of acceleration for their excitation that could possibly be obtained from human movements. 30 different people with different characteristics were thus measured during walking at controlled speeds in order to find the common frequencies and relevant magnitudes in the acceleration waveforms. Different ways of mounting the accelerometer to the head are also presented and the measurement results compared to identify and filter out the parasitic acceleration frequencies.**

Keywords-energy harvesting; biomedical devices; wearable electronics; acceleration measurements

I. INTRODUCTION

Latest technological advances in the field of wearable electronics and in biomedical applications, such as pacemakers, cochlear implants, various sensors and health monitors etc., call for a battery-less power source, that would increase the user comfort and allow for the true autonomy of such applications. Current battery-dependant power sources significantly limit the service life especially of the biomedical sensors. Depleting the battery power of biomedical implants might require a surgical removal of the device to change the battery or the whole device, which lowers the user comfort and increases the stress placed on the users of such devices. The observable trend of lowering the power consumption of such devices in recent years [1], [2] could mean that in the near future the energy harvesting approach will become a feasible way of providing the power to modern low-consumption wearable and medical devices. Energy harvesting is a fast growing discipline dealing with exploiting waste power of ambient environment and converting it into electricity to power up some low-consumption applications [3]. Some industrial applications are already employing the energy harvesting devices and with the progress in the research and development of the smart materials and structures it can be expected that energy harvesters will become even more commonly used.

II. HUMAN WALKING AS A SOURCE OF ENERGY

Human body contains levels of energy high enough to ensure its proper function. Small part of this energy is theoretically possible to exploit for energy harvesting purposes. Various attempts to utilize the human power have been recorded and published many times in the past decade. Some of them rely on the thermoelectric effect to utilize the thermal gradient appearing between the outer environment and human body [4], while others harvest the otherwise wasted mechanical energy from the human activity in order to employ some form of electromechanical energy conversion [5], [6].

Published electromechanical energy harvesters utilize different excitation strategies and conversion methods. The electromechanical harvesters for industrial applications are often designed as velocity damped resonant devices [7], providing maximum power output in a narrow band around the resonant frequency. On the other hand, many designs for harvesting the human power rely on the impact excitation from the foot strikes [8], [9] or even direct force excitation by bending the limbs or flexing the muscles [10].

In the head area of the user the possibilities of direct force or impact-based harvesters are rather limited, with the exceptions of utilizing the ear canal deformation and/or jaw movement [11]. The study shows, that theoretical levels of the available kinetic energy in the head area of the human reach up to 7 mW, considering velocity damped resonant harvester with 48 g proof mass [12]. This weight however might be simply too heavy for the practical applications of powering up the biomedical devices such as cochlear implants. Furthermore the results are bound to be very dependent on the behaviour of the user.

Previous measurements [13] indicated, that walking and running can provide sufficient excitation for inertial electromechanical energy harvester placed in the head area of the user. Other activities, such as random movements, associated with the typically sedentary working style of an average person did not result in acceleration magnitudes that could be easily used for the excitation of the harvester.

However, the experiments raised questions of measured frequencies dependency on the way of fixing the accelerometer to the user and dispersion of available frequencies and magnitudes in a larger number of different users. In this paper we address the mentioned issues by employing two different ways of fixing the accelerometer to the user's head and comparing the measured data in order to identify possible parasitic frequencies caused by the imperfect fixation of the sensor. In the second part of the paper we present basic statistical results from measuring 30 different users during walking at constant speed.

III. MEASUREMENTS

A. Methodology

Acceleration measurements during walking were conducted on the set of 30 testing subjects. The subjects were asked to walk on a flat surface at set constant speed between 3.8 and 4.4 kmph monitored by a personal speedometer. The used device was a wireless data logger Mide Slam Stick, containing a three axis MEMS accelerometer capable of measuring acceleration levels from -16 to +16 g in the frequency range 0-300 Hz. The acceleration during walking was recorded in three axes perpendicular to each other (Fig. 1). The length of each measurement was 60 seconds and the sampling frequency was set to 3.2 kHz in order to prevent any aliasing issues.

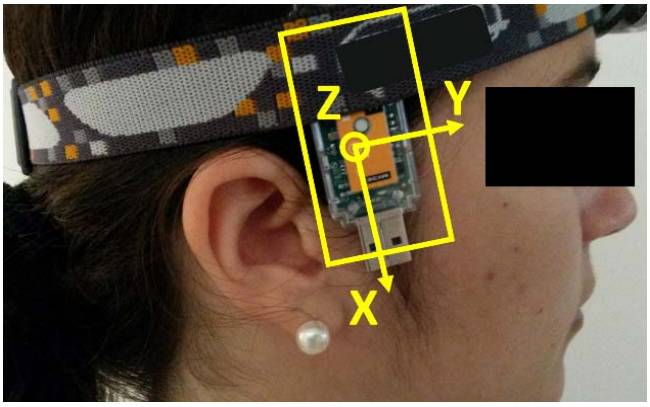

Figure 1. Datalogger fixed by the rubber band with indicated measurement directions

Two different ways of fixing the accelerometer to the head of each testing subject in order to determine the influence of the accelerometer fixing on the recorded data. In the first set of measurements the accelerometer was fixed using a 25mm wide flexible rubber band. The second set of another 30 measurements features the accelerometer fixed by a tight textile headband (Fig. 2).

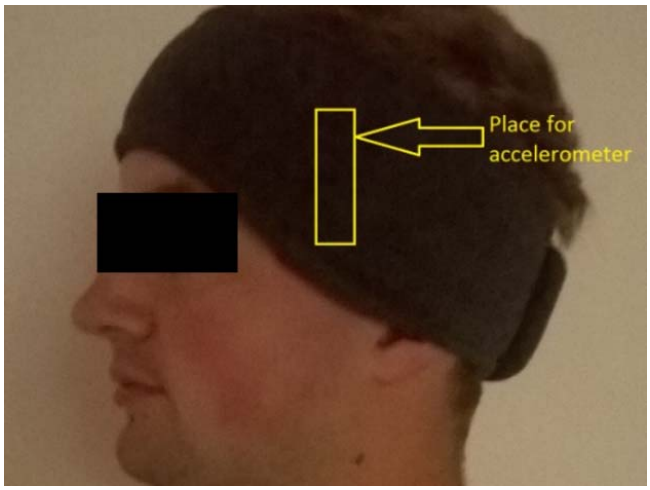

Figure 2. Datalogger fixed by the textile headband

Measured data sets were then processed in Matlab to determine the influence of monitored human features on the measured magnitudes and frequencies. The textile headband fixation data were used in this step for the processing.

B. Testing Subjects Parameters

The monitored features of the testing subjects were their age, height, weight and medium thickness of the shoe sole (Tab. 1).

TABLE I. MONITORED FEATURES OF THE TESTING SUBJECTS

	Mean Value	Variance	Standard Deviation
Age [years]	25.60	96.39	9.82
Height [m]	1.74	0.01	0.08
Weight [kg]	72.20	146.88	12.12
Sole Thickness [mm]	15.40	33.19	5.76

Following histograms represent the distribution of each of the monitored parameters in the observed set of testing subjects (Fig. 3).

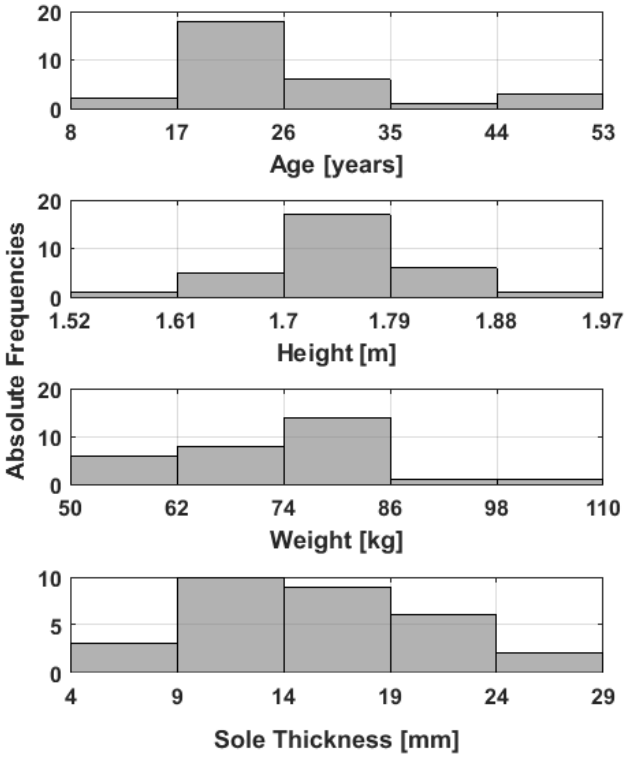

Figure 3. Distributions of the monitored features over the testing set of subjects

The cross-correlations between the monitored features were calculated to help preventing possible future false correlation issues. The calculation results suggest that most of the monitored features are linearly independent, with the exception of weight and height coupling (Tab. 2).

TABLE II. CORRELATION COEFFICIENT TABLE BETWEEN THE MONITORED FEATURES

	Age	Height	Weight	Sole Thickness
Age	X	-0.077	0.198	0.138
Height	-0.077	X	0.775	0.245
Weight	0.198	0.775	X	0.197
Sole thickness	0.138	0.245	0.197	X

IV. RESULTS

A. Fixation Style Comparison

Comparing the FFT of measured data showed, that both ways of fixing the accelerometer to the user's head result in fairly similar spectra obtained (Fig. 4). The differences in some of the data sets are clearly caused by slightly different walking speeds of the subjects during the measurements.

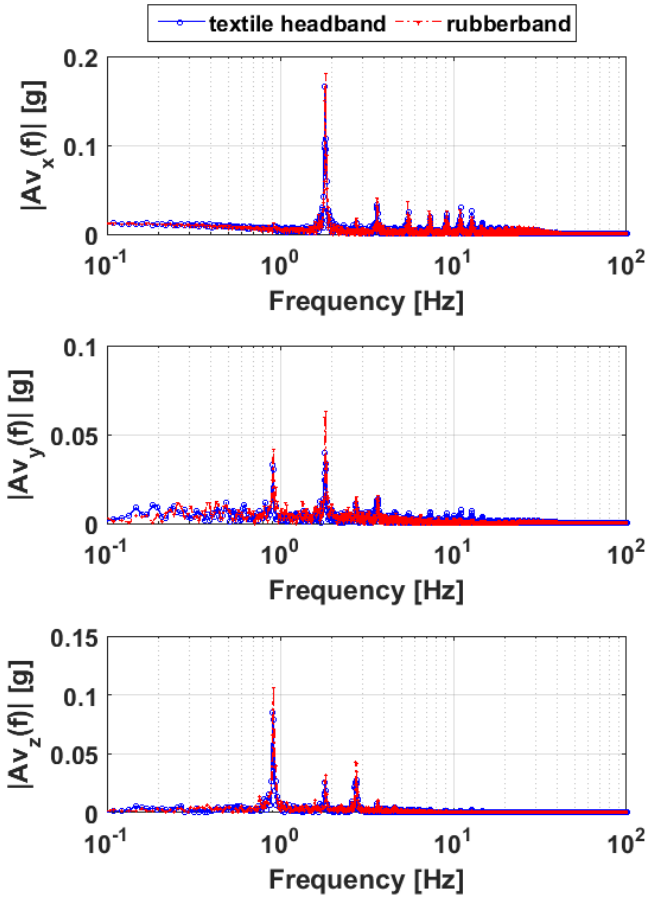

Figure 4. Example of the fixing techniques comparison using FFT on data obtained from measurement axes x, y, z, respectively

The initial assumption was that using imperfectly tight fixation of the accelerometer to the human head might significantly affect the measurements and thus lead to overly optimistic results in follow-up energy harvester design simulations.

However, the expected unmirrored parasitic higher frequencies were observed only in 2 out of the 30 pairs of measurements. In these measurements they are however probably caused by slightly faster walking pace of the user during the measurement, which is observable by comparing the frequencies of the first dominant peak of the acceleration (Fig. 5).

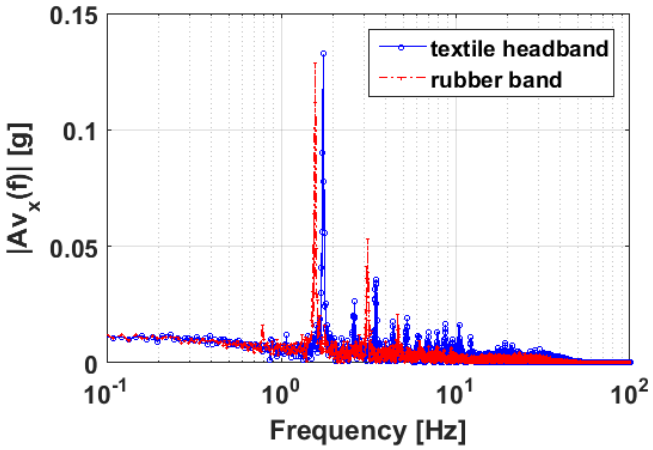

Figure 5. Not matching FFTs caused by different walking pace during the two measurement of the same subject

This change of pace could result in sharper impacts, leading to richer frequency spectrum in the higher frequency area. We therefore cannot confirm, that in any of these two cases the differences in the frequency spectra are caused by bouncing of the sensor in vertical direction due to slightly looser fixation to the head by the textile headband. As the tightness of the two fixation devices used was considerably different from each other, we disprove the original assumption and regard the measured frequency spectra as precise enough for the further simulations of the wearable and biomedical energy harvesting devices.

B. Influence of Monitored Human Features on Measured Acceleration

In the next step we tried to determine whether there is an observable linear relationship between the measured dominant frequencies and magnitudes of the acceleration and the monitored features of the measurement subjects.

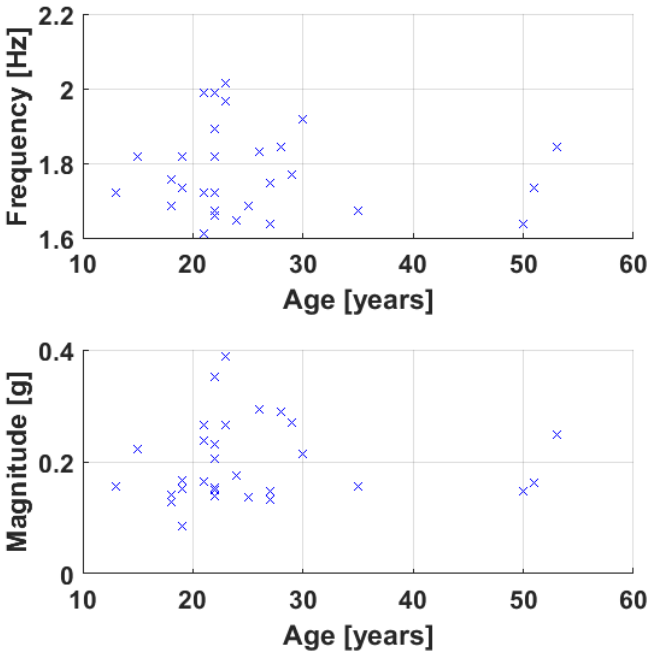

Figure 6. Dominant acceleration peak dependency on the age of the testing subject

Plotting the first dominant frequency and magnitude of the acceleration of this frequency against the monitored features mostly shows, that very little to no correlation can be found between the monitored features and the measured data reflecting the walking style of each particular testing subject (Fig. 6, 7, 8).

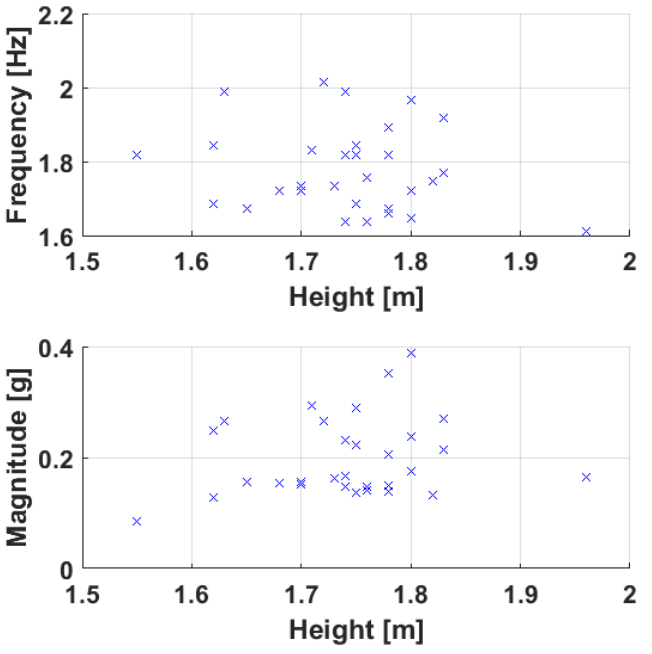

Figure 7. Dominant acceleration peak dependency on the height of the testing subject

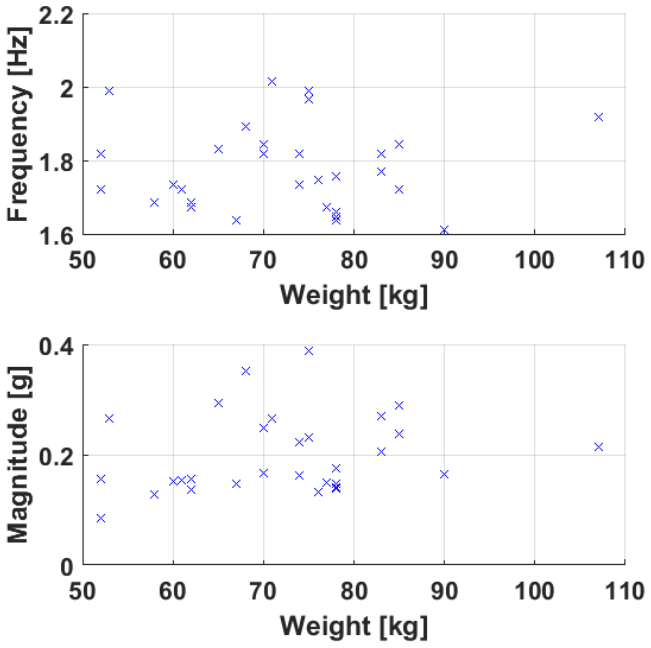

Figure 8. Dominant acceleration peak dependency on the weight of the testing subject

The exception seems to be the dependency of the measured dominant acceleration magnitude on the sole thickness, where the correlation coefficient indicates possible relationship between the two parameters (Fig. 9).

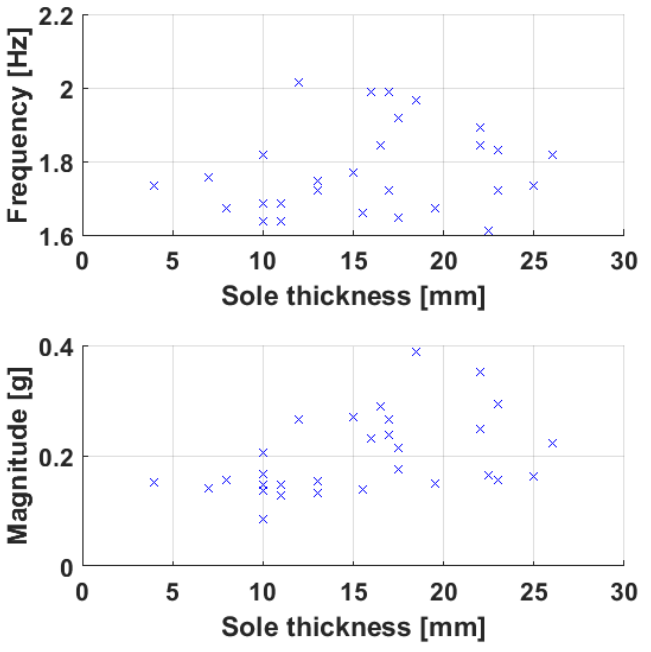

Figure 9. Dominant acceleration peak dependency on the shoe sole thickness of the testing subject

Calculated correlations between the first dominant frequencies and magnitudes of the acceleration and the monitored features for different users are listed in Tab. 3:

TABLE III. CORRELATION COEFFICIENTS BETWEEN THE MONITORED FEATURES AND THE FREQUENCY AND MAGNITUDE OF THE FIRST DOMINANT ACCELERATION PEAK

	Frequency	Magnitude
Weight	0.014	0.210
Height	-0.187	0.185
Age	-0.106	0.034
Sole Thickness	0.161	0.442

As no linear dependency between the monitored features and measured acceleration was observed, we decided to plot an overlay of 20 highest acceleration peaks from all the measured testing subject in order to determine the most common exploitable frequencies in the measured set (Fig. 10). This way it becomes visible that frequencies between 1.5 and 10 Hz could generally provide exploitable acceleration levels, regardless of the particular user's walking style.

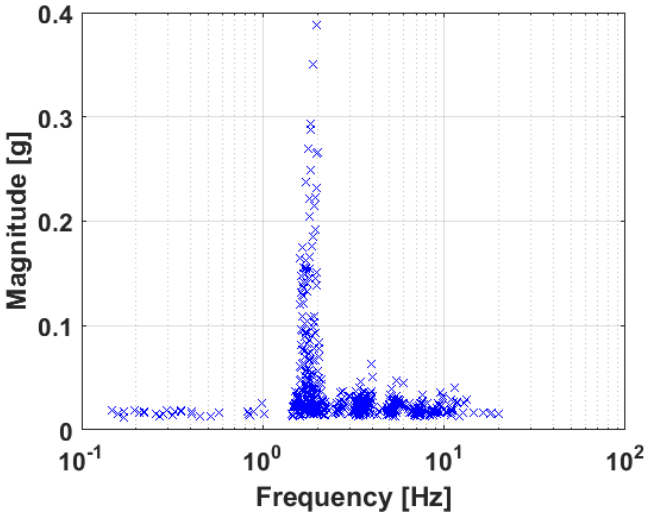

Figure 10. FFT overlay of 20 highest acceleration peaks of all the users.

V. APPLICATION OF THE RESULTS TO DEVELOPMENT OF ENERGY HARVESTERS

The data indicates that no direct correlation can be found between the observed attributes of the perspective users of the wearable energy harvesting devices and the expectable magnitudes of the acceleration available for energy harvester excitation. However, it is observed, that the frequency range in which the dominant frequencies of the measured datasets appear is very narrow. That can be exploited during the design phase of the kinetic energy harvesters for wearable and biomedical devices, as their oscillating mechanism can be tuned to roughly the same natural frequency, with the option of further fine-tuning it for each user individually. Indeed, the possibility of tuning the resonance mechanism to the first dominant frequency might be limited due to physical or technological constraints placed on the harvester and it might be necessary to use some of the higher frequencies present in the spectra for its excitation.

Using the well-known formula [14] we can calculate the power, dissipated in the harvester that is working in resonance with a harmonic excitation acceleration as

$$P_d = m.A_V^2 / (4.\Omega.b_p), \quad (1)$$

where A_V is the acceleration magnitude, m denotes the weight of the proof mass, Ω is the natural frequency of the harvester and b_p is the total damping ratio, evenly split between electrical and mechanical damping b_e and b_m, respectively. It is easy to find out, that the total dissipated power in the system will vary greatly for different users. Assuming the weight of the oscillating proof mass 10 g, which is close to the comfort limit for the head placement of the harvester, the damping ratio of 0.05, and using the first dominant frequency of each of the datasets as the natural frequency of the harvester, the total power dissipated in the harvester ranges from 3 to 58 mW for the measured testing subjects, without taking into account the design limitations of such harvester configurations. Half of this power will be wasted in mechanical losses, and the remaining half represents the harvested electrical power. The large span of dissipated power indicates, that designing an optimal and universal kinetic harvester for the whole range of possible users will be a challenging task and an individual approach of devices being optimized for their particular users might be more feasible.

VI. CONCLUSIONS

In this paper we discuss the acceleration measurements in the area of the human head for the purposes of energy harvester design and simulation. The effect of using different techniques for the fixation of the accelerometer on the testing subject's head are investigated to find out, whether the measured data bears parasitic frequencies caused by improper fixing of the sensor on the human head. As no parasitic frequencies were identified, the measured data were deemed correct and suitable for further processing and simulations. In the second part of the paper the linear relationship between four different monitored features of the test subjects and the measured data is sought. As such relationship is not found, the prediction of the acceleration in the head area of a random person during the walking is not yet possible even with the knowledge of the person's basic features. For that reason a different approach lying in plotting an overlay of selected number of highest acceleration peaks from each measurement set in order to identify the frequencies with the highest densities of acceleration peaks. These frequencies are intended to be used as design natural frequencies for the energy harvester for powering up the wearable and biomedical devices by converting a mechanical energy from the walking of any random user into electricity. However, simple simulations show, that employing a universal harvester design and parameters for the whole range of potential users might not be the best approach, as different users produce very different excitation waveforms, and the

harvester parameters should be optimized to a specific user to ensure the best behavior.

ACKNOWLEDGMENT

This work has been funded by the Faculty of Mechanical Engineering, Brno University of Technology, project FV 16-13 Multidisciplinary models for prototyping independent power sources.

REFERENCES

[1] M. Rasouli and L. S. J. Phee, "Energy sources and their development for application in medical devices.," *Expert Rev. Med. Devices*, vol. 7, no. 5, pp. 693–709, Sep. 2010.

[2] A. Cadei, A. Dionisi, E. Sardini, and M. Serpelloni, "Kinetic and thermal energy harvesters for implantable medical devices and biomedical autonomous sensors," *Meas. Sci. Technol.*, vol. 25, no. 1, p. 012003, Jan. 2014.

[3] D. Accoto, M. Calvano, D. Campolo, F. Salvinelli, and E. Guglielmelli, "Energetic analysis for self-powered cochlear implants.," *Conf. Proc. ... Annu. Int. Conf. IEEE Eng. Med. Biol. Soc. IEEE Eng. Med. Biol. Soc. Annu. Conf.*, vol. 2009, pp. 4860–3, Jan. 2009.

[4] M.-K. Kim, M.-S. Kim, S. Lee, C. Kim, and Y.-J. Kim, "Wearable thermoelectric generator for harvesting human body heat energy," *Smart Mater. Struct.*, vol. 23, no. 10, p. 105002, Oct. 2014.

[5] P. D. Mitcheson, "Energy harvesting for human wearable and implantable bio-sensors.," *Conf. Proc. IEEE Eng. Med. Biol. Soc.*, pp. 3432–3436, 2010.

[6] M. Wahbah, M. Alhawari, B. Mohammad, H. Saleh, and M. Ismail, "Characterization of Human Body-Based Thermal and Vibration Energy Harvesting for Wearable Devices," *IEEE J. Emerg. Sel. Top. Circuits Syst.*, vol. 4, no. 3, pp. 354–363, Sep. 2014.

[7] C. Cepnik, R. Lausecker, and U. Wallrabe, "Review on Electrodynamic Energy Harvesters—A Classification Approach," *Micromachines*, vol. 4, no. 2, pp. 168–196, Apr. 2013.

[8] P. Pillatsch, E. M. Yeatman, and A. S. Holmes, "A scalable piezoelectric impulse-excited energy harvester for human body excitation," *Smart Mater. Struct.*, vol. 21, no. 11, p. 115018, Nov. 2012.

[9] K. Ylli, D. Hoffmann, A. Willmann, P. Becker, B. Folkmer, and Y. Manoli, "Energy harvesting from human motion : exploiting swing and shock excitations," *Smart Mater. Struct.*, vol. 24, no. 2, p. 25029, 2015.

[10] Q. Li, V. Naing, and J. M. Donelan, "Development of a biomechanical energy harvester.," *J. Neuroeng. Rehabil.*, vol. 6, no. 1, p. 22, Jan. 2009.

[11] A. Delnavaz and J. Voix, "Energy Harvesting for In-Ear Devices Using Ear Canal Dynamic Motion," *IEEE Trans. Ind. Electron.*, vol. 61, no. 1, pp. 583–590, Jan. 2014.

[12] E. Goll, H.-P. Zenner, and E. Dalhoff, "Upper bounds for energy harvesting in the region of the human head.," *IEEE Trans. Biomed. Eng.*, vol. 58, no. 11, pp. 3097–103, Nov. 2011.

[13] J. Smilek and Z. Hadas, "A study of kinetic energy harvesting for biomedical application in the head area," *Microsyst. Technol.*, pp. 1–13, Dec. 2015.

[14] S. P. Beeby, M. J. Tudor, and N. M. White, "Energy harvesting vibration sources for microsystems applications," *Meas. Sci. Technol.*, vol. 17, no. 12, pp. R175–R195, Dec. 2006.

ANNEX A4

SMILEK, Jan, Tomas GRISA and Zdenek HADAS.

Statistical modelling of acceleration in the human head area for energy harvester performance prediction.

Smart Materials and Structures [in review, article ID: SMS-106858]

Impact factor: 2.909

Statistical modelling of acceleration in the human head area for energy harvester performance prediction

Jan Smilek[a,*], Tomas Grisa[b], Zdenek Hadas[a]

[a] Faculty of Mechanical Engineering, Brno University of Technology, Technicka 2896/2, 616 69 Brno, Czech Republic
[b] NBC Defence Institute, University of Defence, Vita Nejedleho 691, 682 01 Vyskov, Czech Republic
[*] E-mail: smilek@fme.vutbr.cz

Abstract – This paper deals with the statistical properties of the acceleration waveforms in the area of human head during walking. Statistical models are developed based on the empirical measurements of multiple testing subjects. The purpose of this is a realistic prediction of power outputs of an energy harvester, placed in the area of human head in order to power up a biomedical or wearable electronic application. This harvester must be able to work satisfyingly with different excitation patterns provided by a whole range of potential users. It is therefore essential to know how the acceleration waveforms during similar activities vary both for different measurements of a single person and for different people. Developed models are used to generate artificial acceleration data, which is in turn used to predict the performance limits of an inertial, human motion based linear energy harvester. The results of the analyses show a significant potential for kinetic energy harvesting in the head area, with possible theoretical specific power reaching up to 400 μW per gram of proof mass weight for a half of the potential harvester user population, without taking into account practical limitations, such as proof mass displacement limits.

Keywords – statistical modelling; energy harvesting; linear system; wearable electronics; human motion; power prediction

1. Introduction

Smart textiles, printed electronics and miniaturization of the implantable sensors are allowing for a rapid spread of miniaturized electronic devices. Current trends show a still-increasing use of various wireless sensors in wearable electronics and biomedical applications [1]. A crucial limitation of these devices is the availability of an adequate power source. Use of primary cells is quite limited, as they cannot be recharged, and must be therefore either easily replaceable, or they must provide enough energy to cover the whole designed lifetime of the powered device. Secondary cells are more feasible in the sense, that their maintenance consists of recharging, not replacing, and does not therefore create more waste to be disposed of or recycled. The need for maintenance itself, however, is a limiting factor that decreases the level of user comfort. This need could be mitigated by or even completely eliminated by employing an independent power source, exploiting an energy harvesting principle [2]. There are numerous papers published on the sources of power, available in the ambience of human body [3], [4]. Some of them evaluate utilization of solar [5] energy or the energy of thermal gradient [6], other focus on the conversion of the kinetic energy from the human motion to electricity [7]. For these kinetic energy harvesting devices the levels of kinetic energy available for energy harvesting are essential for an efficient and functional design.

While some of the kinetic energy harvesters exploiting human motion rely on the direct force excitation [8], [9], many the designs are inertial harvesters, where a relative motion of the proof mass against the frame of the harvester is excited by an acceleration of the frame [10].

Previous studies [11], [12] showed, that the available energy levels fluctuate considerably during the different activities of the energy harvester user. It has been reported, that every-day activities other than walking or running usually do not provide high enough magnitudes of the input acceleration for the inertial energy harvesters [13]. However, even during the walking the levels of acceleration available for the harvester excitation vary significantly for different people [14].

Papers published on the topic often work with quite a small sample of measurement subjects, making it difficult to generalize the reported results. Some papers [15] report statistics for moderately high number of measurement subjects, but they focus on the random activities during a whole day observation.

Our goal is to focus on one clearly defined activity instead, in order to develop the statistical models for this particular activity. In our earlier work [16] we tried to find a linear relationships between a set of observed

parameters of the measurement subjects and acceleration waveforms they provided during a series of measurements during walking. As such a relationship was not found, this paper focuses instead on the statistical modelling of the acceleration in the area of human head, regardless of the people's characteristics. Developed statistical models are then used for power output prediction of a linear energy harvester.

2. Acceleration Measurement Methodology

Acceleration data in the human head area were measured empirically. During the first stage of measurements a single subject (male, 28 years, 183 cm, 71 kg) was measured 40 times in the course of three days and during different day times. Second stage comprised of measuring 51 different subjects (Tab. 1), each of them only once. All the subjects were told to walk at their natural walking speed on the predefined smooth and level path. A MIDE Slam stick C wireless datalogger containing a three-axial MEMS accelerometer was firmly attached to the side of the subject's head by a tight headband. This accelerometer can measure acceleration levels between +- 16 g with the 0.004 g resolution in the frequency range 0-500 Hz with 5% accuracy in all three orthogonal measurement axes.

Parameter	Value
Sex	39 M, 12 F
Age [years]	24.67±7.56
Height [cm]	176.96±7.83
Weight [kg]	73.60±10.39

Tab. 1 Basic properties of the measurement set

The fixed sampling rate of 3200 Hz was used during the measurements, and a built-in 100 Hz cut-off filter was employed to reduce the high frequency noise. Each of the measurements lasted 90 seconds. The x-axis of the measurement roughly corresponded with the vertical axis, y-axis was aligned with the side of the head and z-axis was oriented along the approximated lateral axis of the subject's head.

3. Measured Data Treatment

The measured data were treated and reduced in order to obtain datasets suitable for further statistical processing. The first step of treatments employed the Principal Component Analysis (PCA) method, as described in our previous work [17] in order to correct for possible misalignments and misplacements of the datalogger on the head of testing subjects during different measurement sessions. The method is based on filtering the original dataset to obtain only acceleration data on the frequency of interest, and its subsequent rotation in Cartesian space in such a way, so that the magnitude of acceleration is maximized in the first orthogonal axis, and minimized in the third axis. This way the rotation angles for the original dataset are obtained, allowing for the spatial rotation of the data coordinate system so that the acceleration on desired frequency is maximized along the aligned X axis and minimized along the aligned Z axis, regardless of the other frequency components. The dominant frequency of each measurement was used as the reference frequency, the magnitude of which is to be maximized along the X axis by the PCA algorithm.

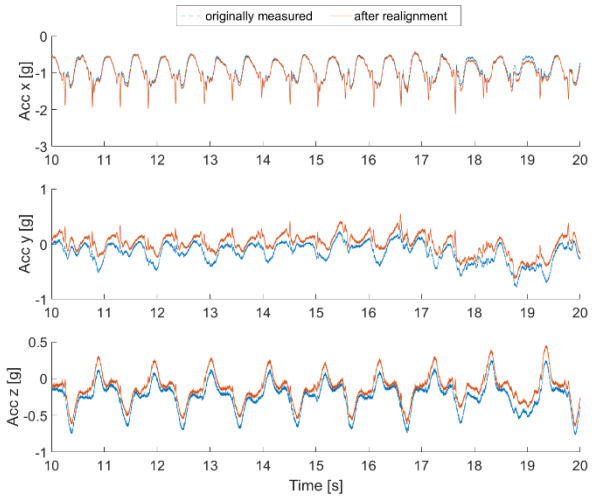

Fig. 1 Example of the acceleration waveforms before and after alignment

Comparison of the waveforms in the three orthogonal axes before and after alignment (Fig. 1), and histograms of the calculated rotation angles (Fig. 2) needed to align the measurement axes with the principal components of the acceleration on the reference frequency show that the orientation of the datalogger mostly did not perfectly correspond with the principal components of the acceleration.

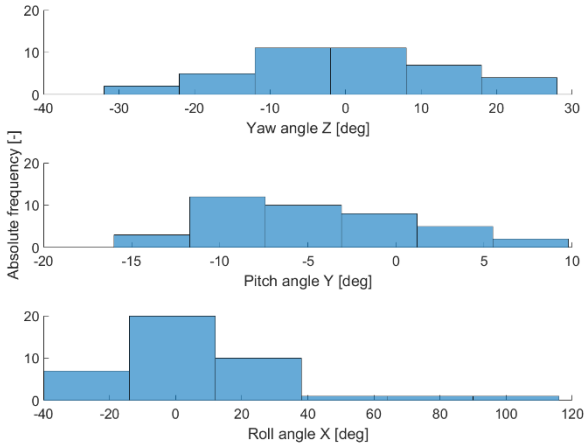

Fig. 2 Distributions of yaw, pitch and roll angles used for data alignment

This can be accounted to the following possible causes: the need for rotation around the Z measurement axis can be caused by a head up or down position during walking or by a misalignment of the datalogger. The necessity of a realignment around the direction of the X measurement axis can be caused by the shape of the human skull, by a rotation of the head during measurements and also in some cases by different placement of the datalogger during the measurement (e.g. on forehead instead on the temple). Corrections needed around Y measurement axis were generally marginal and could be attributed to the shape of the skull again. The calculated correction angles also support the expectation that the principal components of the acceleration during walking can be found along the normals to the transverse, coronal and sagittal planes of the human body (Fig. 3).

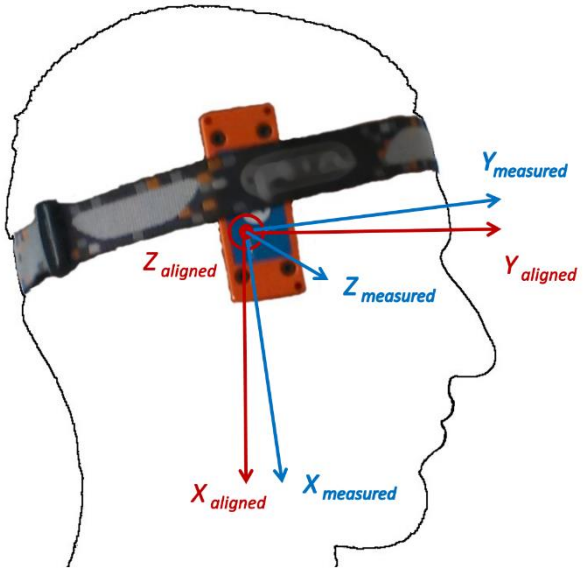

Fig. 3 Datalogger position with visible measurement axes (blue) and axes aligned to the principal components of the acceleration during walking (red)

After all the measured datasets were aligned in the same manner, each set was transferred into the frequency domain by the means of FFT calculation and each axis was reduced to ten frequency-magnitude-initial phase triplets with the frequencies falling within the range 0.6 – 10 Hz. Higher frequencies did not provide any acceleration levels potentially useful for energy harvesting, and they were therefore omitted completely. Even

though in the measured dataset the frequencies over circa 3 Hz do not carry as much energy as the dominant walking frequencies around 2 Hz, it was decided to keep the whole aforementioned frequency range, because it might not be practically feasible for some inertial energy harvester designs to be tuned to work in the lower part of the selected spectrum due to e.g. proof mass displacement limitations. It might thus be beneficial to analyse the higher frequencies as well, for the sake of future practical energy harvester device development.

An attempt to statically parse the frequency range into ten static intervals and to find a dominant acceleration peak in each interval did not provide reliable results especially in the second half of the spectrum of interest. It was therefore decided to adopt an assumption that the dominant peaks contained in the frequency spectra are harmonics of the fundamental frequency, which corresponds to the stride frequency of each person. Assuming this, a dynamic parsing of the spectra was employed. The frequency range was split into ten intervals, each with a length of one fundamental frequency and centred around one assumed harmonic frequency (Fig. 4).

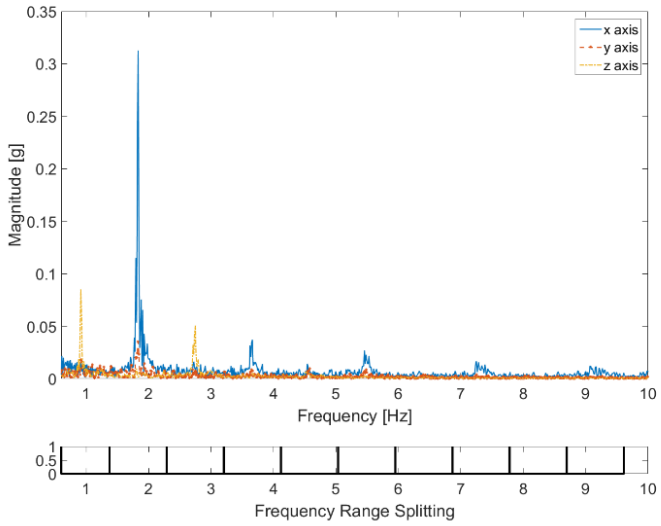

Fig. 4 Example of a measured frequency spectra with dynamic parsing into intervals

Every interval was then searched for its dominant acceleration peak and the corresponding frequency independently in each of the three axes. The correlation coefficients were calculated between the dominant frequency with highest magnitude (principal frequency) and other obtained frequencies within the spectrum of interest in each axis. The results support the expectation that the dominant frequencies found are the harmonics of the fundamental stride frequency (Tab. 2 and 3).

Frequency interval no.	Single test subject			Multiple test subjects		
	X axis	Y axis	Z axis	X axis	Y axis	Z axis
1	0.81	0.13	**1**	0.11	0.16	**1**
2	**1**	**1**	0.15	**1**	**1**	0.68
3	0.83	0.65	0.79	0.69	0.85	0.97
4	0.80	0.82	0.35	0.94	0.76	0.82
5	0.79	0.50	0.87	0.85	0.61	0.90
6	0.89	0.71	0.33	0.94	0.91	0.87
7	0.51	0.55	0.80	0.90	0.77	0.90
8	0.92	0.70	0.40	0.98	0.92	0.91
9	0.35	0.59	0.66	0.89	0.83	0.88
10	0.93	0.67	0.65	0.97	0.87	0.89

Tab. 2 Linear correlation coefficients between the found frequencies in the spectrum and principal frequency of the corresponding axis

	XY dominant peak frequencies cross-correlation	XZ dominant peak frequencies cross-correlation
Single subject	0.85	0.94
Multiple subjects	0.90	0.97

Tab. 3 Cross-correlation coefficients between the principal frequencies in different axes

The results also suggest, that the dominant frequencies in X and Y axes correspond to the second harmonic frequency - the step frequency - and its higher harmonics, which in turn correspond to even harmonics of the fundamental stride frequency. The distinct dominant frequencies in the Z axis correspond to the stride frequency of each subject and its odd harmonics. The odd harmonics in X and Y and the even harmonics in Z axis are mostly diminished. This is visible also from lower correlation coefficients, as the diminished peaks can more easily blend with the measurement noise.

The comparison of the time series recreated from the reduced frequency-domain data, and the original measured data shows, that the dominant features of the waveforms are sufficiently preserved (Fig. 5) even after reducing the dataset size to the fraction of the original size by saving only ten dominant frequencies and corresponding magnitudes and initial phases from the whole measured spectra.

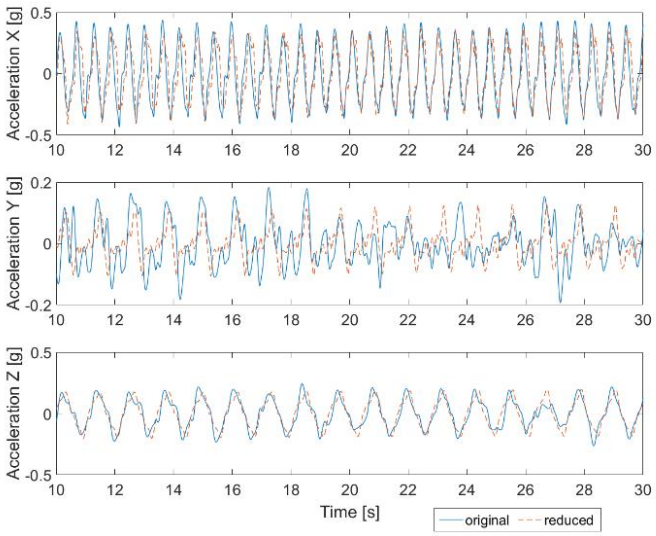

Fig. 5 Comparison of originally measured time series, and waveforms recreated from the reduced frequency domain data

The measured data were truncated by a constant during the processing to get rid of the time delay between the measurement start and the subject actually starting the activity. The waveforms after the processing were therefore misaligned. For that reason also the initial phase shifts obtained from the FFT did not share a common reference point. In order to model the data better, all the saved reduced data were realigned. This was done by recalculating all the initial phase shifts so that the initial phase of the first harmonic waveform in Z axis is nullified and the other phases are shifted accordingly (Fig. 6). The reference frequency for the phase alignment needs to be the lowest dominant frequency present in the spectra, as aligning the data to any higher reference frequency does not ensure the proper alignment of frequency components lower than the reference. Indeed, all three measurement axes in each dataset must be shifted consistently.

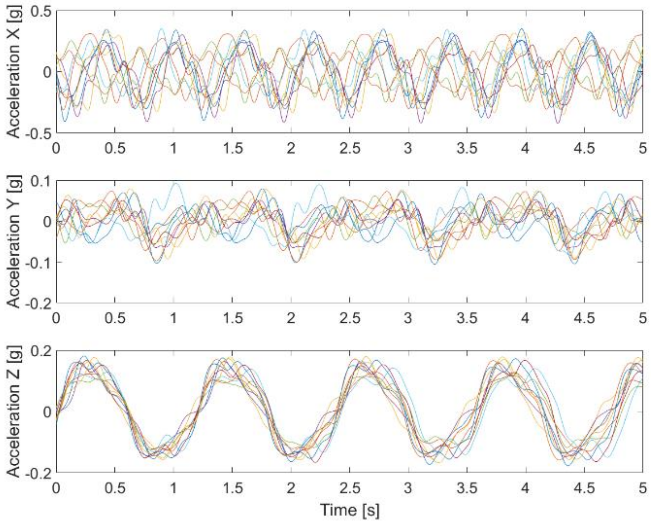

Fig. 6 Overlay of first ten saved waveforms aligned to the first dominant frequency in Z axis

The reduced data in frequency domain (Fig. 7) are easy to analyse in order to find their statistical properties. This will allow generating acceleration datasets for arbitrarily large model population, which can be exploited for predicting and evaluating the average performance of an energy harvesting device for generating electric power from human motion.

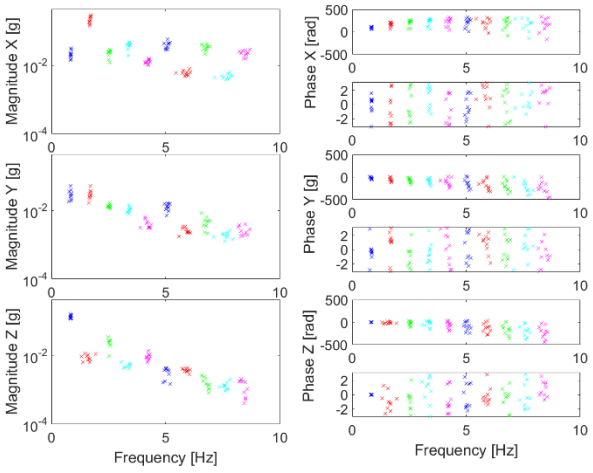

Fig. 7 Reduced data from ten random measurements displayed in frequency domain (left) with the initial phase originally obtained from FFT (right top) and wrapped to <– π,π> interval (right bottom)

4. Statistical processing of the data

Magnitude and frequency couples are sufficient to recreate the acceleration spectra, which can be used for estimating the power output of linear energy harvesting devices using the superposition principle. Nonlinear harvester models would however require also the information about the initial phase offset relationships between the different frequencies in the spectra, so that a time-domain signal could be credibly reconstructed. This information is included in the data obtained by the Fourier transform of the original signal. However, the initial phase obtained from FFT is not wrapped to any interval.

To be able to model whole frequency – magnitude – initial phase triplets for each axis and all ten selected frequency ranges, statistical distribution of such quantities has to be determined. It is natural to assume, that both frequency and magnitude follow normal distribution. In addition, it can be seen that also the initial phase can be assumed to follow a normal distribution. Generally, when wrapped to interval <0,2π>, which might seem useful for reconstructing the time-domain data, the initial phase seems to be uniformly distributed within the whole interval. But when obtained from FFT, initial phase is not wrapped to any interval and follows normal distribution. This is

caused by the fact that normal distribution with variance σ behaves like a uniform distribution when wrapped to interval with length less than 2*σ. Therefore, a simplification to model the initial phase by the uniform distribution would be incorrect, because possible correlations could be lost.

To support the aforementioned assumptions, appropriate statistical tests were deployed. For this reason, let us denote 90-dimensional random vector with multivariate normal random distribution by $\boldsymbol{X} = [X_1, \dots, X_{90}]^T$, where the elements represent frequencies, magnitudes and initial phases of all ten frequency ranges and all three orthogonal measurement axes. Sample mean and sample covariance were used to estimate the mean vector and the covariance matrix.

To begin with, it is important to detect and remove outliers from datasets. Such values could negatively affect estimation of parameters of normal distribution and therefore the test results. Measured values for each quantity were sorted and both tails of probability distributions were searched for repeating deviated measurements within all quantities. The deviated measurements correspond with the measurement runs, where the conditions were affected by external factors. These factors include other people walking together with the subject, forcing their natural speed on the measurement subject; or the subject trying to walk in unnatural style or pace. Such values should be removed.

As a next step, the Kolmogorov-Smirnov test [18] with the null hypothesis that the sample comes from the normal distribution with estimated parameters was used to test, if the normal distribution can be assumed. Then, two sampled Kolmogorov-Smirnov test was applied to check, whether the measured and the random number simulated samples come from the same distribution. This would indicate, whether the randomly generated samples can be used as an approximation of the measured acceleration data in frequency domain. For this purpose, samples of normally distributed random numbers with estimated parameters were generated. Then, the null hypothesis that the samples are drawn from the same distribution was tested.

Finally, this approach was validated by using the repeated random sub-sampling validation. Measured data were randomly split into training and validation subsets. For each such split, random number simulated samples with parameters estimated from training subset were generated and compared to the validation subset by two sampled Kolmogorov-Smirnov test. Ratio of non-rejected to all tests was used as a measure of fit for such a validation.

4.1 Single person measurements

The first step was to verify the statistical behaviour of single person's samples. As described, one sample Kolmogorov-Smirnov test was performed to verify if the samples come from the normal distribution with estimated parameters. Resulting p-values are presented in Tab. 4. It can be seen, that the null hypothesis was rejected at significance level $\alpha = 0.05$ only for Freq. 1, Y-axis and Phase 1, Z-axis. The first case was caused by the fact that the first harmonic frequency component is diminished in the spectra of X and Y axes, as mentioned in previous chapter. Therefore, the obtained values are heavily influenced by the measurement noise. Phase 1, Z-axis was rejected by the fact that this value was used as the reference initial phase, and therefore nullified.

The results of two sampled Kolmogorov-Smirnov test were in agreement with one sample Kolmogorov-Smirnov test. Due to this fact, resulting p-values were omitted. The repeated random sub-sampling validation shows, that 99.25 % of trials was not rejected. This result does not include rejected trials for Phase 1, Z-axis.

Based on the validation results and p-values of Kolmogorov-Smirnov tests, the assumption that frequency – magnitude – initial phase triplets of single person can be approximated by normal distribution is not rejected.

Single person	X axis			Y axis			Z axis		
Interval No.	Frequency	Magnitude	Phase	Frequency	Magnitude	Phase	Frequency	Magnitude	Phase
1	0.31	0.80	0.70	0.00	0.55	0.98	**0.34**	**0.44**	0.00
2	**0.85**	**0.60**	**0.99**	**0.46**	**0.35**	**0.78**	0.72	0.80	0.97
3	0.84	0.64	0.96	0.12	0.51	0.93	**0.38**	**0.83**	**0.99**
4	**0.99**	**0.35**	**0.95**	**0.55**	**0.97**	**0.86**	0.27	0.53	0.64
5	0.51	0.90	0.99	0.19	0.56	0.88	**0.97**	**0.97**	**0.92**
6	**0.84**	**0.74**	**0.92**	**0.95**	**0.90**	**0.56**	0.57	0.74	0.91
7	0.39	0.27	0.95	0.15	0.95	0.85	**0.08**	**0.59**	**0.90**
8	**0.91**	**0.86**	**0.93**	**0.83**	**0.12**	**0.86**	0.75	0.06	0.97
9	0.35	0.38	0.98	0.29	0.97	0.72	**0.49**	**0.76**	**0.52**
10	**0.96**	**0.89**	**0.99**	**0.86**	**0.08**	**0.86**	0.50	0.14	0.58

Tab. 4 p-values of one-sampled KS test for the measured data of the single person

4.2 Multiple people measurements

After non-rejecting the null hypothesis that the sample of single person comes from the normal distribution, the null hypothesis that the samples of multiple people comes from the normal distribution was tested as well. Procedure of the evaluation was identical to single person case.

From 51 measured samples, 6 samples were removed as outliers. Resulted p-values of one sample Kolmogorov-Smirnov test are presented in Tab. 5. Based on the results, the null hypothesis was rejected at significance level $\alpha = 0.05$ only for Freq. 1, X-axis and Phase 1, Z-axis. This is caused by the same facts as for the single person case.

The results of two sampled Kolmogorov-Smirnov test were in agreement with one sample Kolmogorov-Smirnov test. Due to this fact, resulting p-values were omitted. The repeated random sub-sampling validation shows, that 99.82 % of trials was not rejected. This result does not include rejected trials for Phase 1, Z-axis.

Based on the validation results and p-values of Kolmogorov-Smirnov tests, the assumption that frequency – magnitude – initial phase triplets of multiple people can be approximated by normal distribution is not rejected.

Multiple People	X axis			Y axis			Z axis		
Interval No.	Frequency	Magnitude	Phase	Frequency	Magnitude	Phase	Frequency	Magnitude	Phase
1	0.04	0.12	0.34	0.57	0.35	0.78	**0.53**	**0.54**	0.00
2	**0.68**	**0.31**	**0.90**	**0.64**	**0.57**	**0.60**	0.17	0.33	0.26
3	0.63	0.32	0.63	0.54	0.54	1.00	**0.41**	**0.74**	**0.83**
4	**0.98**	**0.68**	**0.72**	**0.93**	**0.55**	**0.98**	0.54	0.13	0.77
5	0.75	0.34	0.63	0.27	0.48	1.00	**0.43**	**0.76**	**0.77**
6	**0.76**	**0.50**	**0.63**	**0.77**	**0.77**	**0.88**	0.72	0.67	0.97
7	0.86	0.08	0.79	0.36	0.32	0.99	**0.89**	**0.22**	**0.68**
8	**0.71**	**0.92**	**0.63**	**0.91**	**0.99**	**1.00**	0.96	0.61	0.89
9	0.78	0.94	0.64	0.48	0.73	0.93	**0.94**	**0.43**	**0.95**
10	**0.96**	**0.76**	**0.57**	**0.59**	**0.34**	**0.89**	0.96	0.29	0.88

Tab. 5 p-values of one-sampled KS test for the measured data of multiple people

4.3 Statistical models

Based on the results of the statistical processing it can be assumed, that the measured acceleration data can be substituted by a modelled dataset. This dataset is entirely described by a normal distribution with the obtained mean vector and covariance matrix. Values of both these variables are provided in the Mendeley Data online repository (doi:10.17632/38fn2d6wp3.1) in order to allow their use for further research.

5. Harvested power predictions

5.1 Linear Energy harvester Model

Previous analyses enable us to generate artificial three-axial frequency or time-domain acceleration data that can be used for prediction of the energy harvester performance and optimization of its design without the necessity to conduct a large number of real-life tests.

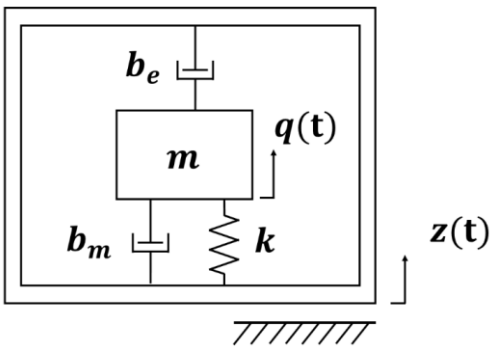

Fig. 8 Single DOF model of inertial energy harvester

A linear kinetic energy harvester with one degree of freedom and inertial excitation is usually modelled as a spring mass damper system (Fig. 8), dynamics of which is described by the 2nd order differential equation of motion

$$m\ddot{q} + (b_e + b_m)\dot{q} + kq = -m\ddot{z}, \tag{1}$$

where m is the proof mass of the harvester, b_e and b_m are the electrical and mechanical damping, respectively; k is the stiffness of the mechanical oscillator spring, $\ddot{z}$ is excitation acceleration and q is the displacement of the harvester proof mass. Defining the harvester natural frequency $\Omega = \sqrt{\frac{k}{m}}$, and its quality factor $Q = \frac{m\Omega}{b_e+b_m}$, Eq. (1) can be written in the form

$$\ddot{q} + \frac{\Omega}{Q}\dot{q} + \Omega^2 \mathrm{q} = -\ddot{z}, \tag{2}$$

where the design variables are the natural frequency of the harvester Ω and its quality factor Q. The quality factor Q can be written as an inversion of the sum of reciprocal values of mechanical and electrical quality factors.

$$Q = \left(\frac{1}{Q_e} + \frac{1}{Q_m}\right)^{-1} \tag{3}$$

The mechanical quality is a function of unavoidable mechanical energy losses in the system:

$$Q_m = \frac{m\Omega}{b_m} \tag{4}$$

while the electrical quality factor represents the extraction of energy from the oscillating system by the means of the electrical damping

$$Q_e = \frac{m\Omega}{b_e} \tag{5}$$

In order to maximize the total electrical power dissipated from the system the electrical and mechanical quality of the system should be the same, so that

$$Q_e = Q_m \tag{6}$$

$$Q = \frac{Q_m}{2} \tag{7}$$

Note that this domain matching [19] ensures maximum electric power dissipation from the system, but not the maximum obtainable power on load. The electric power extracted from the system by the electrical damping force is defined as

$$p(t) = F_e\dot{q} = b_e\dot{q}^2, \tag{8}$$

The proof mass displacement given a harmonic excitation acceleration $\ddot{z} = A_v \cdot \sin(\omega t)$ can be calculated as

$$q(t) = \frac{mA_v}{k\sqrt{\left(\frac{1}{Q}\cdot\frac{\omega}{\Omega}\right)^2 + \left(1 - \left[\frac{\omega}{\Omega}\right]^2\right)^2}} \cdot \sin(\omega t) = \frac{A_v\frac{1}{\Omega^2}}{\sqrt{\left(\frac{1}{Q}\cdot\frac{\omega}{\Omega}\right)^2 + \left(1 - \left[\frac{\omega}{\Omega}\right]^2\right)^2}} \cdot \sin(\omega t) \tag{9}$$

The velocity of the system is then

$$\dot{q}(t) = \frac{dq}{dt} = \frac{A_v\frac{\omega}{\Omega^2}}{\sqrt{\left(\frac{1}{Q}\cdot\frac{\omega}{\Omega}\right)^2 + \left(1 - \left[\frac{\omega}{\Omega}\right]^2\right)^2}} \cdot \cos(\omega t) \tag{10}$$

Combination of Eq. (8) and Eq. (10) leads to the electric power dissipated from the system by each of the harmonic acceleration components with given frequency and magnitude:

$$\mathrm{p(t)} = b_e \cdot \frac{\left(A_v\frac{\omega}{\Omega^2}\right)^2}{\left(\frac{1}{Q}\cdot\frac{\omega}{\Omega}\right)^2 + \left(1 - \left[\frac{\omega}{\Omega}\right]^2\right)^2} \cdot \cos^2(\omega t) \tag{11}$$

Taking into account that $b_e = b_m$, and substituting $\frac{m\Omega}{2Q}$ for b_m, this equation can be written as

$$\mathrm{p(t)} = \frac{{A_v}^2 \cdot \frac{\omega^2}{\Omega^3} \cdot \frac{m}{2Q}}{\left(\frac{1}{Q} \cdot \frac{\omega}{\Omega}\right)^2 + \left(1 - \left[\frac{\omega}{\Omega}\right]^2\right)^2} \cdot \cos^2(\omega t) \tag{12}$$

The steady-state average electric dissipated power of the n-th acceleration component reaches one half of its peak power, due to the harmonic waveform:

$$\mathrm{P}_{avg}(n) = \frac{1}{T}\int_0^T p(t)dt = \frac{m}{4Q} \cdot \frac{{A_v}^2 \cdot \frac{\omega(n)^2}{\Omega^3}}{\left(\frac{1}{Q} \cdot \frac{\omega(n)}{\Omega}\right)^2 + \left(1 - \left[\frac{\omega(n)}{\Omega}\right]^2\right)^2} \tag{13}$$

In the special case of resonance operation, where $\omega = \Omega$, the equation can be further simplified into the well-known form [20].

$$\mathrm{P}_{avg_{res}} = \frac{{A_v}^2 mQ}{4\Omega} = \frac{(A_v m)^2}{8b_m} \tag{14}$$

These formulas are indeed valid for sinusoidal excitation acceleration waveforms, while the anticipated real-life excitation is non-sinusoidal. However, the periodicity of the real-life excitation acceleration waveforms allows for decomposing the excitation into sinusoidal components. Exploiting the linearity of the presented harvester model, superposition principle can then be used to obtain the total average harvested power as a sum of average power contributions from each of the non-zero magnitude sinusoidal components of the excitation acceleration.

$$\mathrm{P}_{avg_{total}} = \sum \mathrm{P}_{avg}(n) \tag{15}$$

The following simulation results are therefore obtained as a sum of harvested power contributions from the ten dominant frequencies (one from each interval) in given axis of interest.

5.2 Simulation Results

Using the statistical models of the acceleration obtained from multiple subjects in the previous chapter as inputs for the linear energy harvester that could potentially be used for generating power from human motion gives a fair idea about the performance limits of a linear kinetic energy harvester. Figures 9, 10 and 11 depict the power harvesting capabilities of generic linear harvesters tuned so that their natural frequency ranges between 1 and 10 Hz, and their quality factor ranging between 1 and 100. Three orthogonal axes of possible proof mass oscillation, aligned with the measurements axes, are investigated separately. The performance evaluation process is presented here on the example of the harvester with 1 DOF. The final design of the harvester can however take advantage of utilizing multiple degrees of freedom to exploit acceleration of different frequencies in two or more axes by utilizing the approach described in this paper iteratively. It should also be noted, that the figures presented show the average electric power dissipated from the system, and do not take into the account the ratio of power dissipated on the actual electric load and on the impedance of the harvester. A realistic design will also have to take into account the physical limitations in the form of maximum possible displacement or achievability of the required quality factor of the oscillator.

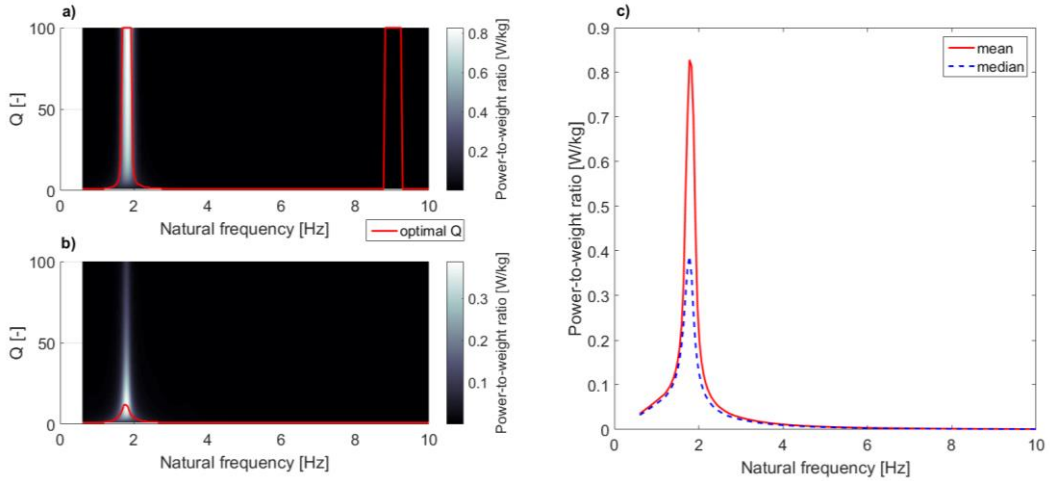

Fig. 9 Mean (a) and median (b) specific power generated in X axis; values of mean and median for optimum Q factor value (c)

An obvious discrepancy between the median and mean values of average harvested electrical power, as is visible on Fig. 10, is caused by the fact that the model acceleration dataset used contains a small number of outlying points that noticeably shift the mean value of the harvested power. From the statistical point of view though, these outliers have a little significance, as they will be rare in the real set of users as well. It is therefore more feasible to use the median value of the average harvested power as a reference for the harvester performance evaluation.

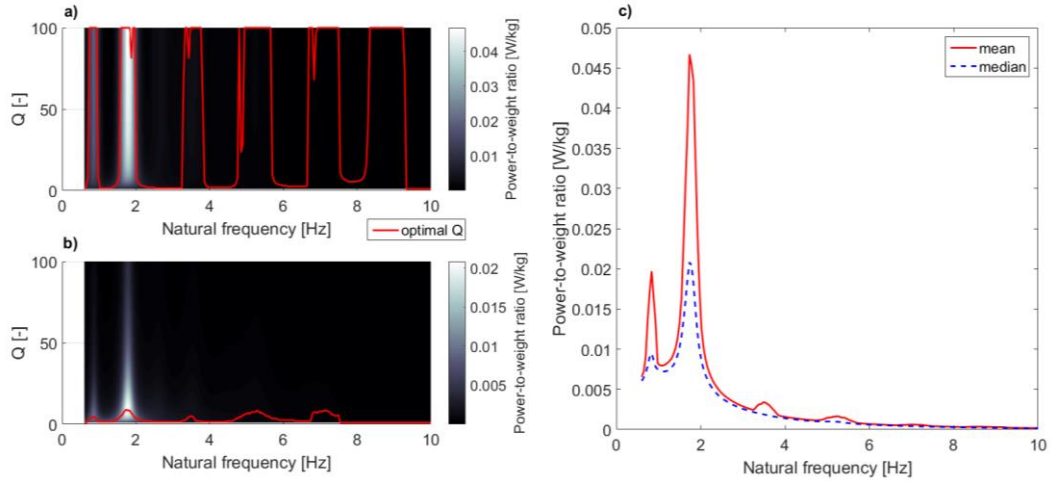

Fig. 10 Mean (a) and median (b) specific power generated in Y axis; values of mean and median for optimum Q factor value (c)

Figures 9-11 also show that implementing the highest achievable quality factor is not the preferred approach when designing a harvester for exploiting the human motion. Higher quality factor means narrower frequency response of the harvester, which limits the power output if the excitation frequency is slightly shifted from the natural frequency of the harvester. As the walking frequencies of different people vary, it seems to be more advantageous to design a linear harvester with a flatter but broader frequency response, which will work satisfyingly for a larger fraction of the potential user population.

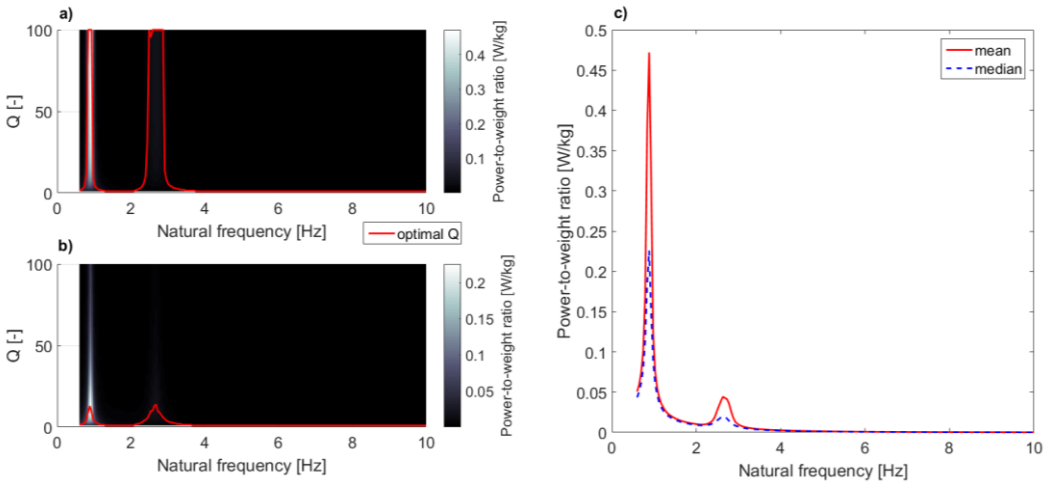

Fig. 11 Mean (a) and median (b) specific power generated in Z axis; values of mean and median for optimum Q factor value (c)

The preliminary analysis reveals three exploitable frequency bands providing a median of average harvested electrical power over 100 µW contained within the spectra. These bands are centred on frequencies that correspond to the most common values of first and third harmonic frequencies in Z axis, and to the second harmonic frequency in the X axis. As was shown in the previous chapters, the acceleration in Y axis contains generally lower magnitudes on the same frequencies compared to X and Z axes. The simulated harvested power results in Y axis are therefore also comparably worse than the other two axes. That makes Y axis less exploitable for energy harvesting purposes than the other axes, and as such it will not be included in further analyses.

The design parameter Q is set in such a way, so that it maximizes the median of average harvested specific power for each of the three investigated frequencies. Fig. 12 then shows the histograms and empirical cumulative distribution functions of the obtainable specific power for given model population and for selected feasible combinations of harvester working axis (only X and Z), its natural frequency, and the Q factor as found above.

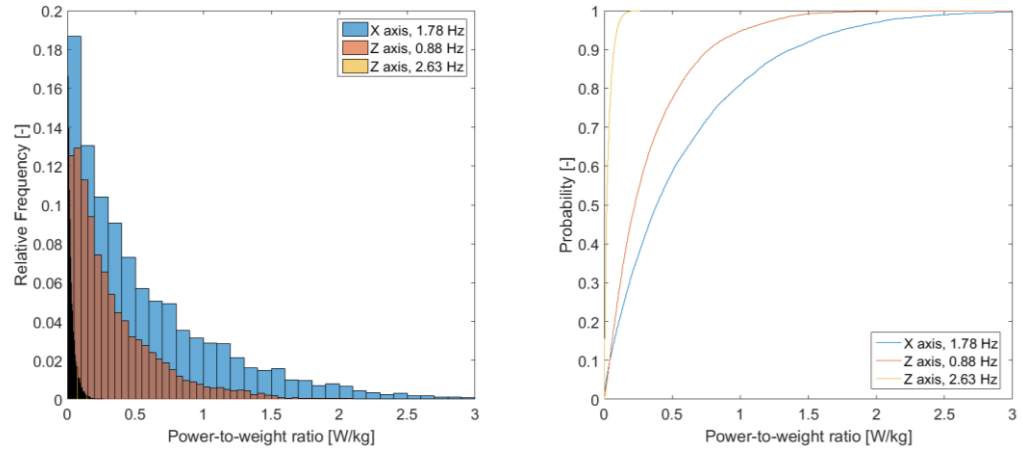

Fig. 12 Estimated histograms (left) and cumulative density functions (right) of average harvested specific power for 10000 samples model population, with harvester tuned to different favourable frequencies in different axes.

The empirical approximation of the complementary cumulative distribution function (reliability function) depicts the least average power that will be harvested for a given percentage of the users from the model population. Each of the following figures (Fig. 13-15) show the reliability function results for one static and one variable design parameter in a single selected axis. This makes it possible to evaluate the harvester performance in case of one design parameter drifting away from its optimal value. That in turn allows setting precision requirements for the

design parameters, so that the lowest acceptable power is certain to be harvested by given percentage of the user population.

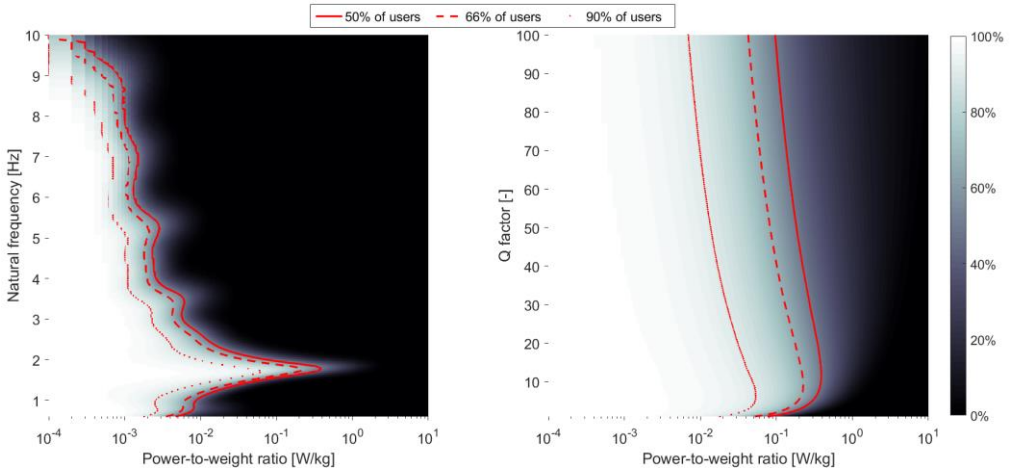

Fig. 13 Complementary cumulative distribution functions showing the percentage of model population that will reach at least the given value of specific power harvested during the walking, with the harvester working in X axis. Static design parameters are the Q factor 13 (left), and the harvester natural frequency 1.78 Hz (right).

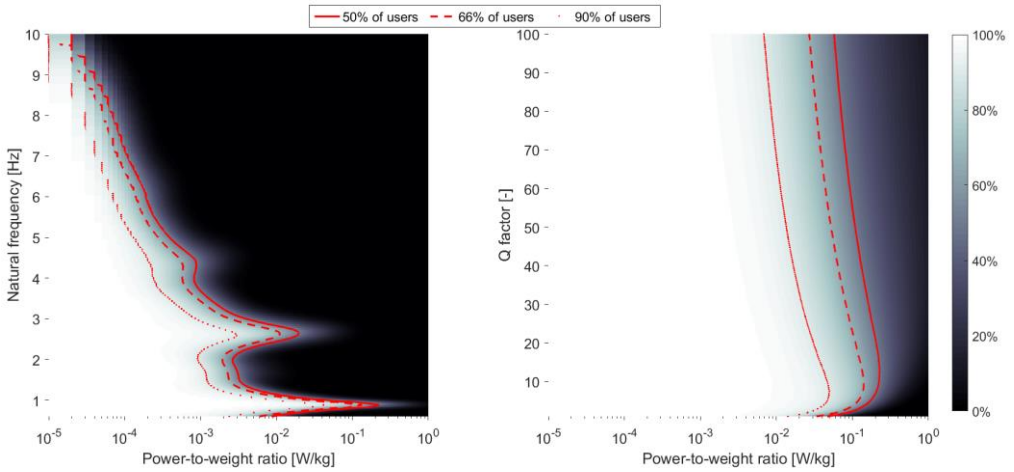

Fig. 14 Complementary cumulative distribution functions showing the percentage of model population that will reach at least the given value of specific power harvested during the walking, with the harvester working in Z axis. Static design parameters are the Q factor 13 (left), and the harvester natural frequency 0.88 Hz (right).

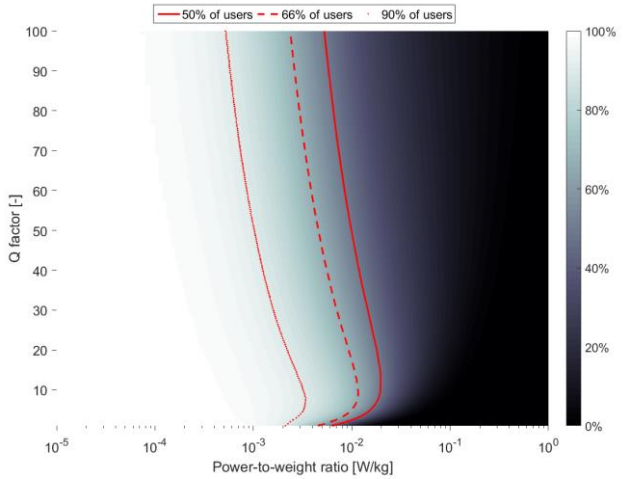

Fig. 15 Complementary cumulative distribution functions showing the percentage of model population that will reach at least the given value of specific power harvested during the walking, with the harvester working in Z axis. Static design parameter is the harvester natural frequency 2.63 Hz (right).

6. Discussion

Simulations indicate, that an inaccuracy in the exact Q factor setting will have less severe effect on the generated power, than mistuning the natural frequency of the harvester. It is also clearly visible, that the exploitable frequency bands widen with increasing frequency. It will therefore be less demanding to roughly tune the harvester to higher natural frequency, then to fine-tune it to the low frequencies. This furthermore allows for more compact designs, as higher natural frequencies are associated with smaller displacements of the proof mass if the Q factor is kept constant.

The reachable specific power results seem quite optimistic for the harvester being tuned to work around the dominant acceleration frequencies in each working axis. It should be noted, though, that the presented simulation results are purely theoretical, and that the real-life harvester will have to deal with technological and spatial limitations, as well as with using a non-ideal energy transducer with nonzero inner impedance. All these factors will introduce additional energy losses into the system. Moreover, theoretically the most promising frequency tunings are in practice difficult to exploit by a linear device due to associated large displacements of the oscillating proof mass, bringing challenges in a form of a stiffness implementation and an overall size of the device. However, exploiting higher frequencies around 3 Hz and more does not result in as high power outputs, as the lower ones. It might thus be challenging to cover the power requirements of the intended electronic application solely by exploiting the third and higher harmonic frequencies of human walking while keeping the energy harvester sufficiently small and lightweight.

Some of these challenges could possibly be mitigated e.g. by employing an energy harvester with a nonlinear stiffness. The statistical models presented in this paper provide a complete information about the acceleration in the head area, and as such they can be used for a performance predictions of nonlinear energy harvester designs as well. However, the nonlinear harvester analysis and comparison for large datasets would be quite time consuming, as the analysis would have to be conducted in the time domain due to unavailability of the superposition principle for nonlinear systems.

Another option is to employ a harvester design, where the proof mass or masses can move in more than one direction. Such a design could take advantage of harvesting the kinetic energy from multiple directions, effectively increasing the output power, while keeping the device weight within acceptable limits.

7. Conclusions

In this paper we have introduced the statistical properties and modelling of acceleration data obtained in the area of human head during walking at natural speed. These models are then exploited for the feasibility study of a human power kinetic energy harvester. The data obtained by measuring acceleration in the head area during walking at natural speed first on a single person 40 times and then on 51 different people, each once, were processed and reduced in the frequency domain in order to allow for their statistical analysis. The Kolmogorov-Smirnov test was deployed to compare the reduced measured samples with the assumed distributions with parameters estimated from the measurements. The results indicate, that the frequencies, magnitudes and initial phases of the significant acceleration frequency components in all measurement axes follow normal distributions, which allowed creating an arbitrarily large set of model data, simulating a large population of potential users of the energy harvester.

A created model dataset was then used for estimating the performance limits of a simple linear energy harvester, depending on its natural frequency and quality factor settings. Optimal values of these parameters were defined with the merit of maximizing the median of average harvested specific power in the sample population. A worst case simulation scenario is presented in a form of the survivor function plots, showing the minimum specific power harvestable for given percentage of the population with given harvester design parameters configuration. These plots are presented for harvester alignment in two different orthogonal working axes, which were evaluated as promising for this purpose. Simulations show that employing the kinetic energy harvesting in the area of human head might be a feasible approach, even though the available acceleration levels and the exploitable dominant frequencies are quite low, making the harvester design complicated. However, in case of having to power up a biomedical implant or other ultra-low power wearable electronic application the kinetic harvester could present a viable solution even with very small and lightweight proof mass, as the lowest specific power theoretically reachable by at least 50% of the population goes up to 400 μW per gram of oscillating mass in the vertical working axis of the harvester.

Acknowledgements

This work is an output of research and scientific activities of NETME Centre, supported through project NETME CENTRE PLUS (LO1202) by financial means from the Ministry of Education, Youth and Sports in Czech Republic under the „National Sustainability Programme I“.

References

[1] P. D. Mitcheson, “Energy harvesting for human wearable and implantable bio-sensors.,” *Conf. Proc. IEEE Eng. Med. Biol. Soc.*, pp. 3432–3436, 2010.

[2] G. Zhou, L. Huang, W. Li, and Z. Zhu, “Harvesting ambient environmental energy for wireless sensor networks: A survey,” *J. Sensors*, vol. 2014, 2014.

[3] E. Romero, R. O. Warrington, and M. R. Neuman, “Energy scavenging sources for biomedical sensors.,” *Physiol. Meas.*, vol. 30, no. 9, pp. R35-62, Sep. 2009.

[4] A. Cadei, A. Dionisi, E. Sardini, and M. Serpelloni, “Kinetic and thermal energy harvesters for implantable medical devices and biomedical autonomous sensors,” *Meas. Sci. Technol.*, vol. 25, no. 1, p. 12003, Jan. 2014.

[5] N. Gomez Estancona, A. G. Tena, J. Torca, L. Urruticoechea, L. Muniz, D. Aristimuno, J. M. Unanue, and A. Urruticoechea, “Solar recharging system for hearing aid cells,” *J Laryngol Otol*, vol. 108, no. 9, pp. 768–769, 1994.

[6] M.-K. Kim, M.-S. Kim, S. Lee, C. Kim, and Y.-J. Kim, “Wearable thermoelectric generator for harvesting human body heat energy,” *Smart Mater. Struct.*, vol. 23, no. 10, p. 105002, Oct. 2014.

[7] P. Patel and M. B. Khamesee, “Electromagnetic micro energy harvester for human locomotion,” *Microsyst. Technol.*, vol. 19, no. 9–10, pp. 1357–1363, Jun. 2013.

[8] C. Dagdeviren, B. D. Yang, Y. Su, P. L. Tran, P. Joe, E. Anderson, J. Xia, V. Doraiswamy, B. Dehdashti, X. Feng, B. Lu, R. Poston, Z. Khalpey, R. Ghaffari, Y. Huang, M. J. Slepian, and J. A. Rogers, “Conformal piezoelectric energy harvesting and storage from motions of the heart, lung, and diaphragm.,” *Proc. Natl. Acad. Sci. U. S. A.*, vol. 111, no. 5, pp. 1927–32, Feb. 2014.

[9] L. Xie and M. Cai, “Increased piezoelectric energy harvesting from human footstep motion by using an amplification mechanism,” *Appl. Phys. Lett.*, vol. 105, no. 14, p. 143901, Oct. 2014.

[10] R. Morais, N. M. Silva, P. M. Santos, C. M. Frias, J. A. F. Ferreira, A. M. Ramos, J. A. O. Simões, J. M. R. Baptista, and M. C. Reis, “Double permanent magnet vibration power generator for smart hip prosthesis,” *Sensors Actuators A Phys.*, vol. 172, no. 1, pp. 259–268, Dec. 2011.

[11] J. Smilek and Z. Hadas, “A study of kinetic energy harvesting for biomedical application in the head area,” *Microsyst. Technol.*, pp. 1–13, Dec. 2015.

[12] E. Goll, H.-P. Zenner, and E. Dalhoff, “Upper bounds for energy harvesting in the region of the human head.,” *IEEE Trans. Biomed. Eng.*, vol. 58, no. 11, pp. 3097–103, Nov. 2011.

[13] H. Hui, G. V. Merrett, and N. M. White, “Human-powered inertial energy harvesters: The effect of orientation, location and activity on obtainable power,” in *Procedia Engineering*, 2011, vol. 25, pp. 815–818.

[14] J.-P. Martin and Q. Li, “Overground vs. treadmill walking on biomechanical energy harvesting: An energetics and EMG study,” *Gait Posture*, vol. 52, pp. 124–128, Feb. 2017.

[15] S. Zhang and A. Seyedi, “Statistical Models for Harvested Power from Human Motion,” *IEEE J. Sel. Areas Commun.*, vol. 33, no. 8, pp. 1–1, 2015.

[16] J. Smilek, F. Cieslar, and Z. Hadas, “Measuring acceleration in the area of human head for energy harvesting purposes,” in *Proceedings of the 2016 17th International Conference on Mechatronics - Mechatronika, ME 2016*, 2017.

[17] J. Smilek and Z. Hadas, “Improving power output of inertial energy harvesters by employing principal component analysis of input acceleration,” *Mech. Syst. Signal Process.*, vol. 85, pp. 801–808, Feb. 2017.

[18] F. James, *Statistical Methods in Experimental Physics*. World Scientific Publishing Company, 2006.

[19] N. G. Stephen, “On energy harvesting from ambient vibration,” *J. Sound Vib.*, vol. 293, no. 1, pp. 409–425, 2006.

[20] S. P. Beeby, M. J. Tudor, and N. M. White, “Energy harvesting vibration sources for microsystems applications,” *Meas. Sci. Technol.*, vol. 17, no. 12, pp. R175–R195, Dec. 2006.

ANNEX A5

SMILEK, Jan, Zdenek HADAS, Jan VETISKA and Steve BEEBY

Rolling mass energy harvester for very low frequency of input vibrations

Mechanical Systems and Signal Processing [online]. 2018. ISSN 08883270. Available at: doi:10.1016/j.ymssp.2018.05.062

Impact factor: 4.116

Mechanical Systems and Signal Processing xxx (2018) xxx–xxx

Contents lists available at ScienceDirect

Mechanical Systems and Signal Processing

journal homepage: www.elsevier.com/locate/ymssp

Rolling mass energy harvester for very low frequency of input vibrations

Jan Smilek [a,*], Zdenek Hadas [a], Jan Vetiska [a], Steve Beeby [b]

[a] Faculty of Mechanical Engineering, Brno University of Technology, Technicka 2896/2, 616 69 Brno, Czech Republic
[b] School of Electronics and Computer Science, University of Southampton, Highfield, Southampton, Hampshire SO17 1BJ, United Kingdom

ARTICLE INFO

Article history:
Received 9 November 2017
Received in revised form 16 May 2018
Accepted 29 May 2018
Available online xxxx

Keywords:
Energy harvesting
Tusi couple
Nonlinear systems
Human motion
Low frequency
Electromagnetic induction

ABSTRACT

This paper presents a novel design of a nonlinear kinetic energy harvester for very low excitation frequencies below 10 Hz. The design is based on a proof mass, rolling in a circular cavity in a Tusi couple configuration. This allows for an unconstrained displacement of the proof mass while maintaining the option of keeping the energy transduction element engaged during the whole cycle and thus reducing the required number of transduction elements. Both the presented model and the fabricated prototype of the device employ electromagnetic induction to harvest energy from low frequency and low magnitude vibrations that are typically associated with human movements. The prototype demonstrated an average power of 5.1 mW from a 1.3 g periodic acceleration waveform at 2.78 Hz. The highest simulated normalized power density reaches up to 230 $\mu W/g^2/cm^3$, but this depends heavily on the excitation conditions.

1. Introduction

Powering up mostly small electronic devices by the means of independent power sources based on energy harvesting principle has attracted a growing interest in recent years. Instead of utilizing traditional primary or secondary battery cells, or using wiring to supply power directly from the grid or a central power source, there is considerable interest in the exploitation of otherwise wasted energy present in the ambient environment of the electronic device. Such energy harvesting approaches enable compact and standalone wireless system nodes, reducing the cost and weight associated with wiring, and the maintenance costs of periodic battery replacement.

Depending on the intended application, the available ambient energy sources might include solar, temperature gradient, fluid flow, pressure variations or kinetic energy. As the amount of ambient energy is usually limited and the size of the energy harvester is constrained, harvesters are being developed mainly for low-power power devices, such as wireless sensor nodes for structural health monitoring [1] in aerospace or industrial environments [2]. With the increasing prevalence of smart electronics for everyday use another widely considered application field is wearable sensors, electronic gadgets, and biomedical implants [3,4].

Ambient energy in the environment of the human body is sometimes captured by the use of thermoelectric generators [5,6] or photovoltaic panels [7], the most common approach lies in exploiting the mechanical energy from human activity. Some locations on the human body allow for utilizing direct force excitation and associated deformation [8]. Examples of

* Corresponding author.
E-mail address: smilek@fme.vutbr.cz (J. Smilek).

https://doi.org/10.1016/j.ymssp.2018.05.062
0888-3270/

direct force harvesters include the deformation of shoe soles [9], the bending of the knee whilst walking [10] and even the deformation of the ear canal when talking or chewing [11]. Some publications also investigate harvesting the energy from the pulsation of arterial vessels or the heart [12].

Another option is to utilize an inertial oscillation mechanism excited by mechanical displacements during human activity. This is the preferred approach in locations where direct forces cannot be exploited, such as at the forearm or hip [13].

Inertial harvesting mechanisms are commonly used in energy harvesters for industrial applications where numerous linear and nonlinear structures have been demonstrated [14,15]. In the environment of the human body, however, this approach bears considerable additional challenges. For example, the characteristics of the human motion differ significantly between different locations on the body, different types of activity and, for a given location and activity, even between different people [16,17]. In addition, both the frequency and magnitude commonly associated with human activities are very low [18,19], and therefore the inertial harvester design becomes quite heavy and bulky in order to satisfy the application power requirements.

However, with the ever decreasing power consumption and increasing efficiency of power-management circuits in modern wearable and biomedical electronic applications, the size of the energy harvesters to power them up is also shrinking down, with some of the designs being small enough to actually present a feasible power source solution [20].

Common methods of transducing the kinetic energy of the vibrating inertial proof mass into electricity include piezoelectric effect, electrostatic conversion, electromagnetic induction, and lately also the triboelectric effect. Piezoelectric transducers are the most commonly used mechanism for harvesting human energy [21–23], regardless of their rather high impedance. Electrostatic harvesters [24,25] are popular due to their compatibility with MEMS fabrication processes, but their need for a priming voltage drags reduces their practicality. Triboelectric harvesters are gaining popularity in last few years, with potential applications including human power [26]. Electromagnetic transducers are quite common in larger scale industrial applications, but scaling these down in size to make them suitable for human power harvesting presents a technical challenge due to reducing the electromechanical coupling coefficient [27]. Complex energy harvesting approaches, such as nonlinear system design [28], frequency up-conversion [29], or parametric resonators [30] are being employed in order to improve the performance of the energy harvesters in certain applications. Various designs of human powered inertial energy harvesters have been demonstrated including linear trajectory oscillation structures (either suspended [31] or free moving with the displacement limited by the use of mechanical bumpers [32,33]), cantilevers with nonlinear frequency response, arrays of independent oscillators or rotational harvesters [34], frequency up-conversion mechanisms and chaotic motion harvesters [35].

However, the excitation by human power is considered unpredictable [36] and only a small fraction of all the kinetic energy harvester designs introduced in the last two decades [37–39] are capable of working in the excitation frequency range below 10 Hz. In this paper we introduce a novel design of nonlinear energy harvester based on a Tusi couple configuration designed for very low excitation frequency in the range between 2 and 10 Hz.

2. Novel mechanism for energy harvesting from low frequency vibrations

The downside of most mechanisms suitable for low frequency excitation is that they are either large in size in order to accommodate the high amplitude proof mass displacements, or they employ mechanical limiters, leading to additional mechanical energy losses and physical wear of components. Pendulum harvesters can theoretically have unlimited displacement, as the pendulum can rotate around its pivotal point. Implementing the transduction mechanism in the pendulum structures with large displacements is challenging and they will either employ multiple transduction elements (e.g., pickup coils in electrodynamic harvester) along the path of the proof mass [40], or increase their total weight by using a proof mass only as a mechanical energy storage element, which is mechanically linked to a separate energy transducing mechanism [41].

The Tusi couple configuration enables unlimited displacements and can be designed in such a way, that a single transduction element can be used irrespective of the inertial mass position. This allows for reduced cost and complexity of the power management electronics whilst slightly increasing the precision required in the mechanical design compared to most common energy harvesting devices.

The proposed mechanism consists of a cylindrical proof mass placed inside a circular cavity in such a way, that only a rolling motion of the proof mass along the cavity wall is possible. During the motion every point on the diameter of the proof mass travels along hypocycloidal path. This can be described using a Cartesian coordinate system, the origin of which lies in the centre of the circular cavity with radius R. The initial position of the proof mass is in the bottom of the cavity.

The position of the centre of the rolling mass C as a function of the angle between the cavity centre and the proof mass centre φ (Fig. 1) is then defined by a set of parametric equations:

$$x_C = (R - r)\sin(\varphi) \tag{1}$$

$$y_C = -(R - r)\cos(\varphi) \tag{2}$$

Please cite this article in press as: J. Smilek et al., Rolling mass energy harvester for very low frequency of input vibrations, Mech. Syst. Signal Process. (2018), https://doi.org/10.1016/j.ymssp.2018.05.062

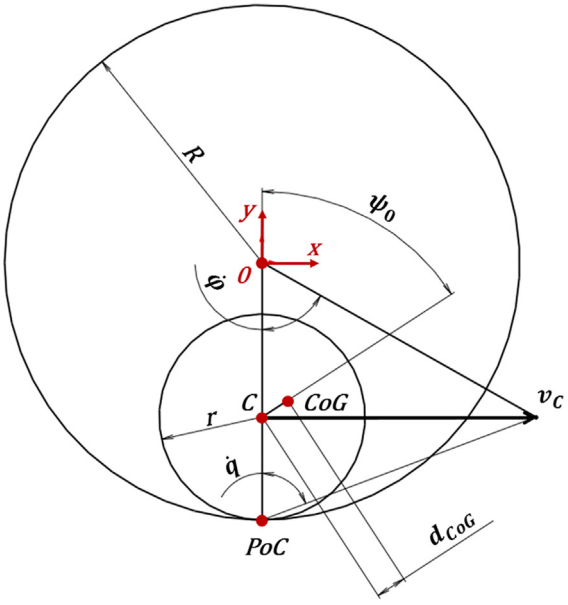

Fig. 1. Rolling mass harvester geometry.

Constants R and r are the radiuses of the cavity and the proof mass, respectively. The position of the point on the rolling mass that is initially in contact with the circular cavity and that moves along the hypocycloidal path (blended with the *PoC* in the figure) can be determined from:

$$x_{hypo} = x_C - r \cdot \sin\left(\frac{R-r}{r}\varphi\right) \tag{3}$$

$$y_{hypo} = y_C - r \cdot \cos\left(\frac{R-r}{r}\varphi\right) \tag{4}$$

In case of the centre of gravity *CoG* not being in the geometric centre of the rolling mass *C*, its position during the proof motion mass follows a hypotrochoid, and is given by a set of equations:

$$x_{CoG} = x_C + d_{CoG} \cdot \sin\left(\frac{R-r}{r}\varphi + \psi_0\right) \tag{5}$$

$$y_{CoG} = y_C + d_{CoG} \cdot \cos\left(\frac{R-r}{r}\varphi + \psi_0\right) \tag{6}$$

where d_{CoG} is the distance of the proof mass centre of gravity from the geometrical centre, and ψ_0 is the initial angle between the vertical and the connector of *C* with *CoG*. The position of the instantaneous point of contact *PoC* between the rolling mass and the cavity is found from:

$$x_{PoC} = R\sin(\varphi) \tag{7}$$

$$y_{PoC} = -R\cos(\varphi) \tag{8}$$

The Tusi couple is a special case of this setup, where the ratio of the cavity radius to the rolling mass radius is 2:1. In this case the hypocycloids created by the points on the outer diameter of the rolling mass blend with the straight lines noting the diameter of the cavity (Fig. 2).

Every point on the diameter of the rolling mass travels through the centre of the cavity twice during each revolution cycle. A point of the proof mass currently aligned with the centre of the cavity also has the largest instantaneous velocity in the mechanism, making this location advantageous for velocity damper type energy transduction element placement (Fig. 3).

Since the movement of the proof mass is constrained in such a way that the rolling motion is ensured, the whole system has only one remaining degree of freedom and can be treated as such. Its dynamics under base excitation is described by the Lagrange's equation of the second kind

$$\frac{d}{dt}\left(\frac{dE_k}{d\dot{q}}\right) - \frac{dE_k}{dq} + \frac{dE_b}{d\dot{q}} + \frac{dE_p}{dq} = -\frac{dA}{dq} = -Q \tag{9}$$

Please cite this article in press as: J. Smilek et al., Rolling mass energy harvester for very low frequency of input vibrations, Mech. Syst. Signal Process. (2018), https://doi.org/10.1016/j.ymssp.2018.05.062

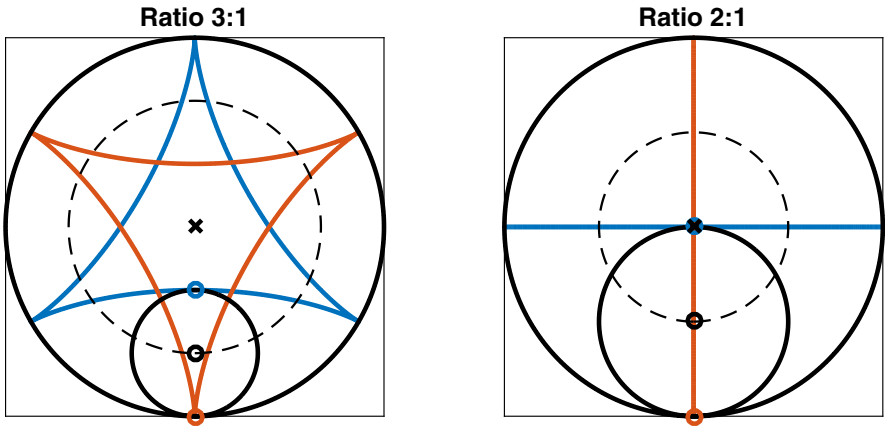

Fig. 2. Comparison of hypocycloidal paths of points on the proof mass for different ratios of cavity to proof mass diameter.

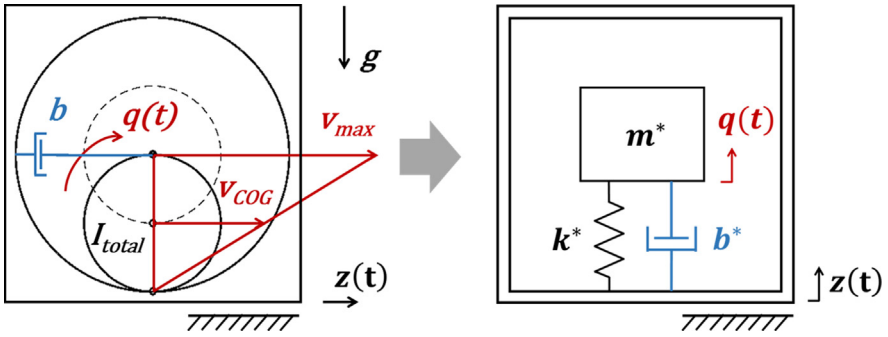

Fig. 3. Tusi couple as spring mass damper system with 1 DoF.

The generalized coordinate q in this case denotes the angular position of the proof mass, which is a function of the angle φ:

$$q = \frac{R-r}{r}\varphi \tag{10}$$

Time derivatives of the generalized coordinate q are denoted with dots above the variable. The rolling movement of the proof mass can be understood as a rotation around a variable axis, which passes through the instantaneous point of contact between the proof mass and the frame, perpendicular to the plane of movement. Employing the parallel axis theorem the kinetic energy of such a movement is:

$$E_k = \frac{1}{2} I_{total} \dot{q}^2 = \frac{1}{2}\left(I_{CoG} + m \cdot d_{PoC-CoG}^2\right)\dot{q}^2 \tag{11}$$

where I_{CoG} denotes the moment of inertia of the proof mass with respect to its centre of gravity, m is the weight of the proof mass and $d_{PoC-CoG}$ is the distance between the instantaneous point of contact and the proof mass centre of gravity. Depending on the mass distribution within the rolling element, the distance between the point of contact *PoC* and the centre of gravity *CoG* is generally a function of the instantaneous position q:

$$d_{CoG-PoC} = \sqrt{(x_{CoG-PoC})^2 + (y_{CoG-PoC})^2} \tag{12}$$

$$x_{CoG-PoC} = (x_{CoG} - x_{PoC}) \tag{13}$$

$$y_{CoG-PoC} = (y_{CoG} - y_{PoC}) \tag{14}$$

In the special case where the centre of gravity is aligned with the centre of the rolling mass, the distance $d_{PoC-CoG}$ is constant:

$$d_{CoG-PoC_{centre}} = r \tag{15}$$

Please cite this article in press as: J. Smilek et al., Rolling mass energy harvester for very low frequency of input vibrations, Mech. Syst. Signal Process. (2018), https://doi.org/10.1016/j.ymssp.2018.05.062

It is clear that in the general case the $d_{CoG-PoC}$ is a function of instantaneous position. Therefore the derivative of the kinetic energy with respect to position $\frac{dE_k}{dq}$ has generally a nonzero value, which needs to be taken into account when modelling the general mechanism.

The potential energy of the system depends on the global orientation of the mechanism, as there are no additional spring elements employed. In the intended orientation, where the proof mass moves in the vertical plane, the potential energy depends on the height of its centre of gravity, and can be written as:

$$E_p = mgh_{COG} \tag{16}$$

The instantaneous height can then be found as:

$$h_{COG} = y_{CoG}(\varphi) - y_{CoG}(\varphi = 0) \tag{17}$$

In the special case of the centre of gravity being in the centre of the rolling mass ($d_{CoG} = 0$), the Eq. (17) can be written as

$$h_{COG_{centre}} = (R - r)[1 - \cos(\varphi)] = (R - r)\left[1 - \cos\left(\frac{r}{R - r}q\right)\right] \tag{18}$$

The mechanical energy of the energy harvester is being dissipated from the system in a form of unavoidable mechanical losses and as an electric energy, part of which is dissipated on the impedance of the transduction mechanism, and other part is being delivered to the electric load. The dissipation energy of this system is thus found as a function of mechanical damping b_m^* and electrical damping b_e^*:

$$E_d = \frac{1}{2}b^*\dot{q}^2 = \frac{1}{2}(b_m^* + b_e^*)\dot{q}^2 \tag{19}$$

The mechanical damping b_m^* is affected significantly by the choice of material, and by the manufacturing and assembly precision. These losses are summarized in the mechanical quality factor Q_m.

$$b_m^* = \frac{I_{total} \cdot \Omega}{Q_m} \tag{20}$$

where Ω is the natural frequency of the mechanism, which can be calculated in the same manner as for a pendulum, assuming small displacements and taking into account the distance between the pivot point and the centre of gravity:

$$\Omega = \sqrt{\frac{k^*}{m^*}} = \sqrt{\frac{mgd_{CoG-PoC}}{I_{total}}} \tag{21}$$

The electrical damping b_e^* is directly proportional to the squared electromechanical coupling coefficient c and indirectly proportional to the total impedance loading Z_{total}:

$$b_e^* = \frac{c^2}{Z_{total}} \tag{22}$$

In case of using the electromagnetic transducer the coupling coefficient is found as

$$c = \frac{d\phi}{dq} \tag{23}$$

where ϕ is total magnetic flux through the coil. The total impedance is a sum of the load impedance Z_L and the transducer inner impedance Z_C.

$$Z_{total} = Z_L + Z_C \tag{24}$$

The inductance of the coreless pickup coil can be neglected, and the assuming the load impedance is resistive, the Eq. (22) can therefore be written as:

$$b_e^* = \frac{\left(\frac{d\phi}{dq}\right)^2}{R_L + R_C} \tag{25}$$

The excitation of the system Q is caused by the input acceleration, creating a torque acting upon the rolling proof mass:

$$Q = m(\ddot{z}_x \cdot y_{CoG-PoC} + \ddot{z}_y \cdot x_{CoG-PoC}) \tag{26}$$

where $\ddot{z}_x$ and $\ddot{z}_y$ are accelerations of the frame in x and y directions, respectively. In this design study, where the centre of gravity is aligned with the centre of the rolling element, the final form of the equation of motion (5) obtained by combining equations (9)–(26) takes the form:

$$I_{total}\ddot{q} - 0 + (b_e^* + b_m^*)\dot{q} + mgr \cdot \sin\left(\frac{r}{R - r}q\right) = -mr\left(\ddot{z}_x \cdot cos\left(\frac{r}{R - r}q\right) + \ddot{z}_y \cdot sin\left(\frac{r}{R - r}q\right)\right) \tag{27}$$

Please cite this article in press as: J. Smilek et al., Rolling mass energy harvester for very low frequency of input vibrations, Mech. Syst. Signal Process. (2018), https://doi.org/10.1016/j.ymssp.2018.05.062

This equation is implemented in the simulation model to predict and evaluate the performance of the harvester in different scenarios.

3. Harvester design and modelling

Model based design [42] was employed using CAD and FEM software tools together with the derived analytical model to sketch, evaluate and improve the mechanism in terms of the generated power output. Multiple design iteration cycles resulted in a variant with 12 permanent magnets arranged in two groups of six, one group on each face of the rolling proof mass (Fig. 4).

The magnetization direction of each two neighbouring magnets is alternated to maximize the electromechanical coupling coefficient (Fig. 5). Material properties and magnetic field parameters through the coil volume were analysed in CAD and FEM software and used as design parameters in the simulation model.

Analysis of the magnetic field distribution (Fig. 6), and its rate of change in the proximity of the cavity face for different displacement angles (Fig. 7) illustrates the optimum coil position above the centre of the circular cavity, as close as possible to the magnet surface plane. The magnets used both in simulations and in fabricated prototype are made of neodymium, iron and boron alloy $Nd_2Fe_{14}B$.

The pair of coils is located at the optimum position on either side sides of the cavity above its centre. A realistic magnetic circuit model can then be developed, taking into account the thickness of the coil wire, the coil fill factor and the number of turns used. The magnetic flux through each of the coil turns is calculated separately and summed to give the total magnetic flux through the coil. This approach prevents the magnetic circuit model from overestimating the induced voltage due to incorrectly estimated magnetic flux change ratio.

The calculated total magnetic flux through the designed coil volume dependency on the proof mass position follows a sinusoidal waveform (Fig. 8). Knowing the magnetic flux change ratio through the volume of space occupied by the coil also allows for future optimization of coil parameters in order to maximize the power output delivered to the electric load.

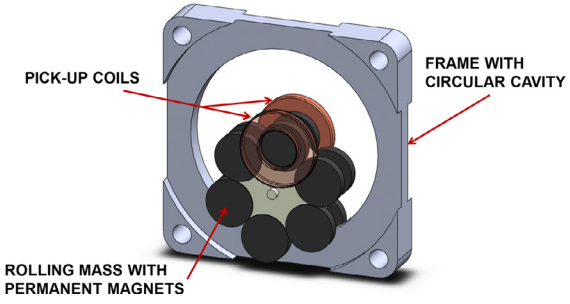

Fig. 4. Design of the energy harvester based on Tusi couple.

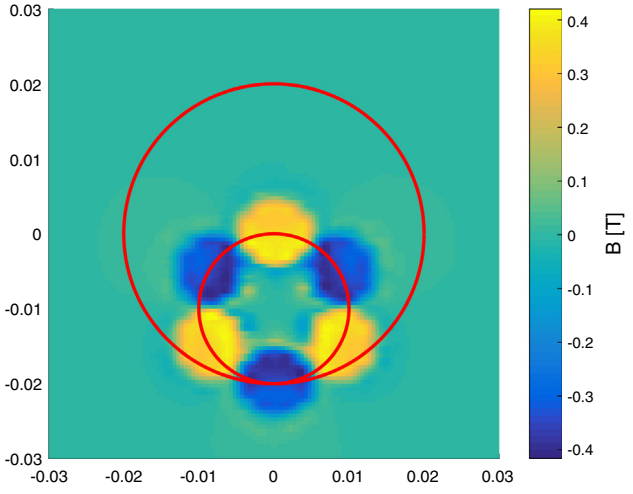

Fig. 5. Magnetic field distribution 0.5 mm above the magnets surface in the default mechanism position. Cavity and rolling mass diameters in red. (For interpretation of the references to colour in this figure legend, the reader is referred to the web version of this article.)

Please cite this article in press as: J. Smilek et al., Rolling mass energy harvester for very low frequency of input vibrations, Mech. Syst. Signal Process. (2018), https://doi.org/10.1016/j.ymssp.2018.05.062

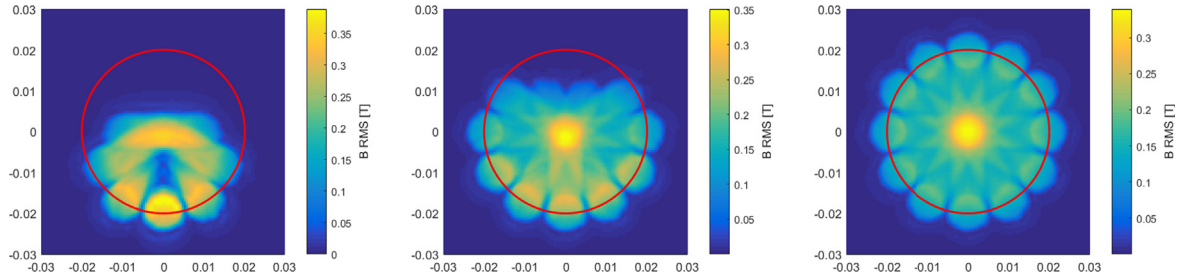

Fig. 6. Effective magnetic flux density 0.5 mm above the magnets surface during a simulated motion of the mechanism with constant speed in limit displacement angles $\pm\frac{\pi}{6}$ (left), $\pm\frac{\pi}{2}$ (middle), and $\pm\pi$ (right). Cavity diameter in red. (For interpretation of the references to colour in this figure legend, the reader is referred to the web version of this article.)

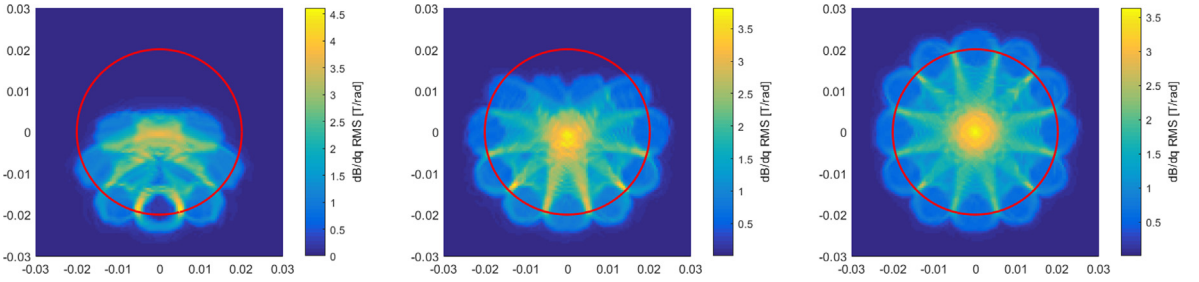

Fig. 7. Effective magnetic flux density rate of change in the cavity area 0.5 mm above the magnets surface during the mechanism motion. Limit displacement angles $\pm\frac{\pi}{6}$ (left), $\pm\frac{\pi}{2}$ (middle), and $\pm\pi$ (right). Cavity diameter in red. (For interpretation of the references to colour in this figure legend, the reader is referred to the web version of this article.)

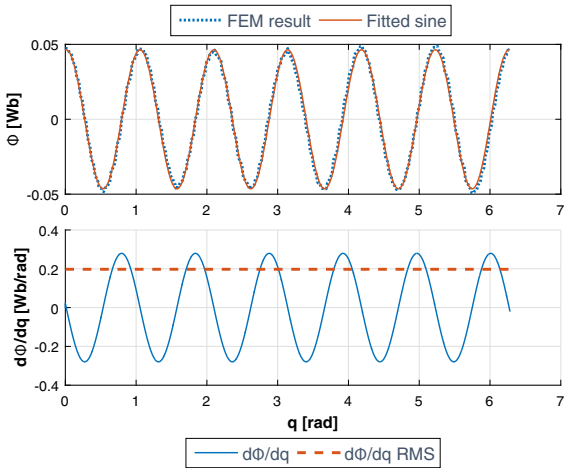

Fig. 8. Total magnetic flux through the coil and its rate of change as a function of proof mass position.

4. Prototype fabrication

A prototype of the harvester (Fig. 9) was manufactured using conventional manufacturing methods. The frame of the harvester was manufactured from non-magnetic and electrically non-conductive materials to prevent the induction of eddy currents in the frame and related energy losses. The pair of cylindrical coreless coils was wound manually using insulated copper wire of 50 μm diameter. The contact surfaces of the proof mass and the frame were roughened to promote the rolling motion without sliding. The leading slots for the pegs that prevent a free movement of the proof mass inside the cavity are milled into covering lids made of low friction plastic material PE 1000 to minimize mechanical losses in the mechanism. The measured and estimated parameters of the harvester prototype are summarized in Table 1. In order to enable reliable manufacture, the initial harvester design was scaled up in size by a factor of 2.

Please cite this article in press as: J. Smilek et al., Rolling mass energy harvester for very low frequency of input vibrations, Mech. Syst. Signal Process. (2018), https://doi.org/10.1016/j.ymssp.2018.05.062

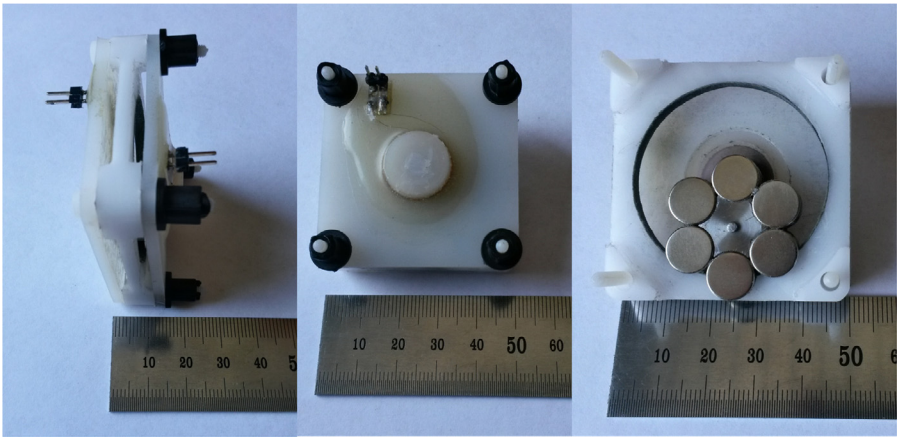

Fig. 9. Prototype of the Tusi couple harvester.

Table 1
Fabricated harvester prototype data.

Parameter	Value	Unit
Total dimensions	$50 \times 50 \times 20$	mm
Total weight	56.3	g
Frame material	POM C	–
Frame cavity radius	40	mm
Covering lids material	PE 1000	–
Rolling body material	Steel	–
Rolling body radius	20	mm
Rolling body weight	12.8	g
Number of magnets	12	–
Magnets material	$Nd_2Fe_{14}B$ N42	–
Magnets dimensions	$ø10 \times 2$	mm
Magnets weight	1.1	g
Total proof mass weight	26	g
Total proof mass moment of inertia I_{COG} (CAD)	2.48e−6	$kg.m^2$
Effective coupling coefficient (FEM)	0.20	Wb/rad
Coil wire diameter	50	μm
Coil outer radius	16	mm
Coil inner radius	6	mm
Coil height	3	mm
Coil turns	2000	–
Coil resistance	2	kΩ
Resistive load	2	kΩ
Mechanical quality factor	3.5	–

5. Experimental analysis

The assembled prototype was tested on a linear drive, oscillating in the horizontal plane with a range of dominant frequencies and magnitudes of acceleration. The linear drive used was not capable of delivering a harmonic excitation acceleration, thus the data presented are obtained from excitation with multiple frequency components. The acceleration data during the measurements were captured using a SlamStick C wireless datalogger containing a three axial accelerometer capable of measuring acceleration frequencies in the range of 0–500 Hz and magnitudes between ±16 g.

The voltage on a 2 kΩ resistive load was recorded for 15 measurements, each with different excitation parameters as shown in Table 2. The load was selected based on empirical results, obtained by exciting the harvester in non-controlled environment.

The measured RMS voltage and power on the load exhibit a good agreement with the simulation results obtained by feeding the recorded acceleration to the model (Fig. 10), considering the manufacturing precision of the prototype and measurement uncertainties. Discrepancy over 10% between the measured and simulated performance was found only in two measurements, which is considered satisfactory.

A comparison of the time domain waveforms measured and simulated also shows a good agreement between the measurement and the simulation (Fig. 11). The higher noise present on the simulated voltage waveforms is due to the numerical derivative used to model the change in total magnetic flux through the coil.

Please cite this article in press as: J. Smilek et al., Rolling mass energy harvester for very low frequency of input vibrations, Mech. Syst. Signal Process. (2018), https://doi.org/10.1016/j.ymssp.2018.05.062

Table 2
Measured and simulated performance comparison.

Measurement No.	Acceleration frequency [Hz]	Acceleration magnitude [g]	Measured RMS voltage [V]	Simulated RMS voltage [V]	Difference [V]	Difference [%]
1	2.88	0.15	**0.60**	0.66	−0.06	10.41
2	5.00	0.34	**1.04**	1.02	0.02	2.01
3	1.34	0.73	**1.05**	0.96	0.09	8.65
4	2.00	0.49	**1.09**	0.98	0.11	10.25
5	1.51	0.52	**1.23**	1.11	0.12	9.40
6	2.50	0.48	**1.33**	1.33	0.00	0.04
7	5.57	0.48	**1.38**	1.33	0.05	3.87
8	2.00	0.98	**1.65**	1.66	−0.01	0.34
9	4.16	0.45	**1.81**	1.65	0.16	8.75
10	4.16	0.65	**2.02**	2.20	−0.18	8.92
11	3.85	0.50	**2.03**	1.94	0.09	4.45
12	4.17	0.61	**2.14**	2.21	−0.07	3.24
13	3.33	0.93	**2.53**	2.71	−0.19	7.48
14	2.94	0.89	**2.63**	2.84	−0.20	7.62
15	2.78	1.30	**3.22**	3.02	0.20	6.30

Bold denote the column used for sorting the measurements in rising value order.

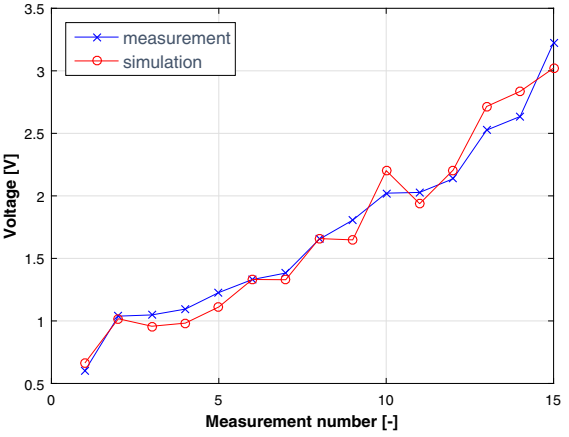

Fig. 10. Fit of the simulation data with the experiment.

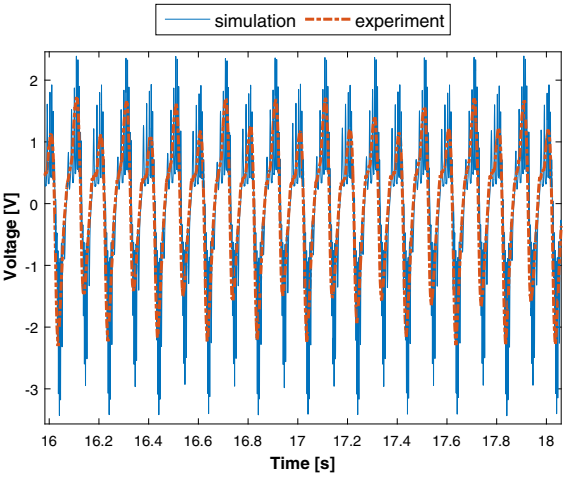

Fig. 11. Time domain voltage waveforms simulation and experiment comparison.

The power delivered to the resistive load for the different excitation parameters is shown in Fig. 12. This indicates a maximum experimentally measured power of 5.2 mW RMS, which is in excellent agreement with the simulated values.

Please cite this article in press as: J. Smilek et al., Rolling mass energy harvester for very low frequency of input vibrations, Mech. Syst. Signal Process. (2018), https://doi.org/10.1016/j.ymssp.2018.05.062

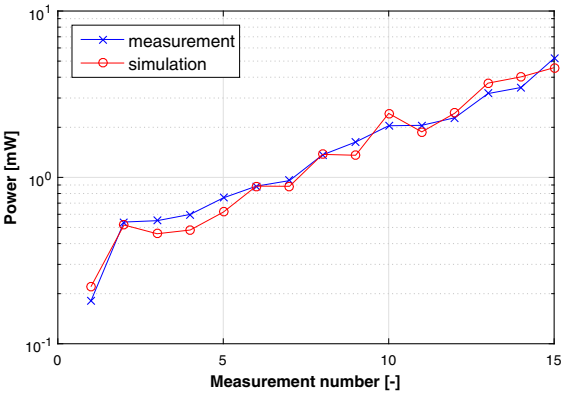

Fig. 12. Average power on load – experiment and simulation fit.

6. Harvester performance evaluation

To enable comparison of the Tusi couple configuration harvester with other designs, normalized power density metrics [43] together with maximum power output is used. Considering the presented prototype dimensions 50x50x20 mm and the simulated voltage output on 2 kΩ resistive load, the simulated NPD of the harvester reaches values up to 230 $\mu W/g^2/cm^3$ depending on the frequency of harmonic excitation acceleration and the degree of nonlinear behaviour (Fig. 13). A comparison with other harvesters working below 10 Hz is shown in Table 3. This shows the Tusi couple design is outperforming all comparable harvesters with a single exception, which is, however, working at almost twice the frequency.

In this case the simulated peak NPD falls with increasing harmonic acceleration magnitude, which is due to the increasing degree of nonlinear behaviour. The NPD is not the optimal performance metric, but as it is at the moment the most widely used metric, it allows for a rough comparison of the different energy harvesters, and information necessary for calculating some other figures of merit [44–46] are rarely available.

Simulated voltage and power output for different resistive loads under a constant acceleration magnitude 0.6 g show a rising RMS voltage on the load with increasing resistance (Fig. 14). In terms of power output, the optimal load [52] for the harmonic excitation was found to be between 2 kΩ and 5 kΩ depending on the harmonic excitation frequency (Fig. 15).

7. Discussion and further research directions

The simulated power outputs demonstrate the significant potential of this harvester design for use in human power energy harvesting and other very low frequency applications. Harvesters based on the Tusi couple could also present a viable

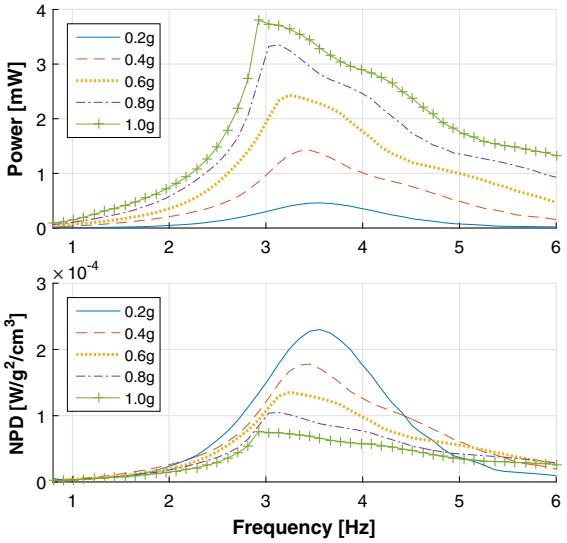

Fig. 13. Simulated performance of the harvester prototype under different harmonic excitation conditions.

Please cite this article in press as: J. Smilek et al., Rolling mass energy harvester for very low frequency of input vibrations, Mech. Syst. Signal Process. (2018), https://doi.org/10.1016/j.ymssp.2018.05.062

Table 3
Comparison of low frequency harvesters performance.

Reference	Size [mm]	Frequency [Hz]	Acceleration [g]	Power output [μW]	NPD [μW/cm^3/g^2]
[47]	20 × 45 × ?	2	0.4	40	?
[48]	ø17 × 55	2	0.5	300	96
[49]	ø 12 × 80	6	0.5	4840	2140
[50]	34 × 34 × 18	8	0.5	430	83
[51]	54 × 46 × 15	9.25	0.5	550	59
This work	50 × 50 × 20	3.45	0.4	1400	178

Question marks denote information unavailable from the literature.

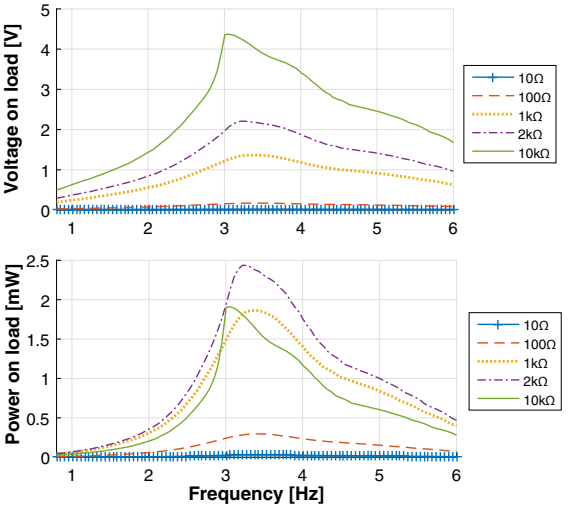

Fig. 14. Comparison of the simulated harvester performance with different resistive loads.

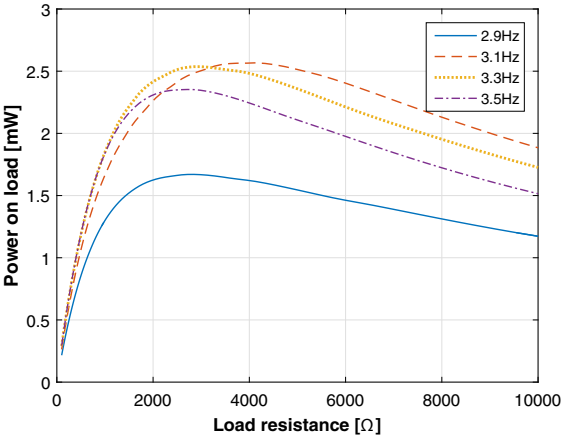

Fig. 15. Optimal resistive loads for different harmonic excitation frequencies.

alternative to current microgenerators used in wristwatches. The energy transduction method is not limited to electromagnetic induction, a similar device could be designed that uses a piezoelectric transducer that could be excited by a variable magnetic force between a magnet, fixed on the piezoelectric transducer, and the magnets on the moving proof mass. The transducing elements excitation principle would then be quite similar to the magnetically plucked [53] harvesting devices presented in [54,55].

The main challenge of the mechanism presented lies in the precision required during assembly, which is necessary to ensure the rolling motion of the proof mass without sliding or sticking during operation.

Material selection is another crucial point, as the contact surfaces between the frame and the rolling mass need to promote the rolling motion without sliding, while the material of the covering lids with the leading slots should be selected so

that lowest possible friction between the proof mass and the lids is achieved. Use of electrically conductive materials for the frame and covering lids structures is not feasible for the presented design due to the eddy currents induction, which would increase the energy losses in the system. However, if the magnetic circuit is reworked so that the magnetic field does extend through the covering lids, the use of metals might be advantageous.

The resulting mechanical damping of the system is affected both by the assembly design and precision, and by the material selection. The future design optimization should include minimizing the mechanical damping, as this will improve the overall harvester performance.

The natural frequency of the device can be changed without changing the main dimensions by changing the weight and its distribution in the proof mass, as this will alter the generalized mass (moment of inertia). Changing the weight of the proof mass will, however, inevitably alter also the stiffness of the system. Unlike standard devices with mechanic or magnetic springs, the natural frequency cannot be changed by simply adjusting the spring stiffness. Fine tuning of the system is therefore complicated and requires redesign of at least one part to adapt the device for different working frequency range.

An asymmetric configuration of the magnets or proof mass weight distribution could be feasible in some applications. The resulting shift of the proof mass centre of gravity position away from the geometric centre of the proof mass would result in a different excitation torque from the same excitation acceleration, compared to the symmetric version. In that case, however, the motion equation becomes more complicated as it needs to account for the effects connected to the varying distance between the centre of gravity and point of contact between the proof mass and the frame.

Another possible future modification is a design with additional stationary magnets fixed on the frame. Depending on their number, orientation, and positioning, they would affect one or both of the equilibrium positions and the stiffness characteristics of the device. This approach could be beneficial especially in case where mainly vertical compound of the acceleration is to be harvested and there is no acceleration in the horizontal plane present to excite the harvester from the default equilibrium position, where it is insensitive to the excitation in the vertical direction. This modification, however, puts more practical demands on the contact between the proof mass and the frame cavity, as the magnetic forces might cause the proof mass to slide in order to align the magnetic fields of the stator and the rotor. A solution for this configuration might be in using geared contact but this would have implications on mechanical friction. It is a matter of further study, whether the increased mechanical losses caused by this would be overweighed by an increase in the harvester performance in given application.

8. Conclusions

In this paper a new design of kinetic, inertial 1DOF energy harvester for human power and other very low frequency environments is presented. The design is based on the Tusi couple, where the cylindrical proof mass rolls in a circular cavity with specified diameter ratio. This configuration allows for exploiting the acceleration inputs from multiple directions, and for an efficient design of the energy transducer itself. The proof mass follows an unrestricted full circular path, which is advantageous for low frequency oscillations, where a path of finite length would lead to either a bulky device, or energy losses due to the proof mass hitting the bumpers at the limits of the path.

A model of the device is built using the derived analytical equation of motion together with CAD and FEM modelling for the design parameters and magnetic field properties. Its performance is compared to the values, measured with the in-house fabricated prototype of the device. A theoretical performance analysis of the verified model is then presented, showing the excellent performance of the design in low frequency excitation environment.

The results of experiments conducted and simulations run on the validated model of the harvester clearly demonstrate the feasibility of the proposed energy harvester design for a low frequency environment, and its superior performance over other comparable designs both in terms of generated power, and normalized power density.

Acknowledgement

This work is an output of research and scientific activities of NETME Centre, supported through project NETME CENTRE PLUS (LO1202) by financial means from the Ministry of Education, Youth and Sports in Czech Republic under the National Sustainability Programme I“.

References

[1] S. Moss, A. Barry, I. Powlesland, S. Galea, G.P. Carman, A broadband vibro-impacting power harvester with symmetrical piezoelectric bimorph-stops, Smart Mater. Struct. 20 (4) (2011) 45013.
[2] K.V. Selvan, M.S. Mohamed Ali, Micro-scale energy harvesting devices: Review of methodological performances in the last decade, Renew. Sustain. Energy Rev. (2016).
[3] E. Romero, R.O. Warrington, M.R. Neuman, Energy scavenging sources for biomedical sensors, Physiol. Meas. 30 (9) (2009) R35–62.
[4] M. Wahbah, M. Alhawari, B. Mohammad, H. Saleh, M. Ismail, Characterization of human body-based thermal and vibration energy harvesting for wearable devices, IEEE J. Emerg. Sel. Top. Circuits Syst. 4 (3) (2014) 354–363.
[5] A. Lay-Ekuakille, G. Vendramin, A. Trotta, and G. Mazzotta, “Thermoelectric generator design based on power from body heat for biomedical autonomous devices,” in: 2009 IEEE International Workshop on Medical Measurements and Applications, 2009, pp. 1–4.
[6] M.-K. Kim, M.-S. Kim, S. Lee, C. Kim, Y.-J. Kim, Wearable thermoelectric generator for harvesting human body heat energy, Smart Mater. Struct. 23 (10) (Oct. 2014) 105002.

Please cite this article in press as: J. Smilek et al., Rolling mass energy harvester for very low frequency of input vibrations, Mech. Syst. Signal Process. (2018), https://doi.org/10.1016/j.ymssp.2018.05.062

[7] N. Gomez Estancona, A.G. Tena, J. Torca, L. Urruticoechea, L. Muniz, D. Aristimuno, J.M. Unanue, A. Urruticoechea, Solar recharging system for hearing aid cells, J. Laryngol. Otol. 108 (9) (1994) 768–769.
[8] L. Xie, M. Cai, Increased piezoelectric energy harvesting from human footstep motion by using an amplification mechanism, Appl. Phys. Lett. 105 (14) (2014) 143901.
[9] S. Niu, X. Wang, F. Yi, Y.S. Zhou, Z.L. Wang, A universal self-charging system driven by random biomechanical energy for sustainable operation of mobile electronics, Nat. Commun. 6 (2015).
[10] M. Pozzi, M. Zhu, Plucked piezoelectric bimorphs for knee-joint energy harvesting: modelling and experimental validation, Smart Mater. Struct. 20 (5) (2011).
[11] A. Delnavaz, J. Voix, Energy harvesting for in-ear devices using ear canal dynamic motion, IEEE Trans. Ind. Electron. 61 (1) (2014) 583–590.
[12] C. Dagdeviren, B.D. Yang, Y. Su, P.L. Tran, P. Joe, E. Anderson, J. Xia, V. Doraiswamy, B. Dehdashti, X. Feng, B. Lu, R. Poston, Z. Khalpey, R. Ghaffari, Y. Huang, M.J. Slepian, J.A. Rogers, Conformal piezoelectric energy harvesting and storage from motions of the heart, lung, and diaphragm, Proc. Natl. Acad. Sci. U.S.A. 111 (5) (2014) 1927–1932.
[13] R. Morais, N.M. Silva, P.M. Santos, C.M. Frias, J.A.F. Ferreira, A.M. Ramos, J.A.O. Simões, J.M.R. Baptista, M.C. Reis, Double permanent magnet vibration power generator for smart hip prosthesis, Sens. Actuat. A Phys. 172 (1) (2011) 259–268.
[14] K. Remick, D. Dane Quinn, D. Michael McFarland, L. Bergman, A. Vakakis, High-frequency vibration energy harvesting from impulsive excitation utilizing intentional dynamic instability caused by strong nonlinearity, J. Sound Vib. 370 (2016) 259–279.
[15] Z. Zhou, W. Qin, P. Zhu, Improve efficiency of harvesting random energy by snap-through in a quad-stable harvester, Sens. Actuat., A Phys. 243 (2016) 151–158.
[16] B.C. Jung, C. Cho, H. Yoon, H. Yoon, B.D. Youn, Y.Y. Kim, Statistical model calibration for energy harvesting skin analysis and design, in: 53rd AIAA/ASME/ASCE/AHS/ASC Structures, Structural Dynamics and Materials Conference 2012, 2012.
[17] J. Smilek, F. Cieslar, Z. Hadas, Measuring acceleration in the area of human head for energy harvesting purposes, in: Proceedings of the 2016 17th International Conference on Mechatronics – Mechatronika, ME 2016, 2017.
[18] J. Smilek, Z. Hadas, A study of kinetic energy harvesting for biomedical application in the head area, Microsyst. Technol. (2015) 1–13.
[19] J. Yun, S.N. Patel, M.S. Reynolds, G.D. Abowd, Design and performance of an optimal inertial power harvester for human-powered devices, IEEE Trans. Mob. Comput. 10 (5) (2011) 669–683.
[20] A. Cadei, A. Dionisi, E. Sardini, M. Serpelloni, Kinetic and thermal energy harvesters for implantable medical devices and biomedical autonomous sensors, Meas. Sci. Technol. 25 (1) (Jan. 2014) 12003.
[21] H. Li, C. Tian, Z.D. Deng, Energy harvesting from low frequency applications using piezoelectric materials, Appl. Phys. Rev. (2014).
[22] J.M. Kluger, T.P. Sapsis, A.H. Slocum, Robust energy harvesting from walking vibrations by means of nonlinear cantilever beams, J. Sound Vib. 341 (Apr. 2015) 174–194.
[23] J. Cao, W. Wang, S. Zhou, D.J. Inman, J. Lin, Nonlinear time-varying potential bistable energy harvesting from human motion, Appl. Phys. Lett. 107 (14) (Oct. 2015) 143904.
[24] Y. Naruse, N. Matsubara, K. Mabuchi, M. Izumi, S. Suzuki, Electrostatic micro power generation from low-frequency vibration such as human motion, J. Micromech. Microeng. 19 (9) (2009) 94002.
[25] R. Tashiro, N. Kabei, K. Katayama, F. Tsuboi, K. Tsuchiya, Development of an electrostatic generator for a cardiac pacemaker that harnesses the ventricular wall motion, J. Artif. Organs 5 (4) (2002).
[26] Y. Zi, H. Guo, Z. Wen, M.-H. Yeh, C. Hu, Z.L. Wang, Harvesting low-frequency (<5 Hz) irregular mechanical energy: a possible killer application of triboelectric nanogenerator, ACS Nano 10 (4) (2016).
[27] S.D. Moss, O.R. Payne, G.A. Hart, C. Ung, Scaling and power density metrics of electromagnetic vibration energy harvesting devices, Smart Mater. Struct. 24 (2) (2015).
[28] W. Yang, S. Towfighian, A hybrid nonlinear vibration energy harvester, Mech. Syst. Signal Process. (2017).
[29] Ö. Zorlu, E.T. Topal, H. Külah, A vibration-based electromagnetic energy harvester using mechanical frequency up-conversion method, IEEE Sens. J. 11 (2) (2011).
[30] M. Scapolan, M.G. Tehrani, E. Bonisoli, Energy harvesting using parametric resonant system due to time-varying damping, Mech. Syst. Signal Process. (2016).
[31] Y. Zhang, C.S. Cai, B. Kong, A low frequency nonlinear energy harvester with large bandwidth utilizing magnet levitation, Smart Mater. Struct. 24 (4) (2015) 45019.
[32] A. Haroun, I. Yamada, S. Warisawa, Study of electromagnetic vibration energy harvesting with free/impact motion for low frequency operation, J. Sound Vib. (2015).
[33] A. Haroun, I. Yamada, S. Warisawa, Micro electromagnetic vibration energy harvester based on free/impact motion for low frequency-large amplitude operation, Sens. Actuat., A Phys. 224 (Apr. 2015) 87–98.
[34] S.-J. Jang, I.-H. Kim, H.-J. Jung, Y.-P. Lee, A tunable rotational energy harvester for low frequency vibration, Appl. Phys. Lett. 99 (13) (2011) 134102.
[35] B.J. Bowers, D.P. Arnold, Spherical, rolling magnet generators for passive energy harvesting from human motion, J. Micromech. Microeng. 19 (9) (2009) 94008.
[36] F.K. Shaikh, S. Zeadally, Energy harvesting in wireless sensor networks: a comprehensive review, Renew. Sustain. Energy Rev. (2016).
[37] A.R.M. Siddique, S. Mahmud, B. Van Heyst, A comprehensive review on vibration based micro power generators using electromagnetic and piezoelectric transducer mechanisms, Energy Convers. Manage. (2015).
[38] C. Wei, X. Jing, A comprehensive review on vibration energy harvesting: modelling and realization, Renew. Sustain. Energy Rev. 74 (2017) 1–18.
[39] C. Cepnik, R. Lausecker, U. Wallrabe, Review on electrodynamic energy harvesters—a classification approach, Micromachines 4 (2) (Apr. 2013) 168–196.
[40] D. Spreemann, Y. Manoli, B. Folkmer, D. Mintenbeck, Non-resonant vibration conversion, J. Micromech. Microeng. 16 (9) (2006) S169–S173.
[41] K. Sasaki, Y. Osaki, J. Okazaki, H. Hosaka, K. Itao, Vibration-based automatic power-generation system, Microsyst. Technol. 11 (8) (2005) 965–969.
[42] Z. Hadas, V. Vetiska, R. Huzlik, V. Singule, Model-based design and test of vibration energy harvester for aircraft application, Microsyst. Technol. 20 (4–5) (Jan. 2014) 831–843.
[43] S.P. Beeby, R.N. Torah, M.J. Tudor, P. Glynne-Jones, T. O'Donnell, C.R. Saha, S. Roy, A micro electromagnetic generator for vibration energy harvesting, J. Micromech. Microeng. 17 (7) (2007).
[44] D. Mallick, A. Amann, S. Roy, Interplay between electrical and mechanical domains in a high performance nonlinear energy harvester, Smart Mater. Struct. 24 (12) (2015) 122001.
[45] G. Sebald, H. Kuwano, D. Guyomar, B. Ducharne, Experimental Duffing oscillator for broadband piezoelectric energy harvesting, Smart Mater. Struct. 20 (10) (2011) 102001.
[46] P.D. Mitcheson, E.M. Yeatman, G.K. Rao, A.S. Holmes, T.C. Green, Energy harvesting from human and machine motion for wireless electronic devices, Proc. IEEE 96 (9) (2008) 1457–1486.
[47] Y. Naruse, N. Matsubara, K. Mabuchi, M. Izumi, S. Suzuki, Electrostatic micro power generation from low-frequency vibration such as human motion, J. Micromech. Microeng. 19 (9) (2009) 94002.
[48] C.R. Saha, T. O'Donnell, N. Wang, P. McCloskey, Electromagnetic generator for harvesting energy from human motion, Sens. Actuat., A Phys. 147 (1) (Sep. 2008) 248–253.
[49] A. Munaz, B.-C. Lee, G.-S. Chung, A study of an electromagnetic energy harvester using multi-pole magnet, Sens. Actuat. A Phys. 201 (2013) 134–140.
[50] S.E. Jo, M.S. Kim, Y.J. Kim, Electromagnetic human vibration energy harvester comprising planar coils, Electron. Lett. 48 (14) (2012) 874.

Please cite this article in press as: J. Smilek et al., Rolling mass energy harvester for very low frequency of input vibrations, Mech. Syst. Signal Process. (2018), https://doi.org/10.1016/j.ymssp.2018.05.062

[51] S. Cheng, D.P. Arnold, A study of a multi-pole magnetic generator for low-frequency vibrational energy harvesting, J. Micromech. Microeng. 20 (2) (2010) 25015.
[52] A. Cammarano, S.A. Neild, S.G. Burrow, D.J. Wagg, D.J. Inman, Optimum resistive loads for vibration-based electromagnetic energy harvesters with a stiffening nonlinearity, J. Intell. Mater. Syst. Struct. (2014).
[53] T. Xue, S. Roundy, On magnetic plucking configurations for frequency up-converting mechanical energy harvesters, Sens. Actuat., A Phys. (2017).
[54] K. Fan, J. Chang, F. Chao, W. Pedrycz, Design and development of a multipurpose piezoelectric energy harvester, Energy Convers. Manag. 96 (2015) 430–439.
[55] P. Pillatsch, E.M. Yeatman, A.S. Holmes, A piezoelectric frequency up-converting energy harvester with rotating proof mass for human body applications, Sens. Actuat., A Phys. (2014).

Please cite this article in press as: J. Smilek et al., Rolling mass energy harvester for very low frequency of input vibrations, Mech. Syst. Signal Process. (2018), https://doi.org/10.1016/j.ymssp.2018.05.062

ANNEX A6

SMILEK, Jan and Zdenek HADAS

Coil optimization for linear electromagnetic energy harvesters with non-uniform magnetic field

In: Tomáš BŘEZINA a Ryszard JABŁOŃSKI, ed. *Mechatronics 2017. Advances in Intelligent Systems and Computing* [online]. Cham: Springer International Publishing, 2018, s. 735–742. ISBN 978-3-319-65960-2. Available at: doi:10.1007/978-3-319-65960-2_90

Coil Optimization for Linear Electromagnetic Energy Harvesters with Non-uniform Magnetic Field

Jan Smilek[1], Zdenek Hadas[1]

[1] Faculty of Mechanical Engineering, Brno University of Technology, Brno, Czech Republic
{smilek,hadas}@fme.vutbr.cz

Abstract. Useful electric power dissipated in the load of kinetic energy harvesters depends among other factors on the electromechanical coupling coefficient and the ratio of the harvester inner impedance and the load impedance. Improving the performance of an electromagnetic harvester is therefore possible by maximizing the electromechanical coupling by optimizing the magnetic circuit design, including the pick-up coil placement, size and shape. At the same time the impedance of the coil needs to be considered and an optimal electric load must be used in order to maximize the useful power. This paper presents a coil optimization algorithm for conditions of known magnetic field and its change in the space exploitable by the coil. The algorithm is based on the greedy search approach with the useful power on load as a cost function to be maximized. It also ensures an optimal and realistic load to be used.

Keywords: Energy Harvesting · Coil Optimization · Greedy Search · Coupling Coefficient · Mechanical Vibrations.

1 Introduction

The design of energy harvesters exploiting the kinetic energy of vibrations or shocks from the environment is a quite well researched topic, which has been discussed in literature numerous times [1–3]. However, in many cases simplifications are being used in order to speed up the design process, which might negatively affect the performance of the final device. A typical example of this can be seen in assuming a uniform magnetic field and its rate of change through all the turns of the pick-up coil in the electromagnetic energy harvesters [4]. In larger harvesting devices this might be close to reality, as the permanent magnets used can be quite large, and the coils can be smaller than the magnets. In small scale harvesters however this is often not the case, as the place for magnets and coil positioning is very limited [5]. Since the time variation of the magnetic flux through the coil turns during the harvester operation then might be non-uniform as well, the simplified models tend to overestimate the real performance [6].

For that reason it is necessary to investigate the magnetic field distribution within the space that can be occupied by the coil. The coil itself then should be optimized in such a way, so that it provides a high electromechanical coupling while keeping its own inner impedance as low as possible.

2 Linear Electromagnetic Harvester Model

A linear kinetic energy harvester using Faraday's law of induction to convert the kinetic energy of vibrations into electricity is typically an oscillating mechanical system with a single degree of freedom and inertial excitation (Fig. 1).

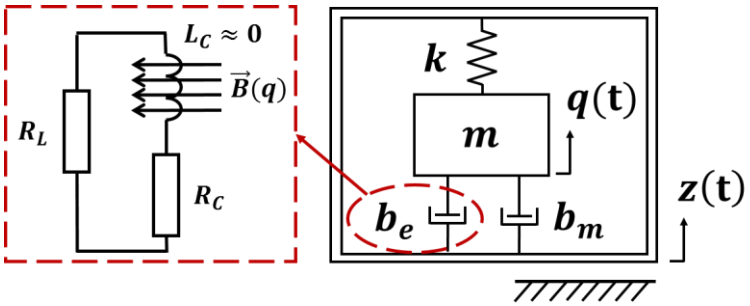

Fig. 1. Spring mass damper model of an energy harvester with 1 DOF

The motion of the harvester is described by the 2nd order differential equation:

$$m\ddot{q} + (b_e + b_m)\dot{q} + kq = -\mathrm{m}\ddot{z} \tag{1}$$

where m is the weight of the proof mass, b_e and b_m denote the electrical and mechanical damping, respectively; k is the stiffness, $\ddot{z}$ is the excitation acceleration of the frame and q is the displacement of the proof mass. If the coil inductance can be considered negligible, the electrical damping is defined as

$$b_e = \frac{c^2}{R_L + R_C} \tag{2}$$

where R_C is the coil resistance, R_L is the load resistance and c is the electromechanical coupling factor given by the rate of change of the magnetic flux $\emptyset$

$$c = \frac{d\emptyset}{dq} = S \cdot \frac{dB}{dq} \tag{3}$$

assuming that the coil area S is constant and the magnetic flux density component B, perpendicular to the coil area is dependent on the position of the mechanism. The electrical damping force

$$F_e = b_e \dot{q} \tag{4}$$

caused by the electromagnetic damping extracts the electrical energy from the system. The displacement of the proof mass of the harvester excited by a harmonic acceleration with an amplitude A_v can be found as

$$q(t) = \frac{A_v \frac{1}{\Omega^2}}{\sqrt{\left(\frac{1}{Q}\frac{\omega}{\Omega}\right)^2 + \left(1 - \left[\frac{\omega}{\Omega}\right]^2\right)^2}} \cdot \sin(\omega t) \tag{5}$$

where Ω is the natural frequency of the harvester, ω is the frequency of harmonic excitation acceleration and Q is the quality factor of the mechanism

$$Q = \frac{m\Omega}{b_e + b_m} \tag{6}$$

Average electrical power on the load R_L is then:

$$\mathrm{P}_{avg} = \frac{1}{2} b_e \dot{q}_A{}^2 \cdot \frac{R_L}{R_L + R_C} = \frac{b_e}{2} \cdot \frac{\left(A_v \frac{\omega}{\Omega^2}\right)^2}{\left(\frac{1}{Q}\frac{\omega}{\Omega}\right)^2 + \left(1 - \left[\frac{\omega}{\Omega}\right]^2\right)^2} \cdot \frac{R_L}{R_L + R_C} \tag{7}$$

where $\dot{q}_A$ denotes the amplitude of proof mass velocity. In the resonance operation of the harvester, where $\omega = \Omega$, equation (7) can be simplified and combined with (2) to

$$\mathrm{P}_{avg} = \frac{b_e \left(A_v Q \frac{1}{\Omega}\right)^2}{2} \cdot \frac{R_L}{R_L + R_C} = \left(\frac{c A_v Q}{\Omega (R_L + R_C)}\right)^2 \cdot \frac{R_L}{2} \tag{8}$$

It was shown in multiple publications [7–9] that in order to achieve the maximum electric power on the load in resonance operation, the load impedance should be set to

$$R_L = \frac{c^2}{b_m} + R_C \tag{9}$$

In that case equations (8) and (9) can be combined into the final form

$$\mathrm{P}_{avg} = \frac{(A_v m)^2}{8 b_m} \cdot \frac{c^2}{c^2 + R_C b_m} \tag{10}$$

In this paper however, the equation (8) is being used as the cost function for the optimization algorithm, as it allows for setting a non-optimal electrical loading, which might be beneficial in some scenarios.

3 Model of Magnetic Field in the Coil Area

Once the basic design of the harvester is decided and its parameters are known, the magnetic field is modelled in FEM software in order to obtain the magnetic field distribution in the coil area. In this paper a harvester with twelve permanent magnets placed on the two opposite faces of a cylindrical proof mass (Fig. 2) is analyzed. The orientation of the magnets is alternating so that each two neighboring magnets have the opposite pole facing the same direction. A single pick-up coil is to be placed above each face of the proof mass in such a way, that the center of the coil is aligned with the circle created by the centers of magnets fixed on the proof mass. The proof mass is designed to rotate around its axis, creating an alternating magnetic field through the coils.

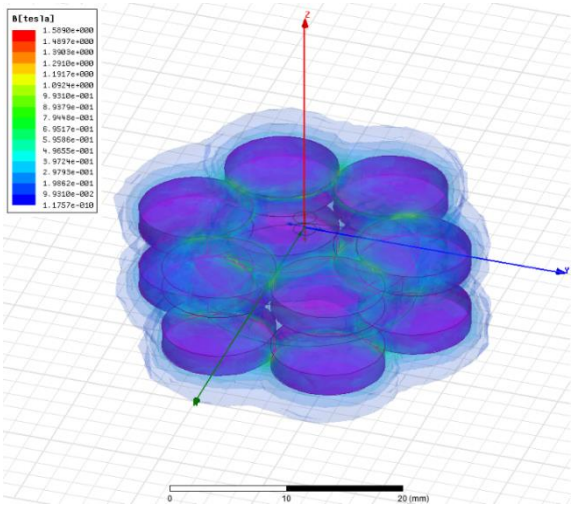

Fig. 2. Magnetic field around the proof mass with 12 magnets

The dimensions and constrains of the harvester investigated are summarized in Tab. 1. The minimal possible distance of the coil from the faces of the magnets is set to 0.5 mm to prevent any mechanical contact and possible damage to the coil. The coil is intended to be cylindrical with the same number of turns in each layer. The coil fill factor is set to 2/3, as a manually wound coil is envisioned to be used for prototype design verification. Minimum and maximum coil diameters are set based on the space limitations and intended coil winding technology constraints.

Parameter	Value	Unit
Magnets diameter	10	mm
Proof mass diameter	20	mm
Coil radius range	2÷30	mm
Coil Height range	0.05÷4.5	mm
Coil wire diameter	50	µm
Coil wire resistivity	1.68e-8	Ωm
Coil fill factor	2/3	-

Tab. 1. Harvester design parameters

For each of the turns of the coil the average magnetic flux rate of the change through the turn during the motion of the mechanism and the impedance of the turn were calculated independently (Fig. 3). These data were then fed as inputs to the calculation of the cost function value.

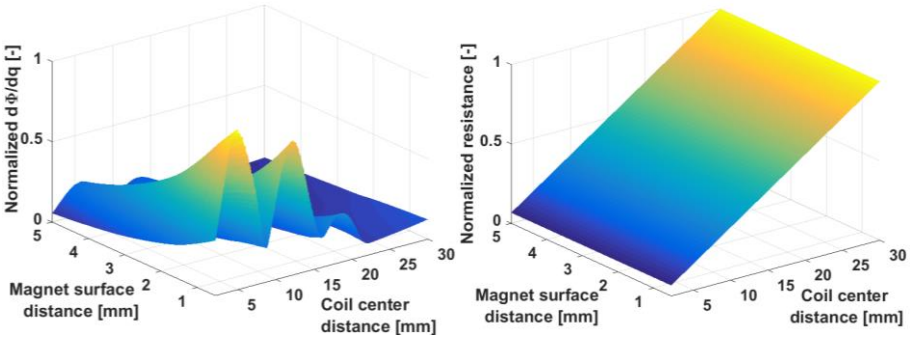

Fig. 3. Normalized magnetic flux rate of change through a single coil turn with given radius and distance from magnets (left) and normalized resistance of a single coil turn (right)

4 Coil Optimization Algorithm

The algorithm used for optimization of the coil shape is based on the greedy search algorithm, finding the locally optimal step in each iteration of the search. The cost function for finding the local optimum is defined as the electric power dissipated in the load, assuming that the load is optimal for reaching optimal electrical and mechanical damping ratio. It should be noted, that the total cost function value cannot be simply obtained by summing the values of cost function for each separate coil turn due to the square dependencies on the coupling c in the power calculation formula (8).

In the first step the algorithm searches for the starting point by evaluating the cost function of every single coil turn in the usable area separately. The highest found value is used as the initial point – the first turn of the coil, placed so that it yields the highest possible power on the optimized load. Every next step then consists of the coil being expanded either in the horizontal direction – towards the coil center or outwards; or in the vertical direction – further away from the magnets or closer to them. The cost function values are always calculated for all the possible advances and they are compared with the current value. The expansion direction with the highest positive increase in the cost function is chosen and the algorithm continues with the next iteration starting from this new coil configuration. The algorithm stops when there is no possible way to extend the coil horizontally or vertically, that would increase the absolute power dissipated on load.

The algorithm is built in such a way, that during the coil expansion it always expands whole row or column in order to keep the coil cylindrical and with the uniform distribution of the wires in each layer.

5 Results and Discussion

Figure 4 shows the results from the coil optimization in few different scenarios. In the first run, the coil was optimized with the assumption that an optimal load for each iteration of the algorithm will be used, as long as the requested optimal load has realistic value, e.g. it is not negative. Even though it is mostly more feasible to change the load impedance than to redesign the coil, in some cases it might be not possible to adjust the load as needed. For that reason several runs were tried to find the optimal coil configurations for given examples of fixed load impedance values of 1, 10, 100, 1000 and 10000 Ohms and fixed harvester parameters and excitation conditions.

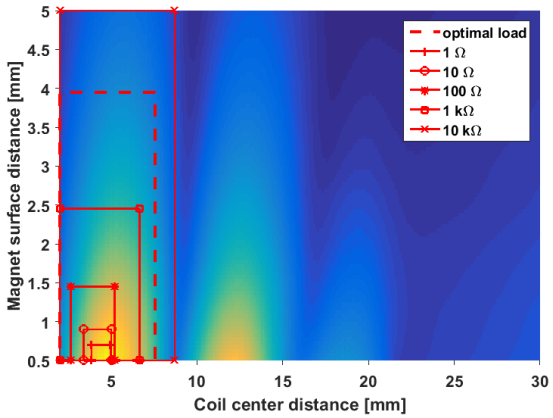

Fig. 4. Boundaries of coils optimized for different loads

Comparison of the total normalized average power on the load is visible on Fig. 5 show, that coil optimized for the optimal load yields the best performance as is expected, even though the ratio of power on load to total power dissipated (Fig. 6) might not be the highest.

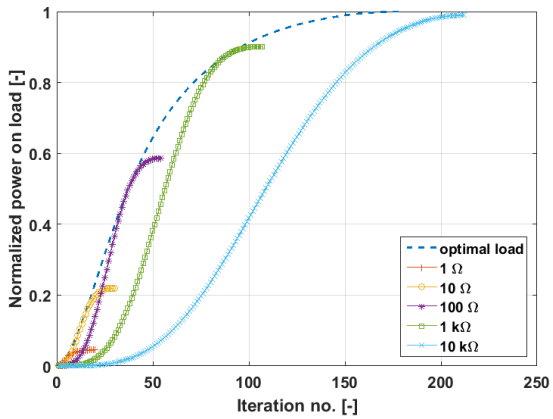

Fig. 5. Comparison of normalized power on load for different loads

It is a matter of further consideration, whether the selected algorithm finds the optimal solution in all possible design configurations of various harvesters, as it is obviously searching for a locally best solution only. More complicated patterns of magnetic field could thus potentially yield solution far from optimal. However, for the given configuration the results obtained are found satisfactory and well in agreement with the intuitive expectations.

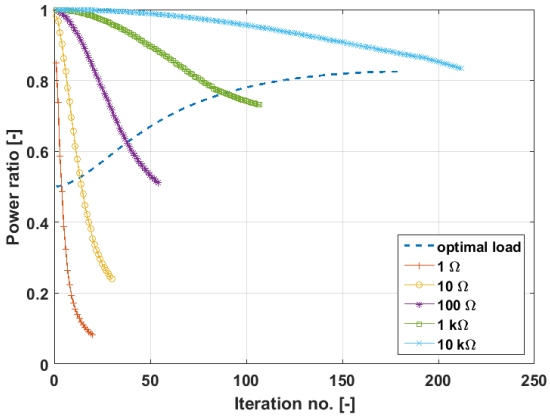

Fig. 6. Ratio of power on load to total power dissipated after optimization for different loads

6 Conclusions

This paper proposes a simple to implement optimization algorithm for the coil design of electromagnetic energy harvesters. The optimization is based on computationally inexpensive greedy search method, maximizing the power on the load of the harvester for given working conditions. The algorithm was tested on the model of a generic linear energy harvester with a given geometry and properties of the magnetic circuit obtained from a FEM simulation. The results show different optimal coil parameters to maximize the harvester performance for different electric loads, which can be useful if for some reason the load of the harvester is not adjustable. Presented implementation of the algorithm takes into account the dynamic feedback of the electrical loading to the oscillating system. The results shown are obtained using the assumption that the linear harvester is working in the resonance operation, which might not be always the case. In non-resonance operation also the value of optimal load would be generally different from the special case mentioned in this paper.

For more general approach one might consider formulating a simplified cost function that will maximize just the ratio of squared coupling coefficient to the coil resistance regardless of the electrical load. This approach yields the same results with the optimal load, as is apparent from a comparison of equations (8) and (10), but in case of different loading, the coil design obtained might not be the best possible solution.

Acknowledgement

This work is an output of research and scientific activities of NETME Centre, supported through project NETME CENTRE PLUS (LO1202) by financial means from the Ministry of Education, Youth and Sports in Czech Republic under the „National Sustainability Programme I“.

References

1. Elvin NG, Elvin AA (2011) An experimentally validated electromagnetic energy harvester. J Sound Vib 330:2314–2324. doi: 10.1016/j.jsv.2010.11.024
2. Arroyo E, Badel A, Formosa F, et al (2012) Comparison of electromagnetic and piezoelectric vibration energy harvesters: Model and experiments. Sensors Actuators A Phys 183:148–156. doi: 10.1016/j.sna.2012.04.033
3. Hadas Z, Vetiska V, Vetiska J, Krejsa J (2016) Analysis and efficiency measurement of electromagnetic vibration energy harvesting system. Microsyst Technol 22:1767–1779. doi: 10.1007/s00542-016-2832-4
4. Beeby SP, Torah RN, Tudor MJ, et al (2007) A micro electromagnetic generator for vibration energy harvesting. J Micromechanics Microengineering. doi: 10.1088/0960-1317/17/7/007
5. Haroun A, Yamada I, Warisawa S (2015) Micro electromagnetic vibration energy harvester based on free/impact motion for low frequency-large amplitude operation. Sensors Actuators, A Phys 224:87–98. doi: 10.1016/j.sna.2015.01.025
6. Khan F, Stoeber B, Sassani F (2014) Modeling of linear micro electromagnetic energy harvesters with nonuniform magnetic field for sinusoidal vibrations. Microsyst Technol 21:683–692. doi: 10.1007/s00542-014-2359-5
7. Smilek J, Hadas Z (2015) Assessment of MEMS energy harvester for medical applications. In: Sánchez-Rojas JL, Brama R (eds) Proc. SPIE. p 95170N
8. Khan F, Sassani F, Stoeber B (2010) Copper foil-type vibration-based electromagnetic energy harvester. J Micromechanics Microengineering 20:125006. doi: 10.1088/0960-1317/20/12/125006
9. Stephen NG (2006) On energy harvesting from ambient vibration. J Sound Vib 293:409–425. doi: 10.1016/j.jsv.2005.10.003

ANNEX A7

SMILEK, Jan and Zdenek HADAS.

Experimental evaluation of Tusi couple based energy harvester for scavenging power from human motion.

In*: Proceedings of VETOMAC 14th international conference on vibration Engineering and Technology of Machinery*. [in press]

Experimental evaluation of Tusi couple based energy harvester for scavenging power from human motion

Jan Smilek[1,*],and *Zdenek* Hadas[1]

[1]Faculty of Mechanical Engineering, Brno University of Technology, Technicka 2896/2, 616 69 Brno, Czech Republic

Abstract. This paper deals with the experimental performance evaluation of the prototype of a novel inertial energy harvester based on Tusi couple mechanism. The harvester was developed as an autonomous power source for environments with very low frequency and magnitude of mechanical vibrations available. The experiments were conducted using human body during different activities as a source of mechanical excitation, with the prospect of using the harvester for powering up future wearable electronic devices. Four different locations on a single measurement specimen were picked for the harvester placement – back of the head, belt, wrist and ankle. Measurements in each location comprised of walking on a straight and level path at natural speed, walking up and down the stairs, jumping, running, and location-specific activities that were expected to provide significant output power. The measured average output power of the device with dimensions 50x50x20 mm on empirically selected 2 kΩ electrical load reached up to 6.5 mW, obtained with the device attached to the ankle while shaking the leg.

1 Introduction

Converting the energy of human motion into electricity has been gaining a significant interest in past few decades thanks to its obvious exploitability in biomedical and low power wearable electronic applications. Various designs of energy harvesters have been presented, utilizing mostly piezoelectric effect [1, 2]; electromagnetic induction [3, 4]; or hybrid approaches [5] to convert the mechanical energy into electricity. Recent works also report utilizing a triboelectric effect [6] or electrochemically driven harvesters [7] for the same goal. The size of devices ranges from large devices integrated into a backpacks or special braces [8, 9], through harvesters small enough to be implemented into apparel or wearable devices [10], to implantable MEMS energy harvesters, meant for powering up biomedical implants [11]. The harvester presented in this paper with its dimensions 50x50x20mm falls into the larger devices category, attachable externally to various parts of human body, or into dedicated pockets in smart clothing products, as close to the intended application as possible.

* Corresponding author: smilek@fme.vutbr.cz

2 Harvester design

The harvester (Fig. 1) comprises of a rolling proof mass with 6 permanent magnets fixed to each face of the rolling mass. Movement of the proof mass with 1 dof in the circular cavity of double the diameter of the proof mass causes the magnets to pass in front of the pick-up coils, placed above the centre of the cavity. The neighbouring magnets are fixed to the rolling mass with alternating magnetization direction to maximize the magnetic flux change during the motion.

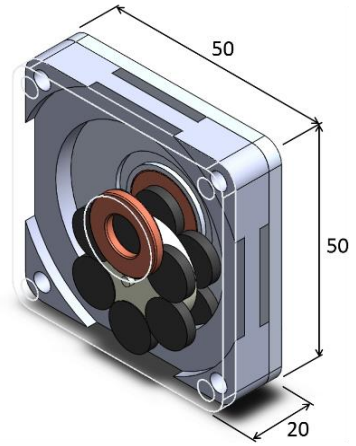

Fig. 1. Tusi couple energy harvester prototype design and main dimensions.

The movement of the proof mass is described by the Lagrange equation of second kind, using q as generalized coordinate:

$$d/dt(dE_k/d\dot{q}) - dE_k/dq + dE_b/d\dot{q} + dE_p/dq = -dA/dq = -Q \quad (1)$$

After a series of mathematical operations the final form of this equation, valid for this design of the harvester where the proof mass centre of gravity is aligned with its geometrical centre, can be derived as:

$$I_{total}\cdot\ddot{q} - 0 + (b_e^*+b_m^*)\cdot\dot{q} + m\cdot g\cdot r\cdot sin[q\cdot r/(R-r)] =$$

$$= -m\cdot r\cdot\{\ddot{z}_x\cdot cos[q\cdot r/(R-r)] + \ddot{z}_y\cdot sin[q\cdot r/(R-r)]\} \quad (2)$$

Where I_{total} the moment of inertia of the proof mass with respect to instantaneous axis of rotation, b_m^* denotes mechanical damping, m is total weight of the proof mass, R is radius of the cavity, and r is radius of the proof mass disc. $\ddot{z}_x$ and $\ddot{z}_y$ denote excitation acceleration in two perpendicular directions in the working plane of the harvester. The useful electrical energy is dissipated on electric load R_L, which contributes to the electrical damping of the system b_e^*, together with the resistance of the pick-up coils connected in series R_C:

$$b_e^* = (d\Phi/dq)^2 / (R_L + R_C) \quad (3)$$

The RMS value of magnetic flux change with respect to the displacement of the harvester $d\Phi/dq$ reaches 0.2 Wb/rad for the evaluated magnetic circuit design.

3 Experimental setup and methodology

The experiment was conducted with the harvester device fixed on a testing rig together with a three-axial accelerometer to log the acceleration in both working axes of the harvester. A single test subject (male, 183 cm, 75 kg) was then performing a series of activities with the harvester mounted on different locations on the body, which were empirically deemed feasible for potential harvester placement (Fig. 2). The locations selected were back of the head, belt, wrist and ankle. Each of the measurement runs lasted 300 s, with six to seven different actions being performed during two runs in each harvester placement. The first measurement in each placement consisted solely of the subject walking at natural speed on level surface inside a building, second measurement contained placement-specific activities. The recorded activities common for all the harvester placements were running, going up and down the stairs, and jumping. The location specific activities included nodding and shaking the head, jumping jacks, different walking style patterns or shaking the limbs violently.

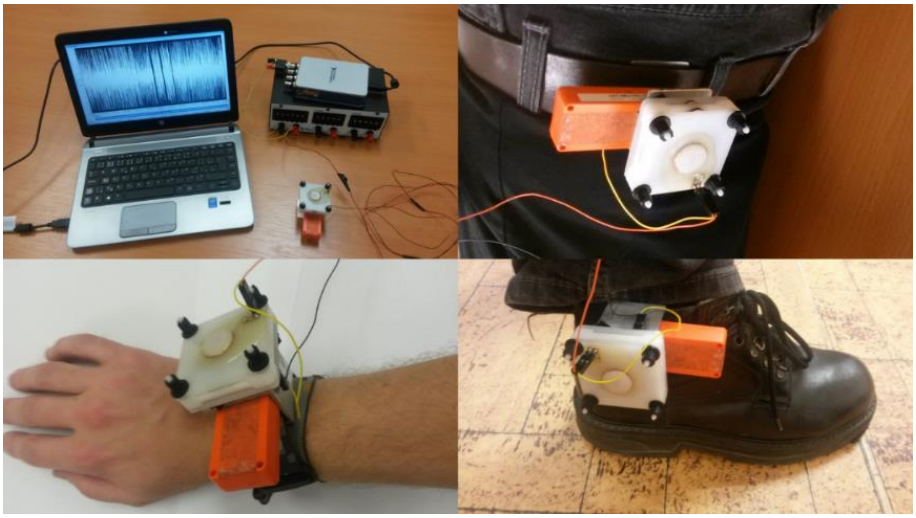

Fig. 2. Measurement setup and the harvester with datalogger in three out of four measured locations.

The harvested power was measured on 2 kΩ electrical load, and recorded using NI-9234 card. Since the peaks of generated voltage on load reached beyond the card ±5 V limits, a voltage divider was employed and the recorded voltages were then recalculated to obtain the power dissipated on the full load.

4 Results

The acceleration measurements were exploited to identify the different recorded activities in the second set of measurements (Fig. 3). Furthermore, the FFT was calculated for each activity and placement, and the dominant acceleration peak in both working directions of the harvester was noted for future analyses. The recorded voltage waveforms on the 2 kΩ electrical load (Fig. 4) were used to calculate the RMS values of voltage and average electrical power dissipated on load (Tab. 1).

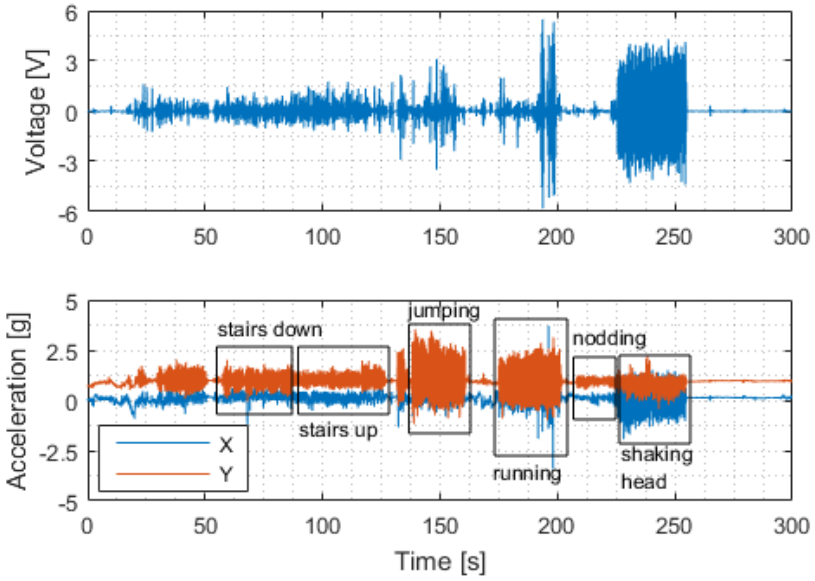

Fig. 3. Voltage on load and acceleration in the relevant axes with harvester placement on head during the second measurement set.

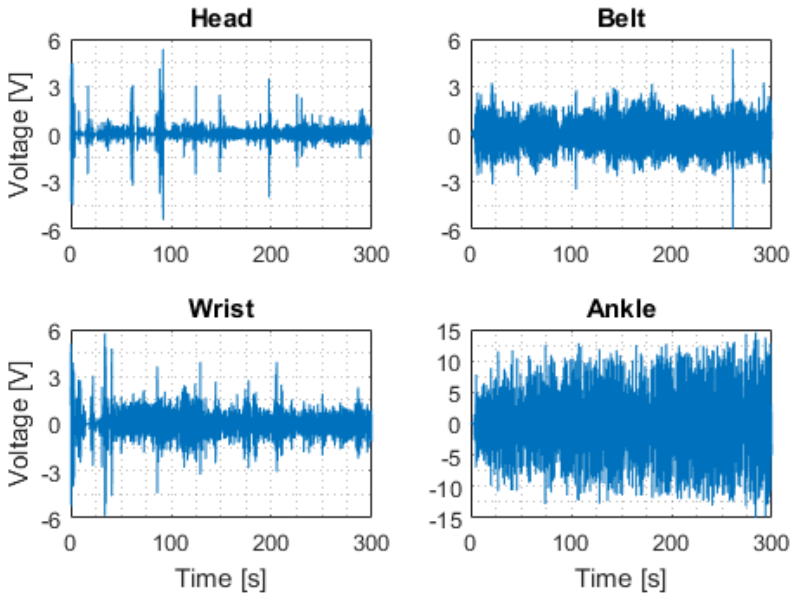

Fig. 4. Generated voltage on load during normal walking in all measured harvester placements.

Table 1. RMS values of voltage and average power on load for different placements and activities.

Harvester Placement	Activity	RMS Voltage on load [V]	Average Power on load [μW]
Head	Walking	0.34	56
	Walking down the stairs	0.24	29
	Walking up the stairs	0.36	66
	Running	0.5	122
	Jumping	0.4	81
	Nodding	0.11	6
	Shaking head	1.35	905
Belt	Walking	0.55	150
	Walking down the stairs	0.75	277
	Walking up the stairs	0.49	120
	Running	2.32	2669
	Jumping	1.9	1779
	Jumping jacks	1.77	1542
Wrist	Walking	0.49	120
	Walking down the stairs	1.01	502
	Walking up the stairs	0.54	147
	Running	1.08	582
	Jumping	1.4	970
	Shaking hand	2.23	2473
	Walking with hand hitting body	1.24	756
Ankle	Walking	1.7	1423
	Walking down the stairs	2.09	2172
	Walking up the stairs	1.66	1367
	Running	1.73	1481
	Jumping	2.36	2752
	Shaking leg	3.62	6501
	Rocking on heels	1.14	643

The results demonstrate, that depending on the placement, this harvester prototype can be used to power up some of the low-power wearable or implantable electronic applications, at least during the time of the user activity. Taking into account the 0.87 hours of average time per day that is spent by walking or exploitable activities [12], the average power available through the whole 24 hours of the day ranges between 2 μW for the head placement (worst case) and 52 μW for the ankle placement (best case).

5 Conclusions

The paper presented an experimental performance evaluation of a novel design of electromagnetic energy harvester developed for human power harvesting. The harvester was tested in real-life conditions, mounted on different locations on testing subject, performing different activities ranging from walking to violent limbs shaking. The harvester was attached in the measurements locations together with a 3-axis acceleration datalogger in order to record the input acceleration data for possible future design

optimization. Average power on load harvested during the normal walking varied between 56 μW for the harvester placed on the back on the head, and 1.4 mW for the device attached on the ankle. The results indicate that, assuming a reasonably active behaviour of the user, the device could provide a feasible alternative power source for modern low-power health sensors and wearable electronics; such as wristwatches, temperature or humidity sensors, accelerometers or pressure sensors. Furthermore, optimization of the harvester design for the conditions in particular locations could increase the output power levels beyond the current results.

This work is an output of research and scientific activities of NETME Centre, supported through project NETME CENTRE PLUS (LO1202) by financial means from the Ministry of Education, Youth and Sports in Czech Republic under the „National Sustainability Programme I“.

References

[1] W. S. Jung, M. J. Lee, M. G. Kang, H. G. Moon, S. J. Yoon, S. H. Baek, and C. Y. Kang, “Powerful curved piezoelectric generator for wearable applications,” Nano Energy, **13**, pp. 174–181, (2015)

[2] P. Pillatsch, E. M. Yeatman, and A. S. Holmes, “A wearable piezoelectric rotational energy harvester,” *2013 IEEE Int. Conf. Body Sens. Networks, BSN 2013*, no. 1, (2013)

[3] S. E. Jo, M. S. Kim, and Y. J. Kim, “Electromagnetic human vibration energy harvester comprising planar coils,” Electron. Lett., **48**, no. 14, p. 874, (2012)

[4] C. R. Saha, T. O'Donnell, N. Wang, and P. McCloskey, “Electromagnetic generator for harvesting energy from human motion,” Sensors Actuators, A Phys., **147**, no. 1, pp. 248–253, Sep. (2008)

[5] R. Hamid and M. R. Yuce, “A wearable energy harvester unit using piezoelectric–electromagnetic hybrid technique,” Sensors Actuators, A Phys., **257**, pp. 198–207, (2017)

[6] Z. L. Wang, “Triboelectric nanogenerators as new energy technology for self-powered systems and as active mechanical and chemical sensors.,” ACS Nano, **7**, no. 11, pp. 9533–57, (2013)

[7] S. Kim, S. J. Choi, K. Zhao, H. Yang, G. Gobbi, S. Zhang, and J. Li, “Electrochemically driven mechanical energy harvesting,” Nat. Commun., **7**, (2016)

[8] R. Riemer and A. Shapiro, “Biomechanical energy harvesting from human motion: Theory, state of the art, design guidelines, and future directions,” J. Neuroeng. Rehabil., **8**, no. 1, pp. 1–13, (2011)

[9] M. Pozzi and M. Zhu, “Plucked piezoelectric bimorphs for knee-joint energy harvesting: Modelling and experimental validation,” Smart Mater. Struct., **20**, no. 5, (2011)

[10] M. A. Halim, H. Cho, M. Salauddin, and J. Y. Park, “A miniaturized electromagnetic vibration energy harvester using flux-guided magnet stacks for human-body-induced motion,” Sensors Actuators, A Phys., **249**, pp. 23–31, (2016)

[11] R. Hinchet and S. W. Kim, “Wearable and Implantable Mechanical Energy Harvesters for Self-Powered Biomedical Systems,” ACS Nano, **9**, no. 8, pp. 7742–7745, (2015)

[12] J. Smilek and Z. Hadas, “A study of kinetic energy harvesting for biomedical application in the head area,” Microsyst. Technol., **22**, no. 7, pp. 1535-1547, (2016)